# Go With the Flow: The Subcellular Compartmentalization of Enzymatic Interactions for Monoterpene Indole Alkaloid Biosynthesis in *Catharanthus roseus*

by

Hannah Caroline Tran

Bachelor of Science in Biology-Chemistry, University of New Brunswick, 2024

A Thesis Submitted in Partial Fulfillment
of the Requirements for the Degree of

Master of Science

in the Graduate Academic Unit of Chemistry

**Supervisor:** Yang Qu, PhD, Chemistry

**Examining Board:** Adam Dyker, PhD, Chemistry, Chair
Jan-Hendrik Poehls, PhD, Chemistry
Bryan Crawford, PhD, Biology

This thesis is accepted by the Dean of Graduate Studies

THE UNIVERSITY OF NEW BRUNSWICK

June, 2026

© Hannah Caroline Tran, 2026

# Abstract

Vinblastine is an important chemotherapeutic drug classified as a monoterpene indole alkaloid (MIA). While its naturally produced by complex biosynthetic pathways in the flowering plant *Catharanthus roseus*, its supply for commercial pharmaceuticals is limited by low yields. Synthetic chemical synthesis is inefficient due to the structural complexity of MIAs, and natural abundance is low. Although recent advances have enabled *de novo* biosynthesis of vinblastine precursors in yeast, yields remain insufficient for commercial viability. A central question that remains in the field is how plants are organizing these biochemical reactions spatially. In this study, I use bimolecular fluorescence complementation (BiFC) assays in *Nicotiana benthamiana* epidermal leaf cells to investigate protein-protein interactions between *C. roseus* enzymes in the vinblastine pathway and their subcellular localization. These findings deepen our understanding of the MIA biosynthesis spatial organization and provide insights into the pathway enzyme interactions; ultimately informing targeted bioengineering strategies to enhance therapeutic MIA production in heterologous systems.

## Acknowledgements

I would like to extend my sincerest gratitude to my supervisor, Dr. Yang Qu, for his invaluable support, wisdom, and guidance throughout the course of my Master's research. I would also like to thank my thesis committee members, Dr. Jan-Hendrik Pöhls and Dr. Bryan Crawford for their insightful feedback and constructive comments. Thank you to all Qu lab students for your technical assistance, advice, and for creating a motivating and supportive research environment. I would also like to thank Nhu Trieu and Steven Cogswell of the UNB Microscopy and Microanalysis Facility for their expertise and help throughout the past two years. I would also like to acknowledge the University of New Brunswick for providing access to the facilities and resources essential for the completion of this project. Finally, I am extremely grateful for my family and friends who have supported me throughout my studies.

# Table of Contents

Abstract ..... ii

Acknowledgements ..... iii

Table of Contents ..... iv

List of Tables ..... viii

List of Figures ..... ix

List of Symbols, Nomenclature, or Abbreviations ..... xi

Chapter 1: Introduction of Monoterpene Indole Alkaloid Biosynthesis ..... 1

1.1 Ancient plant medicines ..... 1

1.1.1 The Transition from Traditional Knowledge to Modern Pharmacology ..... 1

1.1.2 Alkaloids: from *hul gil* to *Oxycontin* ..... 2

1.2 Plant Specialized Metabolites ..... 4

1.2.2 Limited availability of MIA-based drugs ..... 7

1.3 Vinblastine biosynthesis in *C. roseus* ..... 8

1.3.1 Strictosidine aglycone biosynthesis ..... 8

1.3.2 Biosynthesis of Heteroyohimbine MIAs ..... 9

1.3.3 Biosynthesis of Aspidosperma and Iboga MIAs ..... 10

1.3.4 Conversion of Tabersonine to Vindoline ..... 12

1.3.5 Coupling of Catharanthine and Vindoline ..... 13

1.4 Biosynthetic Gene Clusters (BGCs) in plant metabolism ..... 14

1.4.1 Advantage of Plant Biosynthetic Gene Clusters (BGCs) ..... 15

1.4.2 Biosynthetic Gene Clusters (BGCs) in MIA Biosynthesis ..... 16

1.5 CAD Scaffold Protein organizing Geissoschizine Biosynthesis ..... 17

1.5.1 Compartmentalization for Rational Bioengineering in Heterologous Systems . 19
1.6 Techniques to study Protein-Protein Interactions ..... 20
1.6.1 *In vivo* protein-protein interaction methods ..... 21
1.6.1.1 Förster Resonance Energy Transfer (FRET) ..... 21
1.6.1.2 Split-Luciferase Complementation (Split LUC) ..... 21
1.6.1.3 Proximity Labelling (TurboID) ..... 22
1.6.1.4 Yeast Two-Hybrid (Y2H) ..... 23
1.6.2 *In vitro* protein-protein interaction methods ..... 24
1.6.2.1 Pull-Down Assays ..... 24
1.6.2.2 Co-Immunoprecipitation (Co-IP) ..... 24
1.6.2.3 Isothermal Titration Calorimetry (ITC) ..... 25
1.6.2.4 Cryo-Electron Microscopy ..... 26
1.7 Bimolecular Fluorescence Complementation (BiFC) ..... 27
1.7.1 Mechanism of Fluorophore Reconstitution ..... 27
1.7.2 Steric Considerations of BiFC Fusion Proteins ..... 28
1.7.3 Advantages and Limitations of BiFC ..... 29
1.7.4 Application in Plant Biology ..... 30
1.8 Research Hypothesis and Objectives ..... 31
Bibliography 1 ..... 33
Chapter 2: Investigation of *C. roseus* PPIs with BiFC assays in *N. benthamiana* ..... 42
2.1 Research Objective ..... 42
2.2 Preparing Tobacco Plantlets ..... 42
2.3 Chemicals ..... 43

2.4 Molecular Biology Kits ..... 43
2.5 Cloning ..... 43
2.5.1 Generation of GFP tagged Constructs ..... 43
2.5.2 Generation of BiFC tagged Constructs ..... 44
2.5.3 Subcellular localization markers ..... 44
2.5.4 *Escherichia coli* (*E. coli*) Cloning ..... 45
2.5.5 *Agrobacterium tumefaciens* Transformation ..... 46
2.6 Transient gene expression in *Nicotiana benthamiana* ..... 46
2.7 Confocal Scanning Laser Microscopy (CSLM) ..... 47
2.7.1 Sample Preparation for Confocal Scanning Laser Microscopy ..... 47
2.7.2 Confocal Scanning Laser Microscopy Fluorescent Imaging ..... 47
2.7.3 Processing Images using Fiji ..... 48
Bibliography 2 ..... 50
Chapter 3: A BiFC Survey of Core MIA biosynthetic Enzymes in *N. benthamiana* Leaf Epidermal Cells ..... 51
3.1 Interpreting Confocal Microscopy Images ..... 51
3.2 Subcellular Localization of GFP-tagged MIA Biosynthetic Enzymes ..... 51
3.3 Study of Strictosidine β-D-Glucosidase (SGD) Protein-Protein Interaction ..... 55
3.4 Study of Geissoschizine Synthase (GS) Protein-Protein Interactions ..... 62
3.5 *C. roseus* Geissoschizine Oxidase (GO) BiFC in *N. benthamiana* ..... 67
3.6 *C. roseus* Oxidoreductase I (Redox1) BiFC in *N. benthamiana* ..... 73
3.7 *C. roseus* Oxidoreductase II (Redox2) BiFC in *N. benthamiana* ..... 80
3.8 *C. roseus* Stemmadenine Acetyltransferase (SAT) BiFC in *N. benthamiana* ..... 87

3.9 *C. roseus* O-acetylstemmadenine oxidase (ASO) BiFC in *N. benthamiana* ..... 91
3.10 *C. roseus* Dihydroprecondylocarpine Acetate Synthase (DPAS) BiFC in *N. benthamiana* ..... 97
3.11 *C. roseus* Tabersonine Synthase (HL1) BiFC in *N. benthamiana* ..... 104
3.12 *C. roseus* Catharanthine Synthase (HL2) BiFC in *N. benthamiana* ..... 110
3.13 Investigation of the Influence of Native Cinnamyl Alcohol Dehydrogenase ..... 117
3.14 *C. roseus* Cinnamyl Alcohol Dehydrogenase II (CAD2) BiFC in *N. benthamiana* ..... 119
3.15 Summarized BiFC Results ..... 126
Bibliography 3 ..... 129
Chapter 4: Discussion & Future Directions ..... 131
4.1 Discussion of BiFC Results ..... 131
4.1.1 Overexpression of Cytosolic Proteins and Nuclear Localization ..... 133
4.1.2 Negative BiFC Observed for ASO ..... 134
4.2 Future Directions ..... 135
4.2.1 Removing the CAD background ..... 135
4.2.2 Molecular Modelling ..... 135
4.3 Final remarks ..... 136
Bibliography 4 ..... 137
Appendix I Supplementary Information for Chapter 2 ..... 138
Curriculum Vitae

# List of Tables

**Table 3.1:** BiFC subcellular fluorescence of enzymes in the *C. roseus* pathway.....127

**Supplementary Table 1:** Primers used in this study. ..... 138

**Supplementary Table 2:** cDNA sequences of proteins used in this study. ..... 139

# List of Figures

**Figure 1.1:** The reaction of salicin to acetylsalicylic acid (Aspirin) ..... 2

**Figure 1.2:** Chemical structires of caffeine, nicotine, and cocaine ..... 3

**Figure 1.3:** Structures of natural, semi-synthetic, and synthetic opioids ..... 4

**Figure 1.4:** Vinblastine chemical structure. ..... 6

**Figure 1.5:** Formation of strictosidine in *C. roseus* ..... 7

**Figure 1.6:** Enzymatic architecture around the strictosidine aglycones in *C. roseus* ..... 10

**Figure 1.7:** Biosynthetic pathway to tabersonine and catharanthine in *C. roseus* ..... 12

**Figure 1.8:** Coupling of vindoline and catharanthine creates vinblastine and vincristine 14

**Figure 1.9:** CAD2 scaffolds SGD and GS in MIA biosynthesis ..... 18

**Figure 1.10:** Subcellular and cellular synthesis of catharanthine and vindoline ..... 20

**Figure 1.11:** Bimolecular Fluorescence Complementation (BiFC) Mechanism ..... 28

**Figure 1.12:** All possible BiFC tag locations for fusion proteins ..... 29

**Figure 3.1:** Confocal microscopy of GFP-tagged proteins in *N. benthamiana* leaves .... 53

**Figure 3.2:** BiFC assay of mVenus$^{C}$ tagged *C. roseus* SGD ..... 56

**Figure 3.3:** BiFC assay of mVenus$^{N}$ tagged *C. roseus* SGD ..... 59

**Figure 3.4:** SGD protein-protein interaction map ..... 61

**Figure 3.6:** BiFC assay of mVenus$^{N}$ tagged *C. roseus* GS ..... 64

**Figure 3.7:** GS BiFC protein-protein interaction map ..... 66

**Figure 3.8:** BiFC assay of mVenus$^{C}$ tagged *C. roseus* GO ..... 68

**Figure 3.9:** BiFC assay of mVenus$^{N}$ tagged *C. roseus* GO ..... 70

**Figure 3.10:** GO BiFC protein-protein interaction map ..... 73

**Figure 3.11:** BiFC assay of mVenus$^{C}$ tagged *C. roseus* Redox1 ..... 74

**Figure 3.12:** BiFC assay of mVenus$^{N}$ tagged *C. roseus* Redox1 ..... 77

**Figure 3.13:** Redox1 BiFC protein-protein interaction map ..... 79

**Figure 3.14:** BiFC assay of mVenus$^{C}$ tagged *C. roseus* Redox2 ..... 80

**Figure 3.15:** BiFC assay of mVenus$^{N}$ tagged *C. roseus* Redox2 ..... 83

**Figure 3.16:** Redox2 BiFC protein-protein interaction map ..... 86

**Figure 3.17:** BiFC assay of mVenus$^{N}$ tagged *C. roseus* SAT ..... 87

**Figure 3.18:** SAT BiFC protein-protein interaction map ..... 90

**Figure 3.19:** BiFC assay of mVenus$^{N}$ tagged *C. roseus* ASO ..... 91

**Figure 3.20:** ASO BiFC protein-protein interaction map ..... 96

**Figure 3.21:** BiFC assay of mVenus$^{C}$ tagged *C. roseus* DPAS ..... 97

**Figure 3.22:** BiFC assay of mVenus$^{N}$ tagged *C. roseus* DPAS ..... 100

**Figure 3.23:** DPAS BiFC protein-protein interaction map ..... 103

**Figure 3.24:** BiFC assay of mVenus$^{C}$ tagged *C. roseus* HL1 ..... 104

**Figure 3.25:** BiFC assay of mVenus$^{N}$ tagged *C. roseus* HL1 ..... 107

**Figure 3.26:** HL1 BiFC protein-protein interaction map ..... 110

**Figure 3.27:** BiFC assay of mVenus$^{C}$ tagged *C. roseus* HL2 ..... 111

**Figure 3.28:** BiFC assay of mVenus$^{N}$ tagged *C. roseus* HL2 ..... 114

**Figure 3.29:** HL2 BiFC protein-protein interaction map ..... 117

**Figure 3.31:** Reduction of coniferyl aldehyde to coniferyl alcohol by a CAD ..... 118

**Figure 3.32:** BiFC assay of mVenus$^{C}$ tagged *C. roseus* CAD2 ..... 119

**Figure 3.33:** BiFC assay of mVenus$^{N}$ tagged *C. roseus* CAD2 ..... 122

**Figure 3.34:** CAD2 BiFC protein-protein interaction map ..... 125

**Figure 3.35:** Overall BiFC protein-protein interaction map ..... 127

## List of Symbols, Nomenclature, or Abbreviations

AU ..... airy unit

N-terminus ..... amino-terminus

AS ..... alstonine synthase

BGC ..... biosynthetic gene cluster

BiFC ..... bimolecular fluorescent complementation

c ..... circa

CAD ..... cinnamyl alcohol dehydrogenase

CAD1 ..... cinnamyl alcohol dehydrogenase I

CAD2 ..... cinnamyl alcohol dehydrogenase II

C-terminus ..... carboxyl-terminus

Co-IP ..... co-immunoprecipitation

CSLM ..... confocal scanning laser microscopy

CFP ..... cyan fluorescent protein

D4H ..... desacetoxyvindoline 4-hydrolase

DAT ..... deacetylvindoline 4-O-acetyl-transferase

DNA ..... deoxyribonucleic acid

DPAS ..... dihydroprecondylocarpine synthase

ER ..... endoplasmic reticulum

FRET ..... Förster resonance energy transfer

G8H ..... geraniol 8-hydroxylase

GPCR ..... G protein-coupled receptors

GFP ..... green fluorescent protein

GS .....geissoschizine synthase

His .....histidine

HL1 ..... catharanthine synthase

HL2 ..... tabersonine synthase

HYS .....heteroyohimbine synthase

ITC .....isothermal titration calorimetry

$MgCl_2$ .....magnesium chloride

MEP .....methylerythritol phosphate pathway

MIA ..... monoterpenoid indole alkaloid

NLS .....nuclear localization signal

NMT .....N-methyltransferase

NPC .....nuclear pore complex

OD ..... optical density

PPI ..... protein-protein interaction

PRX ..... peroxidase

SGD ..... strictosidine β-D glucosidase

SDS-PAGE ..... sodium dodecyl sulfate-polyacrylamide gel electrophoresis

SS ..... serpentine synthase

STR ..... strictosidine synthase

T16H ..... tabersonine 16-hydroxylase

TDC..... tryptophan decarboxylase

THAS .....tetrahydroalstonine synthase

UPS ..... ubiquitin proteosome system

Y2H.....yeast two-hybrid

YFP .....yellow fluorescent prote

# Chapter 1: Introduction of Monoterpene Indole Alkaloid Biosynthesis

## 1.1 Ancient plant Medicines

The medicinal use of plants has been foundational to human civilization since time immemorial. The earliest documented records of herbal medicine originate from the Sumerian civilization (*circa* 3000 BCE) in Mesopotamia. Cuneiform clay tablets from this era catalog a diverse pharmacopeia, including myrrh for inflammatory conditions and the latex of *Papaver somniferum* (opium poppy) for pain[1]. The Sumerians referred to the poppy as *hul gil* ("the plant of joy"), marking one of the earliest recorded links between a specific botanical species and its psychoactive properties[2]. This plant medicine knowledge was transferred and expanded by subsequent Old World civilizations, most notably within the Ebers Papyrus (*c*. 1550 BCE). In this text, the ancient Egyptians detailed over 800 therapeutic formulations, including the use of *P. somniferum* extract as a sedative[3].

### 1.1.1 The Transition from Traditional Knowledge to Modern Pharmacology

While traditional medicine relied on empirical observation, the development of organic chemistry in the 19th and 20th centuries has improved our understanding of therapeutic compounds through the isolation and structural elucidation of compounds from crude plant extracts. A paramount example of this evolution is Aspirin. From the Sumerians and Egyptians to Indigenous North American populations, extracts from the bark of willow trees (e.g., *Salix alba*) have been used to treat fever and inflammation[4]. In the early 19th century, the therapeutic agent in *Salix* species, salicin, was first isolated.

Salicin acts as a prodrug, which human metabolism initially hydrolyzes into *D*-glucose and salicyl alcohol, then further oxidizes into salicylic acid–the active agent that combats inflammation and fever. To improve the pharmacokinetics, in 1897 Felix Hoffmann synthesized a less acidic analog via an acetylation with acetic anhydride: acetylsalicylic acid, known today as Aspirin[5] (Figure 1.1). This synthetic modification represents a landmark and lasting principle in medicinal chemistry: the optimization of a natural scaffold to improve the therapeutic index and commercial viability of a drug[6].

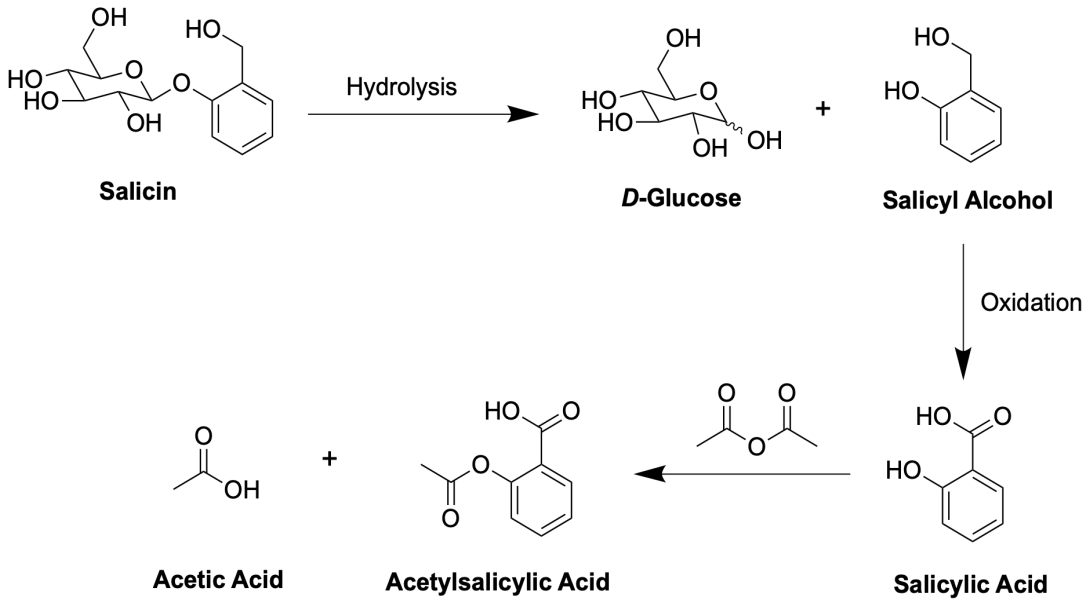



**Figure 1.1:** The *in-vivo* metabolism of salicin to salicylic acid, followed by the synthetic acetylation of salicylic acid to acetylsalicylic acid (Aspirin). Figure reproduced from Mahdi *et al*.[5]

### 1.1.2 Alkaloids: from *hul gil* to *Oxycontin*

The development of opium from *hul gil* represents another remarkable example of natural product medicine development. In 1804, Friedrich Sertürner successfully isolated the analgesic and sleep-inducing agent from opium poppy, *morphium* (morphine), which he named after the Greek god of dreams, *Morpheus*. This was the very first active principle

isolated from a plant source, and triggered the advent of rational drug discovery in the 19th century including other alkaloids such as caffeine, nicotine, and cocaine[7] (Figure 1.2). Remarkably, in 1952, over 100 years later, the structure of morphine was finally elucidated[8].

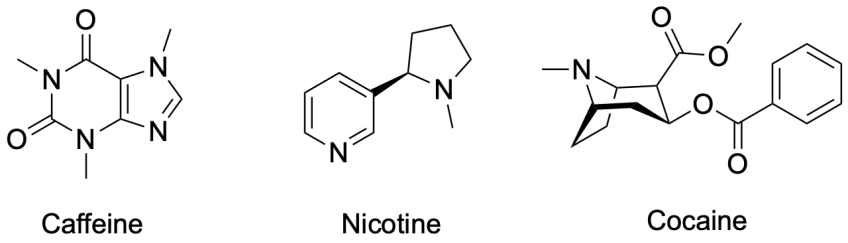



**Figure 1.2:** Chemical structures of commonly known alkaloids: caffeine, nicotine, and cocaine. Adapted from Katerova et al.[9]

Morphine and other opium alkaloids reduce pain by acting as agonists for mu (μ), kappa (κ), and delta (δ) opioid receptors [10]. These are types of G protein-coupled receptors (GPCRs) that work to block nociceptive (pain) signals from reaching the brain[11]. In contemporary medicine, this lineage has expanded to include a diverse array of natural, semisynthetic, and synthetic opioids – such as codeine, oxycodone, hydrocodone, fentanyl, and methadone (Figure 1.3) – which are currently used clinically for moderate to severe pain[11] and inextricably linked to their misuse. The trajectory of opioids from the Sumerians' *hul gil* to Purdue Pharma's *OxyContin* reinforces the power of natural product scaffolds as commercial drugs[12].

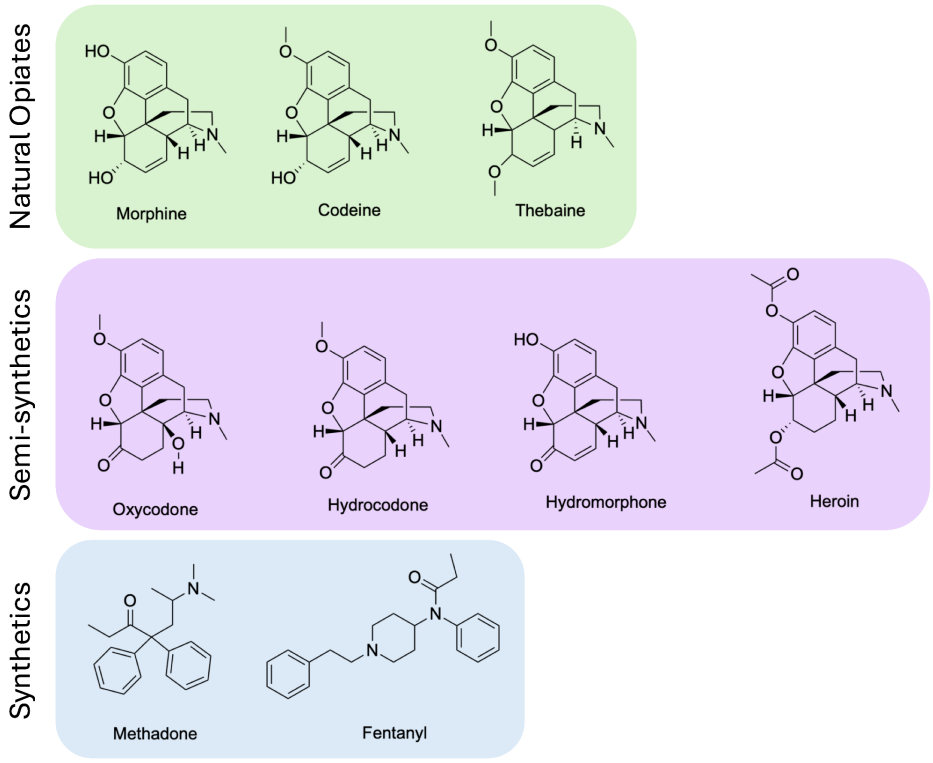



**Figure 1.3:** Structures of natural, semi-synthetic, and synthetic opioids used clinically and recreationally. Adapted from Baldo et al.[13]

### 1.2 Plant Specialized Metabolites

The development of salicylic acid and morphine illustrates the fundamental importance of identifying and optimizing natural products, specifically plant specialized metabolites, as scaffolds for modern pharmaceuticals. Plant metabolism is generally divided into two main classes: primary and specialized (secondary). Primary metabolism generates energy and molecules directly related to plant growth, development, and reproduction. This includes processes such as amino acid synthesis and photosynthesis. Meanwhile, specialized metabolism generates more complex molecules for processes indirectly related to plant development and reproduction. This includes a diversity of compounds that act as plant defense and aid in environmental niche adaptation. While often categorized for simplicity, primary and specialized metabolism are inherently

interconnected; all building blocks of specialized metabolism come directly from primary metabolism[12]. Additionally, it is important to acknowledge that although specialized metabolites have evolved from the products of core metabolism[14,15], there is growing evidence that supports a bidirectional metabolic relationship. Specialized metabolism can influence the flux of core metabolism, just as core metabolism inherently impacts the production of specialized metabolites[16].

Specialized metabolites can be largely categorized into four classes: terpenoids, phenylpropanoids, alkaloids, and glucosinolates, based on their biosynthetic origins and building blocks[17]. Terpenoids derive from simple, five-carbon building block isopentenyl pyrophosphate and are the largest group of specialized metabolites. Phenylpropanoids refers to compounds derive from the amino acid phenylalanine. Alkaloids also constitute one of the largest and most structurally diverse classes of natural products, characterized as nitrogen-containing organic compounds biosynthesized by bacteria, fungi, marine organisms, and most prevalently, terrestrial plants. Specialized metabolites provide a critical evolutionary advantage to plants, serving as a chemical defense mechanism to ward off herbivores, pathogens, and participate in plant communication with the environment[17,18].

### 1.2.1 Monoterpenoid indole alkaloids

The research in this thesis focuses on monoterpenoid indole alkaloids (MIAs), which are a class of specialized metabolites naturally produced by plants within the order *Gentianales*, which includes the *Apocynaceae*, *Loganiaceae*, *Gelsemiaceae*, and *Rubiaceae* families. Many MIAs are renowned for their diverse structures and bioactivities, including the bis-MIA Vinblastine. (Figure 1.4). Derived from the

Madagascar Periwinkle (*Catharanthus roseus*), Vinblastine contains nine chiral centers and acts as an anti-cancer agent by binding to the mitotic spindle during metaphase to prevent cell division. Notably, the anticancer properties of Vinblastine was first discovered in 1958 by Robert Noble and Charles Beer at Western University in London, Ontario[19]. Today, Vinblastine is widely used in chemotherapy for Hodgkins's lymphoma[20] and non-Hodgkins's lymphoma[21], alongside bladder[22], testicular[23], and lung cancer[24].

Since 1958, many other clinically useful MIA therapies have been identified: Vincristine (anticancer)[21], Ajmaline (anti-arrhythmic)[25], Reserpine (hypertension)[26], Vincamine (vasodilator)[27], and Alstonine (anti-psychotic)[28]. From the name 'monoterpenoid indole alkaloids', you can gather that their structure contains a terpene and indole moiety, in addition to nitrogen.

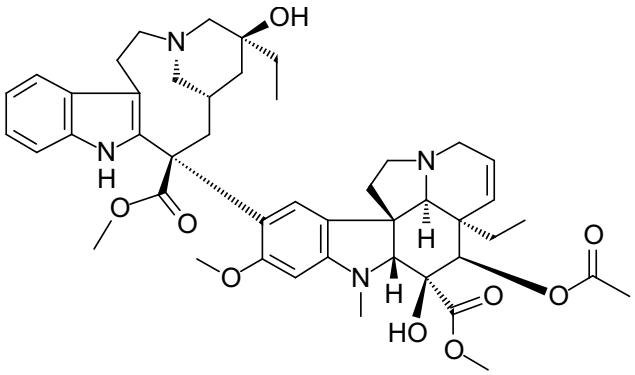



**Figure 1.4:** Vinblastine chemical structure.

The characteristic indole moiety, tryptamine, derives from the decarboxylation of tryptophan from the shikimate pathway by tryptophan decarboxylase (TDC). Meanwhile the monoterpenoid moiety, secologanin, originates from the methylerythritol phosphate pathway (MEP) then feeding into the secoiridoid pathway. Remarkably, these two molecules undergo a Pictet-Spengler condensation reaction to form strictosidine in the

vacuole of epidermal leaf cells in *C. roseus*[29] (Figure 1.5). This process highlights that multiple core metabolic pathways directly feed into specialized metabolism to build these structurally complex compounds *in planta*[30].

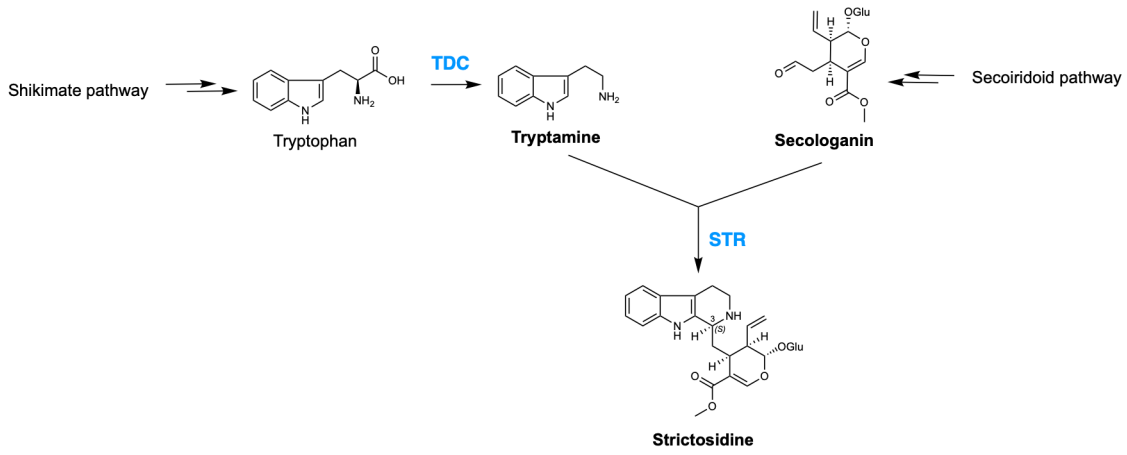



**Figure 1.5:** Formation of strictosidine in *C. roseus*. The Pictet-Spangler condensation of tryptamine and secologanin is catalyzed by strictosidine synthase (STR) to form strictosidine. Adapted from Gao et al.[31]

### 1.2.2 Limited availability of MIA-based drugs

Despite the importance of the medicinal properties of MIAs, their commercial production faces a persistent barrier. MIAs have a high level of stereochemical and structural complexity, which greatly limits the efficiency of synthetic synthesis (e.g., nine chiral centres in vinblastine). Further, MIA accumulation is low *in planta*, generally attributed to them being secondary metabolites compounded with their biosynthesis involving multiple organs, tissue types, and subcellular organelles. For example, harvesting just 1 g of vinblastine requires 500 kg of dried *C. roseus* leaves which uses considerable resources and is how vinblastine is currently obtained by pharmaceutical companies[19]. After decades of research, all but one biosynthetic step to vinblastine has been elucidated, which has enabled *de novo* biosynthesis of vinblastine precursors in yeast, building a foundation for industrial biosynthesis to meet the pharmaceutical demand[31,32].

### 1.3 Vinblastine biosynthesis in *C. roseus*

#### 1.3.1 Strictosidine aglycone biosynthesis

The biosynthesis of vinblastine and over 3000 other MIAs begins with the common precursor strictosidine, which results from a Pictet-Spangler condensation of tryptamine and secologanin by strictosidine synthase (STR) in the vacuole of leaf epidermis cells. Strictosidine is exported from the vacuole by a dedicated transporter NPF2.9 to the nucleus where it is deglycosylated by strictosidine β-D glucosidase (SGD), producing a group of reactive dialdehyde iminiums called strictosidine aglycones that exist in equilibrium[33]. This deglycosylation triggers the secondary amine to spontaneously nucleophilic attack the aldehyde's carbocation, creating a structure with a new ring. This forms 4,21-dehydro-demethylcoryantheine epimers, which will then exist in equilibrium with the other strictosidine aglycone forms (Figure 1.6).

SGD has a bipartite C-terminal nuclear localization signal (NLS) essential for its nuclear localization[34]. Additionally, SGD self-assembles into molecular multimers that form a tubular structure (*i.e.*, octet), which may pacify the reactive strictosidine aglycone[29]. This reactivity is fundamental to the diversity of MIAs, as strictosidine aglycone can spontaneously re-organize into the relatively stable 4,21-dehydrogeissoschizine, cathenamine, and epi-cathenamine, enabling further structural diversification[35].

### 1.3.2 Biosynthesis of Heteroyohimbine MIAs

The formation of heteroyohimbine MIAs begins with strictosidine aglycone intermediates, cathenamine and epi-cathenamine[36]. These compounds are used as substrates by tetrahydroalstonine synthases (THAS1-4) and a heteroyohimbine synthase (HYS). While THASs produce a single product tetrahydroalstonine, HYS produces a mixture of three compounds: tetrahydroalstonine, 19-epi-ajmalicine (mayumbine), and ajmalicine (Figure 1.6). Interestingly, these enzymes interact with SGD multimers in the nucleus[36]. Considering the reactivity of strictosidine aglycones, this interaction likely helps prevent the self-toxicity of aglycone intermediates and promotes their efficient conversion into downstream products. Tetrahydroalstonine and ajmalicine can be further oxidized into alstonine and serpentine by alstonine synthase (AS) and serpentine synthase (SS), respectively. These enzymes are cytochrome P450s located on the endoplasmic reticulum, suggesting that their substrates must move from the nucleus to the cytosol near the ER, either by transport or diffusion[36,37].

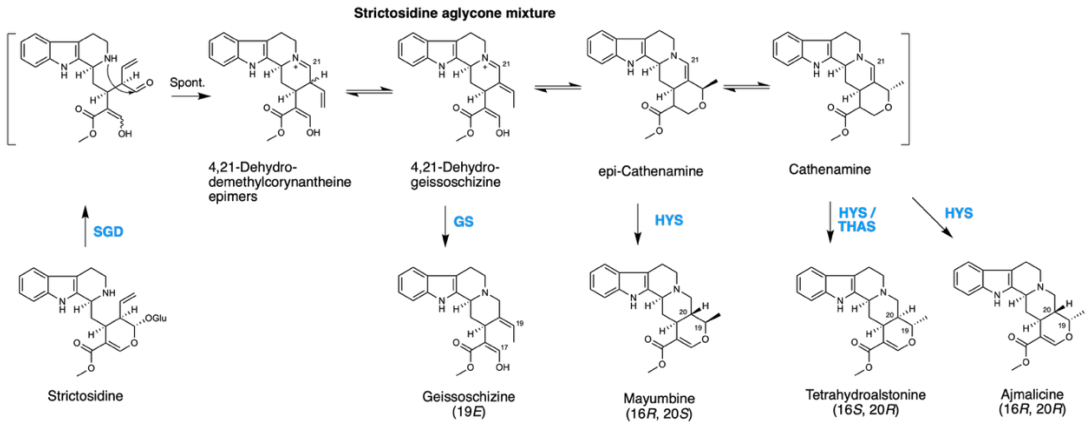



**Figure 1.6:** Strictosidine is deglycosylated by strictosidine beta-D glucosidase (SGD), which spontaneously forms a labile strictosidine aglycone mixture. 4,21-dehydrogeissoschizine is cyclilized by geissoschizine synthase (GS) forming geissoschizine. Heteroyohimbine Synthase (HYS) catalyzes the formation of Mayumbine from epi-Cathenamine, and ajmalicine from cathenamine. The conversion of cathenamine to tetrahydroalstonine can be catalyzed by both HYS and tetrahydroalstonine synthases (THAS1-4). Figure adapted from Stavrinides et al.[37]

### 1.3.3 Biosynthesis of Aspidosperma and Iboga MIAs

One of the strictosidine aglycone intermediates, 4,21-dehydrogeissoschizine, can be reduced by geissoschizine synthase (GS) a nuclear-cytosolic alcohol dehydrogenase, generating geissoschizine, a precursor to vinblastine[38] (Figure 1.6). Geissoschizine is then oxidized by the cytochrome P450 geissoschizine oxidase (GO) , which is anchored to the endoplasmic reticulum (ER) and produces an unstable preakuammicine intermediate (Figure 1.7)[38]. This unstable intermediate is sequentially reduced by a cinnamyl-alcohol dehydrogenase-like enzyme named Redox1, and an aldo-keto-type reductase named Redox2. These consecutive cytosolic reductions create stemmadenine, belonging to the Strychnos-type MIAs. Notably, both the GO product and Redox1 product are highly unstable, which decomposes to akuammicine and 16S/R-dehydroxymethyl-stemmadenine. The lability of these intermediates suggests reaction coordination *in planta*[39].

Stemmadenine is then acetylated by stemmadenine-O-acetyltransferase (SAT), yielding O-acetylstemmadenine[39]. O-acetylstemmadenine is further oxidized into precondylcarpine acetate[40] by the acetylstemmadenine oxidase (ASO) a berberine bridge-like enzyme localized to the vacuole membrane (tonoplast). ASO contains a N-terminal secretive signal peptide, which directs its folding, glycosylation, and eventual targeting to the vacuole [41].

Precondylcarpine acetate is then reduced by the cytosolic homodimer alcohol dehydrogenase dihydroprecondylocarpine synthase (DPAS) into dihydroprecondylocarpine. Interestingly, GS can also catalyze the same reaction despite with low efficiency[41].

DPAS or GS-mediated reduction simultaneously leads to deacetylation, producing another highly labile intermediate dehydrosecodine. From here, two hydrolase-like enzymes, called HL1 (catharanthine synthase) and HL2 (tabersonine synthase), respectively, catalyses two formal [4+2] Diels-Alder cyclizations creating catharanthine and tabersonine. Both HL1 and HL2 have been reported to interact with DPAS[40], which likely helps direct metabolic flux at this critical junction[42].

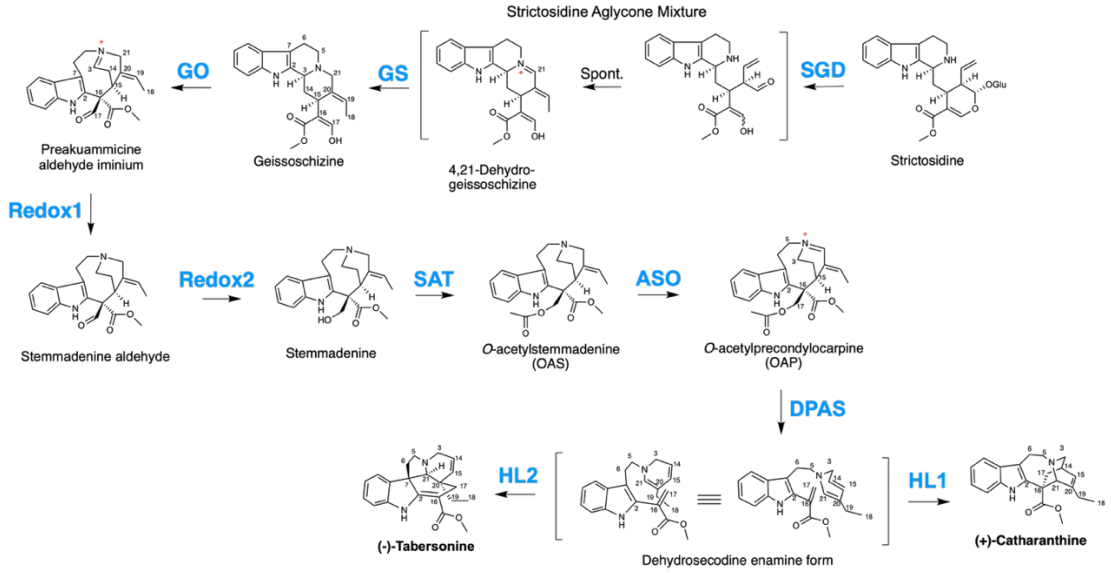



**Figure 1.7:** Biosynthetic pathway to tabersonine and catharanthine in *C. roseus*. Adapted from Gao et al.[31]

### 1.3.4 Conversion of Tabersonine to Vindoline

Catharanthine constitutes a key monomeric unit in vinblastine. The other monomeric unit, vindoline, derives from the further modification of tabersonine via a seven-step biosynthetic route (Figure 1.7). This pathways starts in the leaf epidermal cells and is first catalyzed by tabersonine 16-hydroxylase (T16H) and a 16-hydroxytabersonine,16-O-methyltransferase (16OMT), creating 16-methoxytabersonine[43]. This product is then epoxidized by the cytochrome P450 tabersonine 3-oxygenase (T3O) localized to the ER. Sequentially, it is reduced by the soluble tabersonine 3-reductase (T3R), producing 16-methoxy-2,3-dihydro-3-hydroxytabersonine[44,45]. Notably, in the following step is catalyzed by 16-methoxy-2,3-dihydro-3-hydroxytabersonine *N*-methyltransferase (NMT), targeted to the peroxisomes (via a noncanonical peroxisome targeting signal)[46], and begins the movement of the MIA biosynthetic pathway from the leaf epidermis through the leaf mesophyll[44,47]. This unusual peroxisomal localization influences the transport of the NMT reaction product to the specialized cells (laticifers and idiobasts), although not

yet fully understood. In the laticifer and idioblast cells, desacetoxy-vindoline is hydrolyzed by desacetoxyvindoline 4-hydrolase (D4H) into deactylvindoline, which subsequently reacts with deacetylvindoline 4-O-acetyl-transferase (DAT), to finally create vindoline[44,48]. Travelling from the cytoplasm, vindoline accumulates in the vacuole mediated by an unknown transporter[49].

### 1.3.5 Coupling of Catharanthine and Vindoline

The final steps of vinblastine biosynthesis begin with the coupling of the monomers catharanthine and vindoline (Figure 1.8). Catharanthine and vindoline are initially coupled by an oxidation by a peroxidase (PRX) generating 3',4'-anhydrovinblastine iminium[50,51]. This iminium is then reduced by tetrahydroalstonine synthases (THAS1/2), creating 3',4'-anhydrovinblastine. Finally, the conversion from 3',4'-anhydrovinblastine into vinblastine is catalyzed by enzymes yet to be discovered[40,41]. Consequently, the final assembly of vinblastine stands as the last major uncharacterized step of an otherwise fully elucidated pathway.

Beyond this, the coupling of vindoline and catharanthine is further complicated by cellular and localization of the two compounds. Vindoline accumulates in the vacuole of the laticifers and idioblast cells[49]; meanwhile, catharanthine has been shown to be secreted from epidermal leaf cells to the cuticular waxes by an ATP-binding cassette transporter (CrTPT2) to help the plant defend against pathogens and insects[52]. The low amount of α-3',4'-anhydrovinblastine *in planta* may be partially explained by the physical separation of its two precursors across tissue types, however, recent reports have disputed this catharanthine secretion, instead demonstrating that both may be co-localized in the vacuoles of laticifer and idioblast cells[29,53].

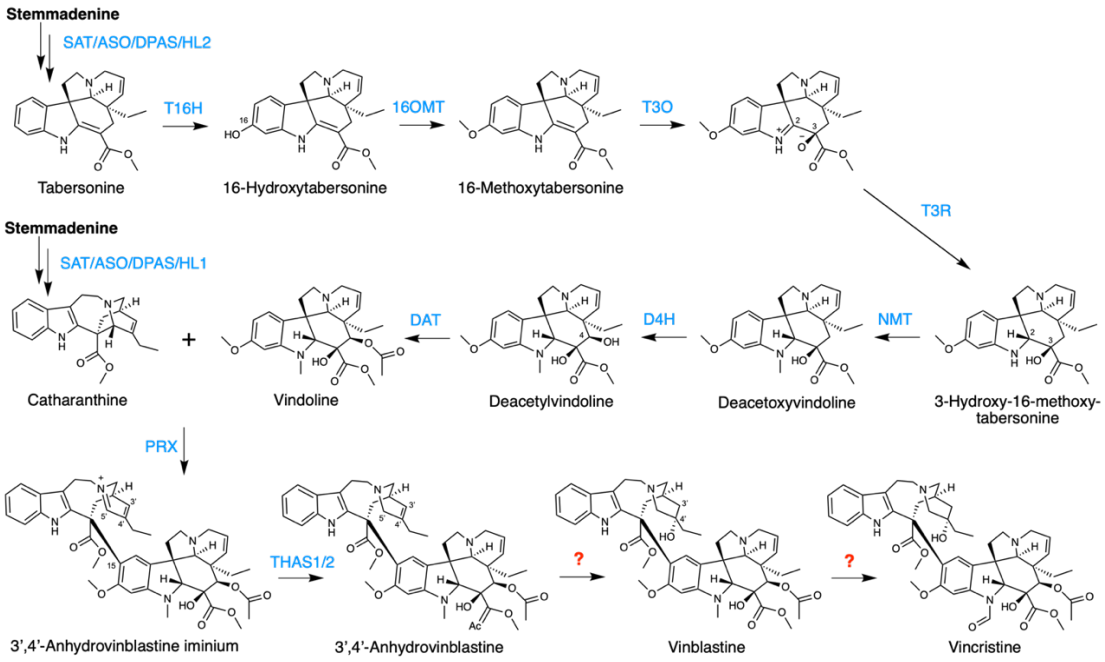



**Figure 1.8:** Coupling of vindoline and catharanthine creates vinblastine and vincristine. Adapted from Zhang et al.[32]

### 1.4 Biosynthetic Gene Clusters (BGCs) in plant metabolism

For decades, the spatial organization of biosynthetic genes in plants were not understood in detail due to their large genome size and limited research tools, contrasting sharply with the comprehensive foundation of polycistronic operons frequently observed in prokaryotes. Recent genomic advances have enabled cost-effective sequencing and assembly of large plant genomes. Accumulating reports have shown that genes involved in plant specialized metabolism may also be found in biosynthetic gene clusters (BGCs)[54]. BGCs are defined as physically co-localized groups of three or more non-homologous genes that participate in a common metabolic pathway [55]. Unlike prokaryotic (bacterial) operons, eukaryotic or plant BGCs consist of individual genes with distinct promoters and terminators, which are transcribed independently rather than as a single mRNA unit[54]. Notable examples across the plant kingdom include the avenacin cluster in

oat (*Avena strigosa*) and the noscapine cluster in opium poppy (*Papaver somniferum*)[55], comprising several to over ten biosynthetic genes.

### 1.4.1 Advantage of Plant Biosynthetic Gene Clusters (BGCs)

It is theorized that plant gene clusters have not evolved by horizontal gene transfer (HGT), unlike their prokaryotic counterparts. Instead, it has been proposed that BGCs in plants evolved via gene duplication, relocalization, neofunctionalization events, and even the independent evolution of genes towards specialized metabolism to cope with harsh environments[56]. In addition, the conservation of BGCs across evolutionary timescales is attributed to several selective advantages. Primarily, clustering genes facilitates coordinated inheritance, ensuring that a full suite of genes required for a specific ecological trait (such as chemical defense) is passed to offspring as a single package, reducing the risk of being disrupted by chromosomal recombination. For example, a plant would benefit from inheriting all the enzymes required to make a compound to defend against herbivory, as opposed to just two enzymes that cannot make this metabolite without the rest[54].

In addition, the physical proximity of these genes is thought to facilitate co-regulation and can be mediated by localized chromatin signatures. Specifically, in *Arabidopsis theliana*, active BGCs are delineated by hallmark chromatin marks (H2A.Z and H3K27me3), and the addition of these marks is associated with changes in BGC expression. Notably, this allows the plant to rapidly switch entire metabolic pathways on or off in response to environmental stimuli[57].

Beyond regulation, BGCs have evolved to limit the accumulation of toxic intermediates. For this reason, acyl transferases and glycosyl transferases are commonly

found in BGCs, as the addition of acyl groups and sugar moieties to pathway intermediates results in reduced cytotoxicity[55,58]. In addition, BGCs may facilitate the formation of a metabolon which is defined as a group of enzymes in a biosynthetic pathway that form a supramolecular complex via protein-protein interactions (PPIs) to efficiently channel metabolites[59]. These metabolons catalyze subsequent reactions quickly, thereby mitigating the accumulation of toxic intermediates in the cell[54].

### 1.4.2 Biosynthetic Gene Clusters (BGCs) in MIA Biosynthesis

The biosynthesis of monoterpene indole alkaloids (MIAs) in *C. roseus* represents one of the most intricate specialized metabolic networks documented to date. The assembly of the scaffolded *C. roseus* genome revealed a physical clustering of numerous MIA biosynthetic genes, which provided critical insight into the complexity of the pathway's genomic regulation. For example, a three-gene cluster has been identified for strictosidine formation, consisting of two biosynthetic genes tryptophan decarboxylase (TDC), strictosidine synthase (STR), and a Multidrug and Toxic Compound Extrusion (MATE) transporter 1 (MATE1)[60,61] that participates in transporting secologanin into vacuole[62]. Downstream in this pathway, two BGCs have also been identified: a geissoschizine synthase BGC and a reserpine BGC. The geissoschizine synthase (GS) BGC consists of GS, THAS2, ASO, an ASO homolog, and several cinnamyl alcohol dehydrogenase-(CAD) type genes including CAD1, CAD2, and 8-hydroxygernaiol oxidoreductase (8HGO) and its homologs. Meanwhile, the reserpine BGC likely derives from a segmental duplication of the GS BGC, which contains a heteroyohimbine/yohimbine/corynanthe C3-oxidase (HYC3O) and a C3-reductase (HYC3R), secologanin synthase 3 (SLS3), THAS1, THAS3, and HYS[63].

In addition to these BGCs, smaller gene clusters have also been discovered. This includes a cluster of DPAS, Redox1, and three uncharacterized CADs[63], and a separate cluster of geraniol 8-hydroxylase (G8H) and iridoid cyclase (ICYC)[64]. These gene clusters suggest selection pressure to preserve these genes, which encourages further investigation into the functions of the uncharacterized enzymes in these clusters[63].

### 1.5 CAD Scaffold Protein organizing Geissoschizine Biosynthesis

In *C. roseus*, after the reactive strictosidine aglycones are created by SGD, MIA biosynthetic flux is primarily directed through the GS-mediated biosynthesis of catharanthine and vindoline, whereas the HYS-mediated MIA route constitutes only a minor side branch[29]. However, HYS physically interacts with SGD in the nucleus, forming a metabolon[36], while the nuclear-cytosolic GS does not interact with SGD and can reside in a distinct subcellular compartment. This reveals a conflict in known metabolon formation and the plant's major metabolic flux; if SGD and GS do not interact, in theory the major metabolic flux should be directed by the SGD-HYS nuclear metabolon[29].

Recently, this conflict has been resolved by the discovery and characterization of the two CAD-like enzymes, CAD1 and CAD2, in the GS BGC. The study addressing this problem, currently unpublished by our group and collaborators, demonstrates that CAD2 forms a heterodimer with GS, which physically mediates the SGD-GS interaction and significantly enhances the GS catalytic efficiency (Figure 1.9). Aside from various *in vivo* and *in vitro* protein-protein interaction studies, our discovery is further supported by virus-induced gene silencing (VIGS) of CAD2 in *C. roseus*, and that when we express CAD2 in a *de novo* catharanthine producing yeast strain we achieve a remarkable 1000-

fold increase in catharanthine titre. Here, I highlight the importance of gene clusters, as our study examines their utility in elucidating biosynthetic pathways, alongside their natural function *in planta* to facilitate the formation of metabolons to drive metabolic flux. Critically, our research suggests the existence of other enzyme complexes in MIA biosynthetic pathways yet to be discovered.

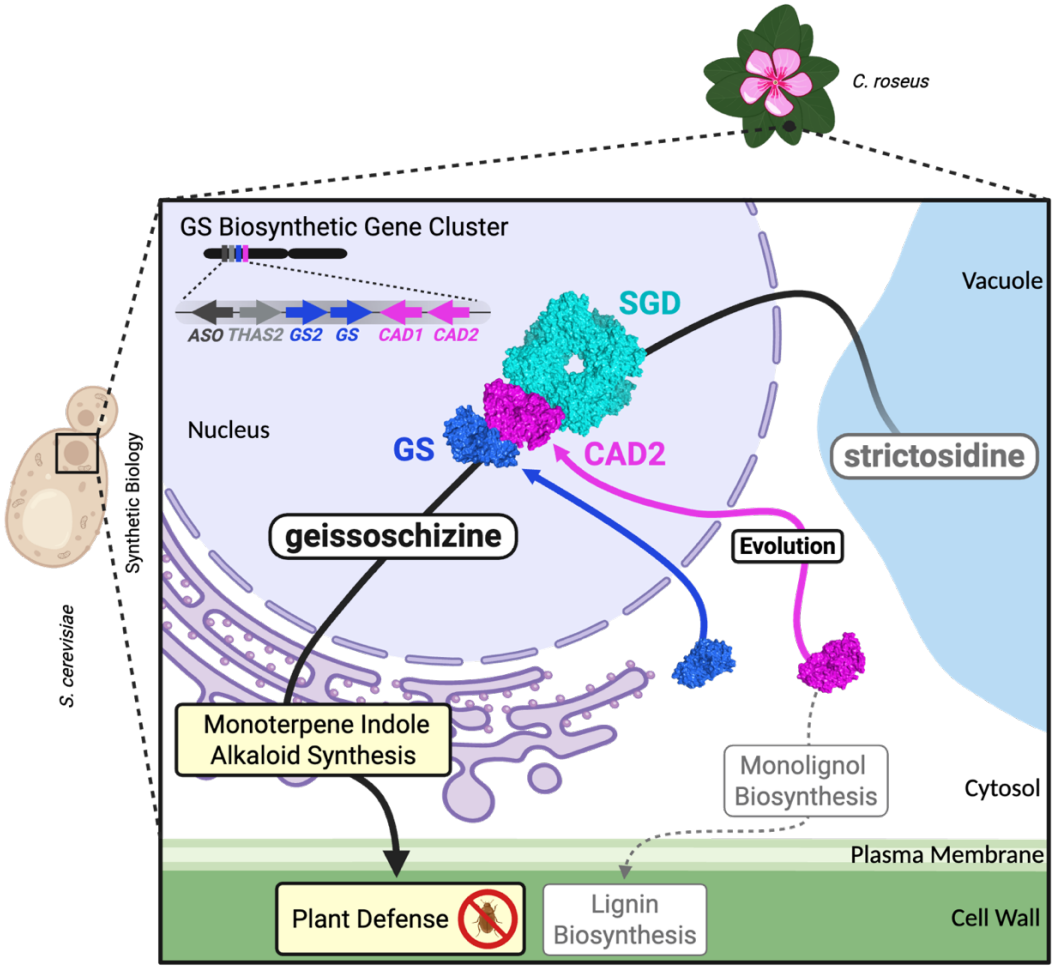



**Figure 1.9: MIA biosynthesis pathway and VinBLAST for scaffolding SGD and GS.** In *C. roseus* and bioengineered yeast cells, CAD2 serves as a scaffold evolved from a CAD-like enzyme that guides GS into the nucleus through protein-protein interactions and interacts with SGD, addressing the spatial barrier between GS and SGD. This eliminates the inefficient transport dilemma of the unstable intermediate strictosidine aglycone caused by the different subcellular localizations of GS and SGD, enabling direct production of geissoschizine from strictosidine in the nucleus. The turquoise protein represents SGD, the magenta protein represents CAD2, and the blue protein represents GS.

### 1.5.1 Compartmentalization for Rational Bioengineering in Heterologous Systems

Advancements over the past four decades of MIA research has allowed the identification of numerous enzymes, alongside unforeseen insight into the subcellular and cellular organization of *C. roseus* MIA pathways and into the incredible complexity of specialized plant metabolism (Figure 1.10). Beyond this, further elucidation of the spatial organization of these pathways are essential for providing new perspectives supporting the rational bioengineering of MIA biosynthesis in heterologous systems[29]. It has been reported that an adapted subcellular localization of biosynthetic enzymes in heterologous hosts, such as targeting a non-native organelle, can increase biosynthetic yields for other natural products[65]. However, efforts to reconstruct these pathways in microbial or alternative plant hosts often face challenges due to the absence of native compartmentalization, improper enzyme localization, and inefficient transport of intermediates. For example, mislocalization of enzymes can lead to reduced pathway flux, accumulation of unstable intermediates, or formation of off-pathway products[66–68].

Consequently, successful metabolic engineering strategies cannot stop at the presence of biosynthetic genes, but must also include targeting specific organelles, reconstruction of metabolon-like assemblies, and, where necessary, engineering of transport processes. In this context, elucidating the mechanisms governing intracellular and intercellular trafficking and compartmentalization in *C. roseus* provides a framework for pathway optimization[69,70].

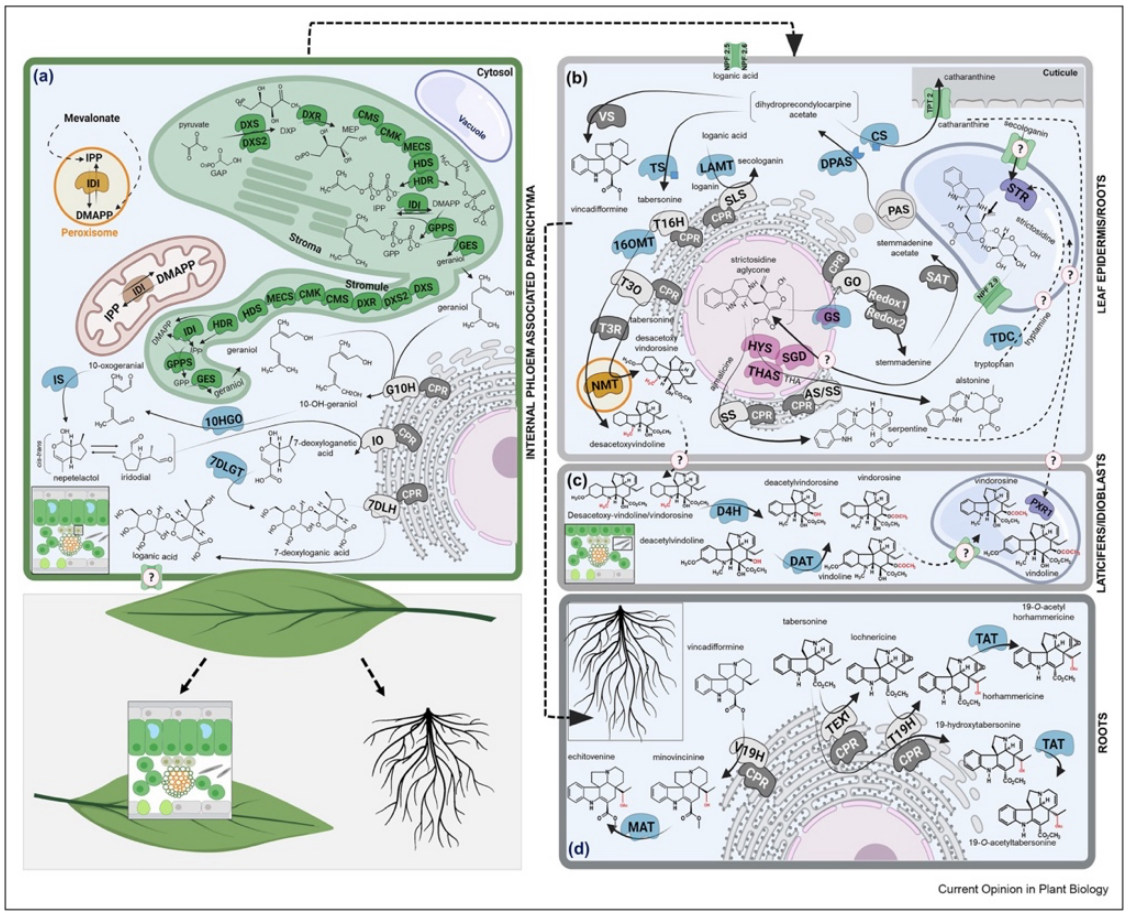



**Figure 1.10:** Subcellular and cellular synthesis of catharanthine and vindoline. Figure reproduced from Kulagina *et al*.[28]

### 1.6 Techniques to study Protein-Protein Interactions

With our recent discovery that CAD2 acts as a scaffold protein to address SGD-GS compartmentalisation mismatch and strictosidine aglycone intermediate instability, we postulate that additional protein-protein interactions (PPIs) exist in MIA biosynthesis due to the existence of many highly unstable intermediates elsewhere in MIA biosynthetic pathways. Characterizing and understanding these protein-protein interactions, with the goal of identifying new scaffold proteins, will significantly contribute to the engineering of efficient heterologous expression systems for MIA biosynthesis. In this section, I

summarize different *in vivo* and *in vitro* techniques that have been used to investigate PPIs, and their respective advantages and disadvantages.

### 1.6.1 In vivo protein-protein interaction methods

#### 1.6.1.1 Förster Resonance Energy Transfer (FRET)

Förster Resonance Energy Transfer (FRET) is a fluorescence-based technique widely used to investigate protein–protein interactions in living plant cells with high spatial and temporal resolution. It relies on the non-radiative transfer of energy from an excited donor fluorophore to an acceptor fluorophore when the two are within ~1–10 nm, a distance consistent with direct molecular interactions[71]. In plant systems, proteins of interest are typically fused to compatible fluorophore pairs (ex: CFP and YFP), and interaction is detected as changes in fluorescence intensity or donor lifetime, commonly measured using fluorescence lifetime imaging microscopy (FRET-FLIM). This approach enables the visualization and quantification of protein interactions *in vivo* with both spatial and temporal resolution, overcoming limitations of purely biochemical assays removed from the cellular environment[72]. Importantly, FRET is reversible and highly sensitive, making it particularly suitable for studying dynamic or transient interactions in plant cells. However, accurate interpretation requires careful control of fluorophore expression levels, spectral overlap, and subcellular localization of fusion proteins[73].

#### 1.6.1.2 Split-Luciferase Complementation (Split LUC)

Luciferase is an enzyme that catalyzes a bioluminescent reaction, emitting visible light through the oxidation of luciferin, a small-molecule substrate. Split-luciferase complementation (Split-LUC) is a sensitive, *in vivo* technique for detecting protein-protein interactions in plant systems. In this approach, luciferase is divided into N- and C-

terminal fragments, which are fused to proteins of interest. Interaction between the two proteins of interest in vivo will reconstitute the luciferase enzymatic activity, and upon addition of luciferin, will produce luminescence[74,75]. Because this reaction does not require external illumination (unlike other fluorescent techniques), split-LUC has extremely low background signal, making them highly sensitive reporters[75].

The luciferin emission can be quantitatively measured, enabling real-time monitoring of protein interactions in living cells. Split-LUC has been widely applied in plant biology due to its low background, high sensitivity, and compatibility with transient expression systems such as *Nicotiana benthamiana* and *Arabidopsis* protoplasts[74,75]. Importantly, the assay allows detection of both stable and dynamic interactions, as stable interactions will have steady signal, whereas dynamic interactions can be monitored post-addition of a stimulus, where the signal would change over time. However, as with other complementation assays, fusion orientation and protein expression levels must be carefully controlled to avoid artifacts[75].

#### 1.6.1.3 Proximity Labelling (TurboID)

Proximity labelling (PL) is an *in vivo* technique where a protein of interest is fused to an engineered enzyme, most commonly a promiscuous biotin ligase, such as TurboID, which covalently labels nearby proteins with biotin in a distance-dependent manner. These labelled proteins can subsequently be purified using streptavidin affinity capture and identified by mass spectrometry, allowing reconstruction of the local interactome[76]. An advantage of PL compared to traditional interaction assays is that it does not require stable or direct binding, making it particularly effective for capturing weak or transient interactions and proteins within dynamic complexes. However, it is important to note that

because it does not require direct physical interactions, it instead detects spatial proximity. Consequently, appropriate controls are required to distinguish true interactions from proteins that are simply co-localized[77]. *In planta*, PL has become increasingly important for studying compartmentalized processes, as it enables interaction mapping within the native cellular context, including specific organelles or membrane-associated environments[78].

#### 1.6.1.4 Yeast Two-Hybrid (Y2H)

The yeast two-hybrid (Y2H) system is a classic *in vivo* method for detecting binary protein–protein interactions. It is based on the reconstitution of a functional transcription factor from two separate domains: a DNA-binding domain fused to a "bait" protein and an activation domain fused to a "prey" protein. Interaction between bait and prey proteins brings the two domains together, initiating transcription of a reporter gene, which is then detected via growth selection, or colorimetric/fluorescent assays[79,80]. Y2H is particularly useful for high-throughput screening of protein interaction networks and for mapping interaction domains, making it valuable in plant molecular biology for exploring complex signaling pathways. However, because the assay occurs in yeast, interactions that depend on plant-specific post-translational modifications or subcellular localization may be missed, and false positives can occur due to overexpression or non-physiological interactions[80,81]. Despite these limitations, Y2H remains a foundational tool for establishing candidate protein interactions prior to *in planta* validation with methods such as co-immunoprecipitation or split-luciferase complementation[80].

### 1.6.2 In vitro protein-protein interaction methods

#### 1.6.2.1 Pull-Down Assays

Pull-down assays are techniques used to study protein-protein interactions by exploiting the affinity of a "bait" protein to capture its binding partners ("prey") from a cell lysate or purified protein mixture. Typically, the bait protein is immobilized on solid beads with a fusion tag (ex. His-tag) and incubated with the prey protein. Here, the fusion tag will bind to the prey protein itself, and interacting proteins will be bound to the prey protein. Therefore, these interacting proteins are co-precipitated, then washed to remove non-specific interactions, and analyzed via SDS-PAGE and Western blotting or mass spectrometry. Pull-down assays are particularly useful for validating direct physical interactions and for probing binding domains through truncated or mutant proteins. However, because these assays are performed under non-physiological conditions, interactions observed *in vitro* may not always reflect those *in vivo*, and weak or transient interactions can be missed. Despite these limitations, pull-down assays remain a foundational tool for initial mechanistic characterization of protein interactions before proceeding to *in vivo* validation methods[82].

#### 1.6.2.2 Co-Immunoprecipitation (Co-IP)

Co-immunoprecipitation (Co-IP) is a widely used technique for detecting protein-protein interactions within plant cells. Co-IP involves several steps, starting with the preparation of a cell-lysate, then isolating the protein of interest from the cell lysate using a specific antibody. Any proteins bound to this protein of interest, either directly or as part of a larger complex, are co-precipitated, while unbound proteins are washed away. Subsequently, the proteins of interest can be identified, typically by Western blotting or

mass spectrometry. Notably, Co-IP can detect both stable and dynamic interactions, such as those regulated by environmental stimuli or signaling events. However, a key limitation is that Co-IP cannot inherently distinguish between direct and indirect interactions, as co-precipitated proteins may be part of multiprotein complexes (i.e. metabolons), and weak or transient interactions may be lost during extraction and washing steps[9]. Because Co-IP is performed using proteins extracted from living tissue, it preserves many native interactions and is considered a robust method for validating physiologically relevant protein complexes *in planta*[83].

#### 1.6.2.3 Isothermal Titration Calorimetry (ITC)

Isothermal Titration Calorimetry (ITC) is a powerful biophysical technique used to determine the thermodynamic parameters of protein-protein interactions (PPIs) in a single experiment. Unlike many affinity-based assays, ITC measures heat changes, either exothermic or endothermic, associated with the binding of a ligand protein into a solution containing a macromolecule partner[84]. The instrument consists of two identical cells: a reference cell containing buffer and a sample cell containing the protein of interest. As the titration progresses via controlled injections, the calorimeter measures the electrical power required to maintain a zero-temperature difference between the two cells. The resulting thermogram provides a raw data set of heat pulses that, upon integration and normalization against the molar concentration of the titrant, yields a binding isotherm[85].

The primary advantage of ITC in the study of PPIs is its ability to provide a complete thermodynamic profile without the need for fluorescent labeling or immobilization, which can often perturb the native states of the proteins. From a single titration curve, one can directly calculate the association constant ($K_a$), the stoichiometry

($n$), and the change in enthalpy ($\Delta H$). Then, using the fundamental thermodynamic relationship:

$$\Delta G = -RTlnK_a = \Delta H - T\Delta S \quad (1)$$

The change in Gibbs energy ($\Delta G$) and the change in entropy ($\Delta S$) can be derived, offering profound insights into the molecular forces driving the interaction, such as hydrophobic effects or hydrogen bonding. While ITC is highly sensitive and provides the gold standard for affinity measurement, its application is occasionally limited by the requirement for very high sample concentrations and the necessity for precise buffer matching to avoid large heats of dilution[84].

#### 1.6.2.4 Cryo-Electron Microscopy

Cryo-electron microscopy (Cryo-EM) has emerged as a transformative tool for the structural characterization of protein-protein interactions (PPIs), enabling the visualization of macromolecular complexes at near-atomic resolution without the requirement for protein crystallization. By vitrifying samples in liquid ethane, the technique preserves the proteins in a native-like, hydrated environment, thereby maintaining the integrity of delicate binding interfaces that might otherwise be disrupted by traditional crystal packing forces[86]. A significant advantage of Cryo-EM in studying PPIs is its capacity to resolve structural heterogeneity; through advanced computational 3D classification, researchers can disentangle multiple conformational states or varying stoichiometries from a single dataset[87]. This ability to capture "snapshots" of dynamic or transient complexes provides critical insights into the molecular forces stabilizing the interaction, making the technique indispensable for mapping the architectures of both

large-scale assemblies and smaller, flexible heteromeric complexes[88]. However, a primary limitation of Cryo-EM is the high infrastructure cost[89].

### 1.7 Bimolecular Fluorescence Complementation (BiFC)

To investigate the spatial dynamics of protein-protein interactions (PPIs) within a cellular environment, Bimolecular Fluorescent Complementation (BiFC) has emerged as a valuable imaging technique. BiFC analysis allows for the direct visualization of protein complexes in living cells, allowing for high sensitivity and spatial resolution without requiring exogenous chemical reagents or cell lysis.

#### 1.7.1 Mechanism of Fluorophore Reconstitution

The chemical basis of BiFC relies on the fragmentation of a fluorescent protein (FP), such as Green Fluorescent Protein (GFP) or its variants (e.g., YFP, Venus). The FP is bisected into two non-fluorescent fragments, typically designated as the N-terminal and C-terminal fragments. These fragments are individually fused to two proteins of interest, forming two distinct “fusion proteins”.

If the two proteins of interest interact, their association will also bring the non-fluorescent fragments into close proximity, facilitating their folding and the subsequent reconstitution of the functional fluorophore (Figure 1.11). The maturation of the reconstituted fluorophore then produces a visible emission that can be detected using fluorescence microscopy[90].

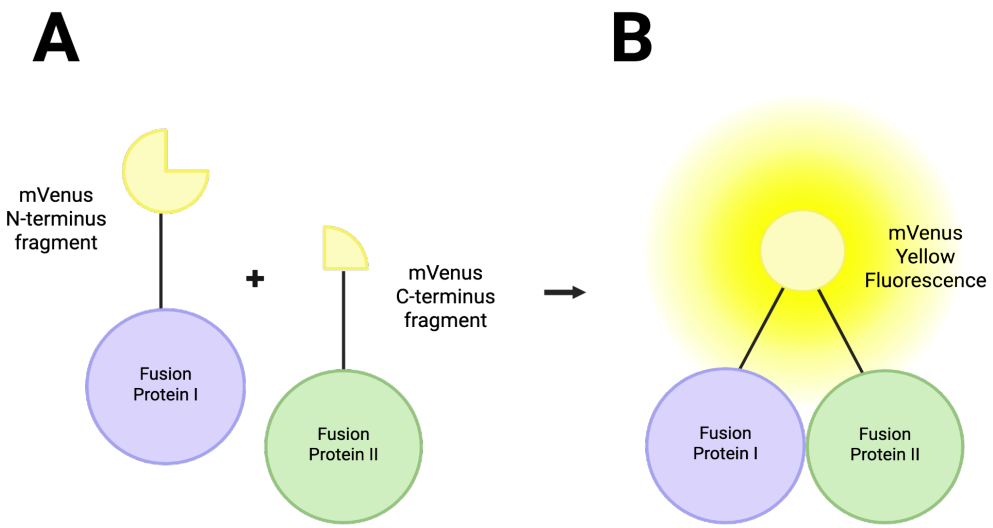



**Figure 1.11: Schematic representation of the Bimolecular Fluorescence Complementation (BiFC) Mechanism.** (A) The target proteins of interest (Protein I and Protein II) are expressed as fusion constructs with non-fluorescent N-terminal (YN) and C-terminal (YC) fragments of a bisected fluorescent protein (e.g. mVenus). (B) Upon the physical interaction of Protein I and II, the tethered non-fluorescent fragments are brought into close proximity. This proximity facilitates the structural reconstruction and folding of the fragments into a functional fluorophor. Following the chemical maturation of the chromophore, the reconstituted protein emits fluorescence upon excitation, indicating the spatial localization of the protein-protein interaction (PPI) within the living cell. Figure adapted from Kerppola et al.[90]

### 1.7.2 Steric Considerations of BiFC Fusion Proteins

When building BiFC tags onto our proteins of interest, it is essential to consider its steric effects on the putative interaction. For association of the fluorescent fragment proteins, the fusion protein complex must have sufficient freedom of motion to allow the fragments to collide with each other with enough frequency to create bimolecular fluorescent complex formation. Therefore, combinations of fusion proteins with varying BiFC tag orientation must be tested empirically to achieve an arrangement that produces maximal signal. It is suggested to test both fusions to the carboxyl-terminal (C-terminal) and amino-terminal (N-terminal) of the proteins of interest, unless there are functional

disruptions expected with tagging at a specific terminus[90]. The possible orientations of mVenus BiFC tags are depicted in Figure 1.12.

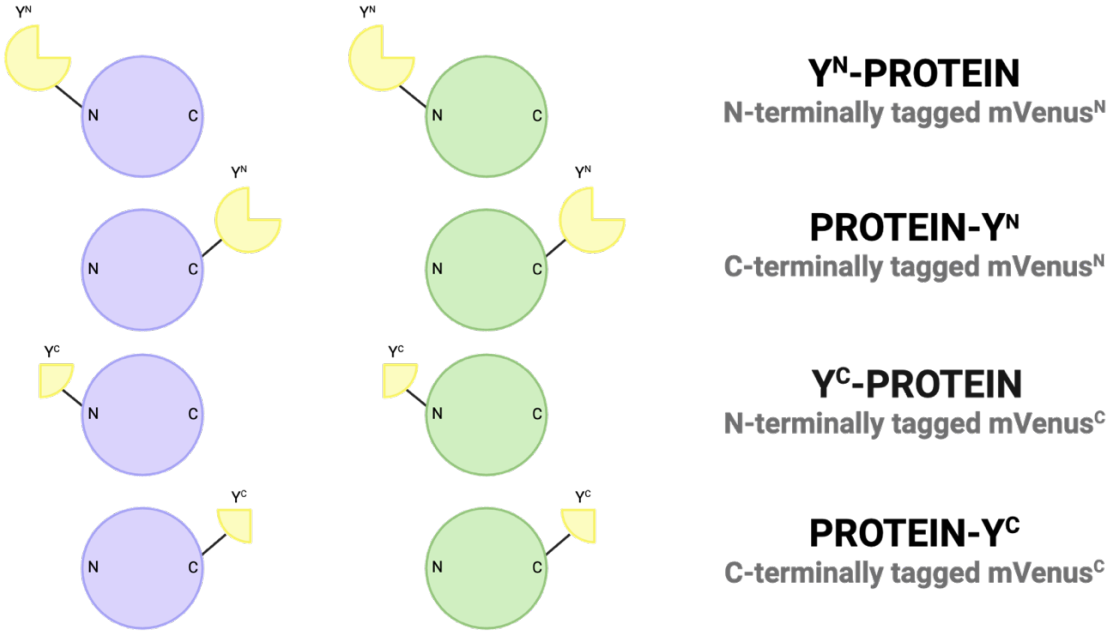



**Figure 1.12: All possible BiFC tag locations for fusion protein I (purple) and fusion protein II (green).** Labels "YN-protein" denotes that mVenusN is tagged on the N-terminal of a protein; "protein-YN" denotes mVenusN is tagged on the C-terminal of a protein; "YC-protein" denotes mVenusC is tagged on the N-terminal of a protein; and "protein-YC" denotes mVenusC is tagged on the C-terminal of a protein.

### 1.7.3 Advantages and Limitations of BiFC

The widespread adoption of BiFC in chemical biology and proteomics is driven by several distinct advantages over *in vitro* methods. Most notably, BiFC enables the detection of interactions at near-physiological expression levels in a hydrated, living environment, preserving the influence of cellular pH, ionic strength, and endogenous chaperones. Because the fluorescent signal is generated only upon complex formation, the technique offers an exceptional signal-to-noise ratio, making it sensitive enough to detect low-abundance interactions[90]. Furthermore, the development of multicolor BiFC allows for the simultaneous visualization of multiple distinct complexes within the same

cell by using fragments from different FPs (e.g., combining YFP and CFP fragments), which is invaluable for studying competitive binding or multi-protein assembly[91].

However, BiFC is not without significant biochemical constraints. The most critical limitation is the irreversibility of the reconstituted fluorophore. Once the FP fragments associate and the chromophore matures, the complex is essentially locked under most physiological conditions. While this molecular memory is advantageous for capturing transient or weak interactions that might be missed by other assays, it precludes the study of real-time dissociation and can lead to an overestimation of the complex's stability[92]. Additionally, the maturation time of the reconstituted fluorophore, introduces a temporal delay that makes it difficult to study rapid signaling events. Finally, the risk of false positives is inherently high due to the possibility of spontaneous self-assembly of the split fragments, necessitating rigorous controls, such as the use of non-interacting mutant variants of the target proteins to establish a baseline for non-specific complementation[90]. False positives can also be influenced by the local concentration of the BiFC fusion proteins in the cell, as adequately high concentrations may cause the fluorescent fragments to associate with each other independently[93]. Therefore, it is generally recommended to express proteins at the lowest level possible that will allow detection of fluorescence, which is ideally the same level as their endogenous equivalents. However, the ability of the fragments to independently associate has been shown to be reduced when they are tagged to proteins which do not interact with each other. Regardless, it is greatly advantageous to test interaction mutants to assess its effect on fluorescence complementation[90].

### 1.7.4 Application in Plant Biology

In plant science, BiFC is particularly useful for showing the subcellular localization of PPIs within the plant cell. A landmark application of BiFC was the characterization of the core abscisic acid (ABA) signaling pathway in *Arabidopsis thaliana*. Researchers used BiFC to demonstrate the physical interaction between the ABA receptor PYR1 and the type 2C protein phosphatase ABI1. By expressing these proteins as BiFC fusions in leaves, it was observed that the PYR1-ABI1 complex formed exclusively in the presence of ABA, localizing predominantly in the nucleus and cytosol. This study provided visual proof of how plants perceive and translate environmental stress signals into biochemical responses[94].

### 1.8 Research Hypothesis and Objectives

In this chapter, I gave an overview of the MIA biosynthetic pathway to the anti-cancer drug vinblastine in *C. roseus*, which has almost reached complete elucidation due to the past four decades of targeted research[29]. With the extensive knowledge of this pathway, there have been successful attempts of producing *de novo* catharanthine and vindoline in *S. cerevisiae*. Despite the huge accomplishment of replicating this complex metabolic pathway in a heterologous system, yields are far too low for commercial pharmaceutical demand[31,32]. The recent discovery of CAD2 scaffold, which has led to nearly 1,000- fold increase in catharanthine titre in yeast has contributed significantly to this goal.

I hypothesize that protein-protein interactions may play a significant role in organizing the core vinblastine biosynthetic pathway (geissoschizine to catharanthine and tabersonine) and that the BiFC technique can be leveraged to decipher the unknown PPIs in this section of the pathway. My objective is to use BiFC to study the binary PPIs among the 11 proteins in this core pathway using agrobacterium-mediated protein

expression in *Nicotiana benthamiana* (tobacco) leaves. Through BiFC assays in *N. benthamiana*, this study aims to elucidate protein-protein interactions, the subcellular localization of these interactions, and to ultimately determine if the pathway has unknown metabolons.

# Bibliography 1


(1) Borchardt, J. K. The Beginnings of Drug Therapy: Ancient Mesopotamian Medicine. *Drug News Perspect.* **2002**, *15* (3), 187–192. https://doi.org/10.1358/dnp.2002.15.3.840015.

(2) Brownstein, M. J. A Brief History of Opiates, Opioid Peptides, and Opioid Receptors. *Proc. Natl. Acad. Sci. U. S. A.* **1993**, *90* (12), 5391–5393. https://doi.org/10.1073/pnas.90.12.5391.

(3) Moosavyzadeh, A.; Ghaffari, F.; Mosavat, S. H.; Zargaran, A.; Mokri, A.; Faghihzadeh, S.; Naseri, M. The Medieval Persian Manuscript of *Afyunieh*: The First Individual Treatise on the Opium and Addiction in History. *J. Integr. Med.* **2018**, *16* (2), 77–83. https://doi.org/10.1016/j.joim.2018.02.004.

(4) Desborough, M. J. R.; Keeling, D. M. The Aspirin Story - from Willow to Wonder Drug. *Br. J. Haematol.* **2017**, *177* (5), 674–683. https://doi.org/10.1111/bjh.14520.

(5) Mahdi, J. G.; Mahdi, A. J.; Mahdi, A. J.; Bowen, I. D. The Historical Analysis of Aspirin Discovery, Its Relation to the Willow Tree and Antiproliferative and Anticancer Potential. *Cell Prolif.* **2006**, *39* (2), 147–155. https://doi.org/10.1111/j.1365-2184.2006.00377.x.

(6) Sneader, W. The Discovery of Aspirin: A Reappraisal. *BMJ* **2000**, *321* (7276), 1591–1594. https://doi.org/10.1136/bmj.321.7276.1591.

(7) Atanasov, A. G.; Waltenberger, B.; Pferschy-Wenzig, E.-M.; Linder, T.; Wawrosch, C.; Uhrin, P.; Temml, V.; Wang, L.; Schwaiger, S.; Heiss, E. H.; Rollinger, J. M.; Schuster, D.; Breuss, J. M.; Bochkov, V.; Mihovilovic, M. D.; Kopp, B.; Bauer, R.; Dirsch, V. M.; Stuppner, H. Discovery and Resupply of Pharmacologically Active Plant-Derived Natural Products: A Review. *Biotechnol. Adv.* **2015**, *33* (8), 1582–1614. https://doi.org/10.1016/j.biotechadv.2015.08.001.

(8) Facchini, P. J. ALKALOID BIOSYNTHESIS IN PLANTS: Biochemistry, Cell Biology, Molecular Regulation, and Metabolic Engineering Applications. *Annu. Rev. Plant Biol.* **2001**, *52*, 29–66. https://doi.org/10.1146/annurev.arplant.52.1.29.

(9) Katerova, Z.; Todorova, D.; Tasheva, K.; Sergiev, I. INFLUENCE OF ULTRAVIOLET RADIATION ON PLANT SECONDARY METABOLITE PRODUCTION; 2013.

(10) Waldhoer, M.; Bartlett, S. E.; Whistler, J. L. Opioid Receptors. *Annu. Rev. Biochem.* **2004**, *73* (1), 953–990. https://doi.org/10.1146/annurev.biochem.73.011303.073940.

(11) Pathan, H.; Williams, J. Basic Opioid Pharmacology: An Update. *Br. J. Pain* **2012**, *6* (1), 11–16. https://doi.org/10.1177/2049463712438493.

(12) Jalali, M. S.; Botticelli, M.; Hwang, R. C.; Koh, H. K.; McHugh, R. K. The Opioid Crisis: A Contextual, Social-Ecological Framework. *Health Res. Policy Syst.* **2020**, *18*, 87. https://doi.org/10.1186/s12961-020-00596-8.

(13) Baldo, B. A.; Rose, M. A. The Anaesthetist, Opioid Analgesic Drugs, and Serotonin Toxicity: A Mechanistic and Clinical Review. *Br. J. Anaesth.* **2020**, *124* (1), 44–62. https://doi.org/10.1016/j.bja.2019.08.010.

(14) Maeda, H. A. Evolutionary Diversification of Primary Metabolism and Its Contribution to Plant Chemical Diversity. *Front. Plant Sci.* **2019**, *10*, 881. https://doi.org/10.3389/fpls.2019.00881.

(15) Carrington, Y.; Guo, J.; Le, C. H.; Fillo, A.; Kwon, J.; Tran, L. T.; Ehlting, J. Evolution of a Secondary Metabolic Pathway from Primary Metabolism: Shikimate and Quinate Biosynthesis in Plants. *Plant J.* **2018**, *95* (5), 823–833. https://doi.org/10.1111/tpj.13990.
(16) Erb, M.; Kliebenstein, D. J. Plant Secondary Metabolites as Defenses, Regulators, and Primary Metabolites: The Blurred Functional Trichotomy. *Plant Physiol.* **2020**, *184* (1), 39–52. https://doi.org/10.1104/pp.20.00433.
(17) Sana; Aftab, T.; Naeem, M.; Jha, P. K.; Prasad, P. V. V. Production of Secondary Metabolites under Challenging Environments: Understanding Functions and Mechanisms of Signalling Molecules. *Front. Plant Sci.* **2025**, *16*. https://doi.org/10.3389/fpls.2025.1569014.
(18) Austen, N.; Walker, H. J.; Lake, J. A.; Phoenix, G. K.; Cameron, D. D. The Regulation of Plant Secondary Metabolism in Response to Abiotic Stress: Interactions Between Heat Shock and Elevated CO2. *Front. Plant Sci.* **2019**, *10*. https://doi.org/10.3389/fpls.2019.01463.
(19) Noble, R. L. The Discovery of the Vinca Alkaloids—Chemotherapeutic Agents against Cancer. *Biochem. Cell Biol.* **1990**, *68* (12), 1344–1351. https://doi.org/10.1139/o90-197.
(20) Warren, R. D.; Bender, R. A.; Norton, L.; Young, R. C. The Treatment of Combination Chemotherapy-Resistant Hodgkin Disease with Single-Agent Vinblastine. *Am. J. Hematol.* **1978**, *4* (1), 47–55. https://doi.org/10.1002/ajh.2830040107.
(21) Zhang, Y.-W.; Kong, X.-Y.; Wang, J.-H.; Du, G.-H. Vinblastine and Vincristine. In *Natural Small Molecule Drugs from Plants*; Du, G.-H., Ed.; Springer: Singapore, 2018; pp 551–557. https://doi.org/10.1007/978-981-10-8022-7_91.
(22) Neoadjuvant Cisplatin,Methotrexate,and Vinblastine Chemotherapy for Muscle-Invasive Bladder Cancer: A Randomised Controlled Trial. *The Lancet* **1999**, *354* (9178), 533–540. https://doi.org/10.1016/S0140-6736(99)02292-8.
(23) Samuels, M. L.; Howe, C. D. Vinblastine in the Management of Testicular Cancer. *Cancer* **1970**, *25* (5), 1009–1017. https://doi.org/10.1002/1097-0142(197005)25:5%3C1009::AID-CNCR2820250504%3E3.0.CO;2-B.
(24) Grunberg, S. M.; Crowley, J. J.; Livingston, R. B.; Muggia, F. M.; MacDonald, J. S.; Williamson, S. K.; Stephens, R. L. Treatment of Non-Small-Cell Lung Cancer with Vinblastine and Very High-Dose Cisplatin. A Southwest Oncology Group Study. *Cancer Chemother. Pharmacol.* **1991**, *28* (3), 211–213. https://doi.org/10.1007/BF00685511.
(25) Yang, Z.-H.; Wang, S.-B.; Du, G.-H. Ajmaline. In *Natural Small Molecule Drugs from Plants*; Du, G.-H., Ed.; Springer: Singapore, 2018; pp 5–11. https://doi.org/10.1007/978-981-10-8022-7_1.
(26) Weir, M. R. Reserpine: A New Consideration of an Old Drug for Refractory Hypertension. *Am. J. Hypertens.* **2020**, *33* (8), 708–710. https://doi.org/10.1093/ajh/hpaa069.
(27) Ren, Y.; DeRose, K.; Li, L.; Gallucci, J. C.; Yu, J.; Douglas Kinghorn, A. Vincamine, from an Antioxidant and a Cerebral Vasodilator to Its Anticancer Potential. *Bioorg. Med. Chem.* **2023**, *92*, 117439. https://doi.org/10.1016/j.bmc.2023.117439.

(28) Linck, V. M.; Herrmann, A. P.; Piato, Â. L.; Detanico, B. C.; Figueiró, M.; Flório, J.; Iwu, M. M.; Okunji, C. O.; Leal, M. B.; Elisabetsky, E. Alstonine as an Antipsychotic: Effects on Brain Amines and Metabolic Changes. *Evid.-Based Complement. Altern. Med. ECAM* **2011**, *2011*, 418597. https://doi.org/10.1093/ecam/nep002.
(29) Kulagina, N.; Méteignier, L.-V.; Papon, N.; O'Connor, S. E.; Courdavault, V. More than a Catharanthus Plant: A Multicellular and Pluri-Organelle Alkaloid-Producing Factory. *Curr. Opin. Plant Biol.* **2022**, *67*, 102200. https://doi.org/10.1016/j.pbi.2022.102200.
(30) Tang, M.; Li, B.; Zhou, X.; Bolt, T.; Li, J. J.; Cruz, N.; Gaudinier, A.; Ngo, R.; Clark-Wiest, C.; Kliebenstein, D. J.; Brady, S. M. A Genome-scale TF–DNA Interaction Network of Transcriptional Regulation of Arabidopsis Primary and Specialized Metabolism. *Mol. Syst. Biol.* **2021**, *17* (11), MSB202110625. https://doi.org/10.15252/msb.202110625.
(31) Gao, D.; Liu, T.; Gao, J.; Xu, J.; Gou, Y.; Pan, Y.; Li, D.; Ye, C.; Pan, R.; Huang, L.; Xu, Z.; Lian, J. De Novo Biosynthesis of Vindoline and Catharanthine in *Saccharomyces Cerevisiae*. *BioDesign Res.* **2022**, *2022*, 0002. https://doi.org/10.34133/bdr.0002.
(32) Zhang, J.; Hansen, L. G.; Gudich, O.; Viehrig, K.; Lassen, L. M. M.; Schrübbers, L.; Adhikari, K. B.; Rubaszka, P.; Carrasquer-Alvarez, E.; Chen, L.; D'Ambrosio, V.; Lehka, B.; Haidar, A. K.; Nallapareddy, S.; Giannakou, K.; Laloux, M.; Arsovska, D.; Jørgensen, M. A. K.; Chan, L. J. G.; Kristensen, M.; Christensen, H. B.; Sudarsan, S.; Stander, E. A.; Baidoo, E.; Petzold, C. J.; Wulff, T.; O'Connor, S. E.; Courdavault, V.; Jensen, M. K.; Keasling, J. D. A Microbial Supply Chain for Production of the Anti-Cancer Drug Vinblastine. *Nature* **2022**, *609* (7926), 341–347. https://doi.org/10.1038/s41586-022-05157-3.
(33) Payne, R. M. E.; Xu, D.; Foureau, E.; Teto Carqueijeiro, M. I. S.; Oudin, A.; Bernonville, T. D. de; Novak, V.; Burow, M.; Olsen, C.-E.; Jones, D. M.; Tatsis, E. C.; Pendle, A.; Ann Halkier, B.; Geu-Flores, F.; Courdavault, V.; Nour-Eldin, H. H.; O'Connor, S. E. An NPF Transporter Exports a Central Monoterpene Indole Alkaloid Intermediate from the Vacuole. *Nat. Plants* **2017**, *3* (2), 16208. https://doi.org/10.1038/nplants.2016.208.
(34) Guirimand, G.; Courdavault, V.; Lanoue, A.; Mahroug, S.; Guihur, A.; Blanc, N.; Giglioli-Guivarc'h, N.; St-Pierre, B.; Burlat, V. Strictosidine Activation in Apocynaceae: Towards a "Nuclear Time Bomb"? *BMC Plant Biol.* **2010**, *10*, 182. https://doi.org/10.1186/1471-2229-10-182.
(35) Carqueijeiro, I.; Koudounas, K.; Dugé de Bernonville, T.; Sepúlveda, L. J.; Mosquera, A.; Bomzan, D. P.; Oudin, A.; Lanoue, A.; Besseau, S.; Lemos Cruz, P.; Kulagina, N.; Stander, E. A.; Eymieux, S.; Burlaud-Gaillard, J.; Blanchard, E.; Clastre, M.; Atehortùa, L.; St-Pierre, B.; Giglioli-Guivarc'h, N.; Papon, N.; Nagegowda, D. A.; O'Connor, S. E.; Courdavault, V. Alternative Splicing Creates a Pseudo-Strictosidine β-d-Glucosidase Modulating Alkaloid Synthesis in Catharanthus Roseus. *Plant Physiol.* **2020**, *185* (3), 836–856. https://doi.org/10.1093/plphys/kiaa075.
(36) Stavrinides, A.; Tatsis, E. C.; Foureau, E.; Caputi, L.; Kellner, F.; Courdavault, V.; O'Connor, S. E. Unlocking the Diversity of Alkaloids in *Catharanthus Roseus*:

Nuclear Localization Suggests Metabolic Channeling in Secondary Metabolism. *Chem. Biol.* **2015**, *22* (3), 336–341. https://doi.org/10.1016/j.chembiol.2015.02.006.
(37) Stavrinides, A.; Tatsis, E. C.; Caputi, L.; Foureau, E.; Stevenson, C. E. M.; Lawson, D. M.; Courdavault, V.; O'Connor, S. E. Structural Investigation of Heteroyohimbine Alkaloid Synthesis Reveals Active Site Elements That Control Stereoselectivity. *Nat. Commun.* **2016**, *7* (1), 12116. https://doi.org/10.1038/ncomms12116.
(38) Tatsis, E. C.; Carqueijeiro, I.; Dugé de Bernonville, T.; Franke, J.; Dang, T.-T. T.; Oudin, A.; Lanoue, A.; Lafontaine, F.; Stavrinides, A. K.; Clastre, M.; Courdavault, V.; O'Connor, S. E. A Three Enzyme System to Generate the Strychnos Alkaloid Scaffold from a Central Biosynthetic Intermediate. *Nat. Commun.* **2017**, *8* (1), 316. https://doi.org/10.1038/s41467-017-00154-x.
(39) Qu, Y.; Easson, M. E. A. M.; Simionescu, R.; Hajicek, J.; Thamm, A. M. K.; Salim, V.; De Luca, V. Solution of the Multistep Pathway for Assembly of Corynanthean, Strychnos, Iboga, and Aspidosperma Monoterpenoid Indole Alkaloids from 19E-Geissoschizine. *Proc. Natl. Acad. Sci.* **2018**, *115* (12), 3180–3185. https://doi.org/10.1073/pnas.1719979115.
(40) Caputi, L.; Franke, J.; Farrow, S. C.; Chung, K.; Payne, R. M. E.; Nguyen, T.-D.; Dang, T.-T. T.; Soares Teto Carqueijeiro, I.; Koudounas, K.; Dugé de Bernonville, T.; Ameyaw, B.; Jones, D. M.; Vieira, I. J. C.; Courdavault, V.; O'Connor, S. E. Missing Enzymes in the Biosynthesis of the Anticancer Drug Vinblastine in Madagascar Periwinkle. *Science* **2018**, *360* (6394), 1235–1239. https://doi.org/10.1126/science.aat4100.
(41) Qu, Y.; Safonova, O.; De Luca, V. Completion of the Canonical Pathway for Assembly of Anticancer Drugs Vincristine/Vinblastine in Catharanthus Roseus. *Plant J.* **2019**, *97* (2), 257–266. https://doi.org/10.1111/tpj.14111.
(42) Carr, S. C.; McDonald, A.; Langley, C.; Grabe, V.; Gase, K.; O'Connor, S. E. Protein–Protein Interactions Modulate a Key Branch Point in Monoterpene Indole Alkaloid Biosynthesis. *ACS Chem. Biol.* **2026**, *21* (1), 8–13. https://doi.org/10.1021/acschembio.5c00485.
(43) Courdavault, V.; Papon, N.; Clastre, M.; Giglioli-Guivarc'h, N.; St-Pierre, B.; Burlat, V. A Look inside an Alkaloid Multisite Plant: The *Catharanthus* Logistics. *Curr. Opin. Plant Biol.* **2014**, *19*, 43–50. https://doi.org/10.1016/j.pbi.2014.03.010.
(44) Qu, Y.; Easson, M. L. A. E.; Froese, J.; Simionescu, R.; Hudlicky, T.; De Luca, V. Completion of the Seven-Step Pathway from Tabersonine to the Anticancer Drug Precursor Vindoline and Its Assembly in Yeast. *Proc. Natl. Acad. Sci. U. S. A.* **2015**, *112* (19), 6224–6229. https://doi.org/10.1073/pnas.1501821112.
(45) Kellner, F.; Geu-Flores, F.; Sherden, N. H.; Brown, S.; Foureau, E.; Courdavault, V.; O'Connor, S. E. Discovery of a P450-Catalyzed Step in Vindoline Biosynthesis: A Link between the Aspidosperma and Eburnamine Alkaloids. *Chem. Commun.* **2015**, *51* (36), 7626–7628. https://doi.org/10.1039/C5CC01309G.
(46) Koudounas, K.; Guirimand, G.; Hoyos, L. F. R.; Carqueijeiro, I.; Cruz, P. L.; Stander, E.; Kulagina, N.; Perrin, J.; Oudin, A.; Besseau, S.; Lanoue, A.; Atehortùa, L.; St-Pierre, B.; Giglioli-Guivarc'h, N.; Papon, N.; O'Connor, S. E.; Courdavault, V. Tonoplast and Peroxisome Targeting of γ-Tocopherol N-Methyltransferase

Homologs Involved in the Synthesis of Monoterpene Indole Alkaloids. *Plant Cell Physiol.* **2022**, *63* (2), 200–216. https://doi.org/10.1093/pcp/pcab160.
(47) DeLuca, V.; Balsevich, J.; Tyler, R. T.; Kurz, W. G. W. Characterization of a Novel N-Methyltransferase (NMT) from Catharanthus Roseus Plants. *Plant Cell Rep.* **1987**, *6* (6), 458–461. https://doi.org/10.1007/BF00272782.
(48) St-Pierre, B.; Vazquez-Flota, F. A.; De Luca, V. Multicellular Compartmentation of Catharanthus Roseus Alkaloid Biosynthesis Predicts Intercellular Translocation of a Pathway Intermediate. *Plant Cell* **1999**, *11* (5), 887–900. https://doi.org/10.1105/tpc.11.5.887.
(49) Carqueijeiro, I.; Noronha, H.; Duarte, P.; Gerós, H.; Sottomayor, M. Vacuolar Transport of the Medicinal Alkaloids from Catharanthus Roseus Is Mediated by a Proton-Driven Antiport1[W]. *Plant Physiol.* **2013**, *162* (3), 1486–1496. https://doi.org/10.1104/pp.113.220558.
(50) Sottomayor, M.; López-Serrano, M.; DiCosmo, F.; Ros Barceló, A. Purification and Characterization of α-3′,4′-Anhydrovinblastine Synthase (Peroxidase-like) from Catharanthus Roseus (L.) G. Don. *FEBS Lett.* **1998**, *428* (3), 299–303. https://doi.org/10.1016/S0014-5793(98)00551-1.
(51) Sottomayor, M.; Ros Barceló, A. Peroxidase from Catharanthus Roseus (L.) G. Don and the Biosynthesis of α-3′,4′-Anhydrovinblastine: A Specific Role for a Multifunctional Enzyme. *Protoplasma* **2003**, *222* (1), 97–105. https://doi.org/10.1007/s00709-003-0003-9.
(52) Yu, F.; De Luca, V. ATP-Binding Cassette Transporter Controls Leaf Surface Secretion of Anticancer Drug Components in Catharanthus Roseus. *Proc. Natl. Acad. Sci.* **2013**, *110* (39), 15830–15835. https://doi.org/10.1073/pnas.1307504110.
(53) Yamamoto, K.; Takahashi, K.; Mizuno, H.; Anegawa, A.; Ishizaki, K.; Fukaki, H.; Ohnishi, M.; Yamazaki, M.; Masujima, T.; Mimura, T. Cell-Specific Localization of Alkaloids in Catharanthus Roseus Stem Tissue Measured with Imaging MS and Single-Cell MS. *Proc. Natl. Acad. Sci. U. S. A.* **2016**, *113* (14), 3891–3896. https://doi.org/10.1073/pnas.1521959113.
(54) Nützmann, H.-W.; Huang, A.; Osbourn, A. Plant Metabolic Clusters – from Genetics to Genomics. *New Phytol.* **2016**, *211* (3), 771–789. https://doi.org/10.1111/nph.13981.
(55) Bharadwaj, R.; Kumar, S. R.; Sharma, A.; Sathishkumar, R. Plant Metabolic Gene Clusters: Evolution, Organization, and Their Applications in Synthetic Biology. *Front. Plant Sci.* **2021**, *12*. https://doi.org/10.3389/fpls.2021.697318.
(56) Field, B.; Fiston-Lavier, A.-S.; Kemen, A.; Geisler, K.; Quesneville, H.; Osbourn, A. E. Formation of Plant Metabolic Gene Clusters within Dynamic Chromosomal Regions. *Proc. Natl. Acad. Sci.* **2011**, *108* (38), 16116–16121. https://doi.org/10.1073/pnas.1109273108.
(57) Yu, N.; Nützmann, H.-W.; MacDonald, J. T.; Moore, B.; Field, B.; Berriri, S.; Trick, M.; Rosser, S. J.; Kumar, S. V.; Freemont, P. S.; Osbourn, A. Delineation of Metabolic Gene Clusters in Plant Genomes by Chromatin Signatures. *Nucleic Acids Res.* **2016**, *44* (5), 2255–2265. https://doi.org/10.1093/nar/gkw100.
(58) Itkin, M.; Rogachev, I.; Alkan, N.; Rosenberg, T.; Malitsky, S.; Masini, L.; Meir, S.; Iijima, Y.; Aoki, K.; de Vos, R.; Prusky, D.; Burdman, S.; Beekwilder, J.; Aharoni, A. GLYCOALKALOID METABOLISM1 Is Required for Steroidal Alkaloid

Glycosylation and Prevention of Phytotoxicity in Tomato[W]. *Plant Cell* **2011**, *23* (12), 4507–4525. https://doi.org/10.1105/tpc.111.088732.
(59) Barone, R. P.; Knittel, D. K.; Ooka, J. K.; Porter, L. N.; Smith, N. T.; Owens, D. K. The Production of Plant Natural Products Beneficial to Humanity by Metabolic Engineering. *Curr. Plant Biol.* **2020**, *24*, 100121. https://doi.org/10.1016/j.cpb.2019.100121.
(60) Rai, A.; Hirakawa, H.; Nakabayashi, R.; Kikuchi, S.; Hayashi, K.; Rai, M.; Tsugawa, H.; Nakaya, T.; Mori, T.; Nagasaki, H.; Fukushi, R.; Kusuya, Y.; Takahashi, H.; Uchiyama, H.; Toyoda, A.; Hikosaka, S.; Goto, E.; Saito, K.; Yamazaki, M. Chromosome-Level Genome Assembly of Ophiorrhiza Pumila Reveals the Evolution of Camptothecin Biosynthesis. *Nat. Commun.* **2021**, *12* (1), 405. https://doi.org/10.1038/s41467-020-20508-2.
(61) Kellner, F.; Kim, J.; Clavijo, B. J.; Hamilton, J. P.; Childs, K. L.; Vaillancourt, B.; Cepela, J.; Habermann, M.; Steuernagel, B.; Clissold, L.; McLay, K.; Buell, C. R.; O'Connor, S. E. Genome-Guided Investigation of Plant Natural Product Biosynthesis. *Plant J.* **2015**, *82* (4), 680–692. https://doi.org/10.1111/tpj.12827.
(62) Li, F.; Shahsavarani, M.; Handy-Hart, C.-J.; Côté, A.; Brasseur-Trottier, X.; Montgomery, V.; Beech, R. N.; Liu, L.; Bayen, S.; Qu, Y.; De Luca, V.; Dastmalchi, M. Characterization of a Vacuolar Importer of Secologanin in Catharanthus Roseus. *Commun. Biol.* **2024**, *7* (1), 939. https://doi.org/10.1038/s42003-024-06624-5.
(63) Hwang, J.; Kirshner, J.; Deschênes, D. A. R.; Richardson, M. B.; Fleck, S. J.; Mann, S. G. A.; Guo, J.; Perley, J. O.; Shahsavarani, M.; Garza-Garcia, J. J. O.; Seveck, A. D.; Doiron, S. S.; Mai, Z.; Silliphant, S. N.; Englehart, S. A.; Blight, B. A.; Calhoun, L.; Gao, D.; Lian, J.; Deslongchamps, G.; Albert, V. A.; Qu, Y. Ancient Gene Clusters Govern the Initiation of Monoterpenoid Indole Alkaloid Biosynthesis and C3 Stereochemistry Inversion. bioRxiv September 20, 2025, p 2025.01.07.631695. https://doi.org/10.1101/2025.01.07.631695.
(64) Colinas, M.; Tymen, C.; Wood, J. C.; David, A.; Wurlitzer, J.; Morweiser, C.; Gase, K.; Alam, R. M.; Titchiner, G. R.; Hamilton, J. P.; Heinicke, S.; Dirks, R. P.; Lopes, A. A.; Caputi, L.; Buell, C. R.; O'Connor, S. E. Discovery of Iridoid Cyclase Completes the Iridoid Pathway in Asterids. *Nat. Plants* **2025**, *11* (11), 2204–2216. https://doi.org/10.1038/s41477-025-02122-6.
(65) Yocum, H. C.; Pham, A.; Da Silva, N. A. Successful Enzyme Colocalization Strategies in Yeast for Increased Synthesis of Non-Native Products. *Front. Bioeng. Biotechnol.* **2021**, *9*. https://doi.org/10.3389/fbioe.2021.606795.
(66) Liu, G.-S.; Li, T.; Zhou, W.; Jiang, M.; Tao, X.-Y.; Liu, M.; Zhao, M.; Ren, Y.-H.; Gao, B.; Wang, F.-Q.; Wei, D.-Z. The Yeast Peroxisome: A Dynamic Storage Depot and Subcellular Factory for Squalene Overproduction. *Metab. Eng.* **2020**, *57*, 151–161. https://doi.org/10.1016/j.ymben.2019.11.001.
(67) Dusséaux, S.; Wajn, W. T.; Liu, Y.; Ignea, C.; Kampranis, S. C. Transforming Yeast Peroxisomes into Microfactories for the Efficient Production of High-Value Isoprenoids. *Proc. Natl. Acad. Sci.* **2020**, *117* (50), 31789–31799. https://doi.org/10.1073/pnas.2013968117.
(68) Gerke, J.; Frauendorf, H.; Schneider, D.; Wintergoller, M.; Hofmeister, T.; Poehlein, A.; Zebec, Z.; Takano, E.; Scrutton, N. S.; Braus, G. H. Production of the

Fragrance Geraniol in Peroxisomes of a Product-Tolerant Baker's Yeast. *Front. Bioeng. Biotechnol.* **2020**, *8*. https://doi.org/10.3389/fbioe.2020.582052.
(69) Liu, T.; Huang, Y.; Jiang, L.; Dong, C.; Gou, Y.; Lian, J. Efficient Production of Vindoline from Tabersonine by Metabolically Engineered Saccharomyces Cerevisiae. *Commun. Biol.* **2021**, *4* (1), 1089. https://doi.org/10.1038/s42003-021-02617-w.
(70) Kulagina, N.; Guirimand, G.; Melin, C.; Lemos-Cruz, P.; Carqueijeiro, I.; De Craene, J.-O.; Oudin, A.; Heredia, V.; Koudounas, K.; Unlubayir, M.; Lanoue, A.; Imbault, N.; St-Pierre, B.; Papon, N.; Clastre, M.; Giglioli-Guivarc'h, N.; Marc, J.; Besseau, S.; Courdavault, V. Enhanced Bioproduction of Anticancer Precursor Vindoline by Yeast Cell Factories. *Microb. Biotechnol.* **2021**, *14* (6), 2693–2699. https://doi.org/10.1111/1751-7915.13898.
(71) Gnanasekaran, P.; Pappu, H. R. Forster Resonance Energy Transfer (FRET) to Visualize Protein–Protein Interactions in the Plant Cell. In *Protein-Protein Interactions: Methods and Protocols*; Mukhtar, S., Ed.; Springer US: New York, NY, 2023; pp 133–135. https://doi.org/10.1007/978-1-0716-3327-4_13.
(72) Liput, D. J.; Nguyen, T. A.; Augustin, S. M.; Lee, J. O.; Vogel, S. S. A Guide to Fluorescence Lifetime Microscopy and Förster's Resonance Energy Transfer in Neuroscience. *Curr. Protoc. Neurosci.* **2020**, *94* (1), e108. https://doi.org/10.1002/cpns.108.
(73) Rios, A. F.; Radoeva, T.; De Rybel, B.; Weijers, D.; Borst, J. W. FRET-FLIM for Visualizing and Quantifying Protein Interactions in Live Plant Cells. In *Plant Hormones: Methods and Protocols*; Kleine-Vehn, J., Sauer, M., Eds.; Springer: New York, NY, 2017; pp 135–146. https://doi.org/10.1007/978-1-4939-6469-7_13.
(74) Fujikawa, Y.; Kato, N. TECHNICAL ADVANCE: Split Luciferase Complementation Assay to Study Protein–Protein Interactions in Arabidopsis Protoplasts. *Plant J.* **2007**, *52* (1), 185–195. https://doi.org/10.1111/j.1365-313X.2007.03214.x.
(75) Chen, H.; Zou, Y.; Shang, Y.; Lin, H.; Wang, Y.; Cai, R.; Tang, X.; Zhou, J.-M. Firefly Luciferase Complementation Imaging Assay for Protein-Protein Interactions in Plants. *Plant Physiol.* **2008**, *146* (2), 323–324. https://doi.org/10.1104/pp.107.111740.
(76) Branon, T. C.; Bosch, J. A.; Sanchez, A. D.; Udeshi, N. D.; Svinkina, T.; Carr, S. A.; Feldman, J. L.; Perrimon, N.; Ting, A. Y. Efficient Proximity Labeling in Living Cells and Organisms with TurboID. *Nat. Biotechnol.* **2018**, *36* (9), 880–887. https://doi.org/10.1038/nbt.4201.
(77) Li, Y.; Zhang, Y.; Dinesh-Kumar, S. P. TurboID-Based Proximity Labeling: A Method to Decipher Protein-Protein Interactions in Plants. *Methods Mol. Biol.* **2024**, *2724*, 257–272. https://doi.org/10.1007/978-1-0716-3485-1_19.
(78) Zhang, Y.; Li, Y.; Yang, X.; Wen, Z.; Nagalakshmi, U.; Dinesh-Kumar, S. P. TurboID-Based Proximity Labeling for In Planta Identification of Protein-Protein Interaction Networks. *J. Vis. Exp. JoVE* **2020**, No. 159, 10.3791/60728. https://doi.org/10.3791/60728.
(79) Fields, S.; Song, O. A Novel Genetic System to Detect Protein–Protein Interactions. *Nature* **1989**, *340* (6230), 245–246. https://doi.org/10.1038/340245a0.

(80) Snider, J.; Kotlyar, M.; Saraon, P.; Yao, Z.; Jurisica, I.; Stagljar, I. Fundamentals of Protein Interaction Network Mapping. *Mol. Syst. Biol.* **2015**, *11* (12), MSB156351. https://doi.org/10.15252/msb.20156351.
(81) High-Quality Binary Interactome Mapping. In *Methods in Enzymology*; Academic Press, 2010; Vol. 470, pp 281–315. https://doi.org/10.1016/S0076-6879(10)70012-4.
(82) Phizicky, E. M.; Fields, S. Protein-Protein Interactions: Methods for Detection and Analysis. *Microbiol. Rev.* **1995**, *59* (1), 94–123. https://doi.org/10.1128/mr.59.1.94-123.1995.
(83) Jiang, Z.; Yang, M.; Cao, Q.; Zhang, Y.; Li, D. A Powerful Method for Studying Protein–Protein Interactions in Plants: Coimmunoprecipitation (Co-IP) Assay. In *Plant Virology : Methods and Protocols*; Wang, A., Li, Y., Eds.; Springer US: New York, NY, 2022; pp 87–92. https://doi.org/10.1007/978-1-0716-1835-6_9.
(84) Ghai, R.; Falconer, R. J.; Collins, B. M. Applications of Isothermal Titration Calorimetry in Pure and Applied Research—Survey of the Literature from 2010. *J. Mol. Recognit.* **2012**, *25* (1), 32–52. https://doi.org/10.1002/jmr.1167.
(85) Duff, M. R.; Grubbs, J.; Howell, E. E. Isothermal Titration Calorimetry for Measuring Macromolecule-Ligand Affinity. *J. Vis. Exp. JoVE* **2011**, No. 55, 2796. https://doi.org/10.3791/2796.
(86) Kühlbrandt, W. The Resolution Revolution. *Science* **2014**, *343* (6178), 1443–1444. https://doi.org/10.1126/science.1251652.
(87) Lyumkis, D. Challenges and Opportunities in Cryo-EM Single-Particle Analysis. *J. Biol. Chem.* **2019**, *294* (13), 5181–5197. https://doi.org/10.1074/jbc.REV118.005602.
(88) Renaud, J.-P.; Chari, A.; Ciferri, C.; Liu, W.; Rémigy, H.-W.; Stark, H.; Wiesmann, C. Cryo-EM in Drug Discovery: Achievements, Limitations and Prospects. *Nat. Rev. Drug Discov.* **2018**, *17* (7), 471–492. https://doi.org/10.1038/nrd.2018.77.
(89) Ltd, C. M. I. P. *Cryo Electron Microscopy Market Size and Forecast, 2026-2033*. Coherent Market Insights. https://www.coherentmarketinsights.com/industry-reports/cryo-electron-microscopy-market (accessed 2026-04-08).
(90) Kerppola, T. K. BIMOLECULAR FLUORESCENCE COMPLEMENTATION: VISUALIZATION OF MOLECULAR INTERACTIONS IN LIVING CELLS. *Methods Cell Biol.* **2008**, *85*, 431–470. https://doi.org/10.1016/S0091-679X(08)85019-4.
(91) Waadt, R.; Schmidt, L. K.; Lohse, M.; Hashimoto, K.; Bock, R.; Kudla, J. Multicolor Bimolecular Fluorescence Complementation Reveals Simultaneous Formation of Alternative CBL/CIPK Complexes in Planta. *Plant J. Cell Mol. Biol.* **2008**, *56* (3), 505–516. https://doi.org/10.1111/j.1365-313X.2008.03612.x.
(92) Kodama, Y.; Hu, C.-D. Bimolecular Fluorescence Complementation (BiFC): A 5-Year Update and Future Perspectives. *BioTechniques* **2012**, *53* (5), 285–298. https://doi.org/10.2144/000113943.
(93) Cabantous, S.; Terwilliger, T. C.; Waldo, G. S. Protein Tagging and Detection with Engineered Self-Assembling Fragments of Green Fluorescent Protein. *Nat. Biotechnol.* **2005**, *23* (1), 102–107. https://doi.org/10.1038/nbt1044.
(94) Park, S.-Y.; Fung, P.; Nishimura, N.; Jensen, D. R.; Fujii, H.; Zhao, Y.; Lumba, S.; Santiago, J.; Rodrigues, A.; Chow, T. F.; Alfred, S. E.; Bonetta, D.; Finkelstein, R.;

Provart, N. J.; Desveaux, D.; Rodriguez, P. L.; McCourt, P.; Zhu, J.-K.; Schroeder, J. I.; Volkman, B. F.; Cutler, S. R. Abscisic Acid Inhibits PP2Cs via the PYR/PYL Family of ABA-Binding START Proteins. *Science* **2009**, *324* (5930), 1068–1071. https://doi.org/10.1126/science.1173041.

# Chapter 2: Investigation of *C. roseus* Protein-Protein Interactions with Bimolecular Fluorescence Complementation assays in *N. benthamiana*

## 2.1 Research Objective

*Catharanthus roseus*, more commonly known as the Madagascar Periwinkle, is known to produce 344 bioactive compounds[1]. The monoterpene indole alkaloid (MIA) vinblastine, produced through an intricate 11-step biosynthetic pathway in *C. roseus*, is a chemotherapeutic agent used to treat Hodgkin's[2] and non-Hodgkin's lymphoma[3], and bladder[4], breast[5], and lung cancers[6]. In an attempt to overcome its low natural abundance[7], recent advances have enabled the *de novo* biosynthesis of vinblastine precursors, catharanthine and vindoline, in yeast; however, yields remain insufficient for commercial pharmaceutical viability[8,9].

Understanding how *C. roseus* spatially organizes these biochemical reactions may help unlock the full potential of MIA-based therapies. To deepen our understanding of enzymatic trafficking in vinblastine synthesis, in this study I investigate protein-protein interactions and their subcellular localization. This chapter discusses the cloning of *C. roseus* enzymes into *Agrobacterium tumefaciens* for use in bimolecular fluorescence complementation (BiFC) assays in *Nicotiana benthamiana* epidermal leaf cells.

## 2.2 Preparing Tobacco Plantlets

Dried *N. benthamiana* plants were used to collect seeds, which were then grown on an autoclaved standard soil mix moistened with sterile water. Plants were grown inside a grow chamber with full-spectrum LEDs set to 26°C and followed a 16 hour light/8 hour dark photoperiod. Following germination, individual seedlings were transplanted into the

wells of seedling trays and maintained in the growth chamber. Plants were watered regularly as needed. Tobacco plants were grown for at least four weeks prior to infiltration with *Agrobacterium tumefaciens* LBA4404.

### 2.3 Chemicals

All chemicals used in this research were purchased as molecular biology grade or higher from these commercial vendors unless denoted differently: Bio Basic Inc., CD BioSciences, Eurofins Genomics, *FroggaBio*, Geneaid Biotech Ltd©, New England Biolabs®, and Thermo Fisher Scientific.

### 2.4 Molecular Biology Kits

All molecular biology kits were used according to the manufacturer's specifications unless denoted differently. For genes or gene fragments destined for downstream applications, Q5 High-Fidelity DNA Polymerase (New England Biolabs®) was used for amplification. All oligonucleotide primers were synthesized and obtained from *Eurofins Genomics*. For Gateway™ cloning, BP Clonase™ II Enzyme mix and BP polymerase and LR Clonase™ II Enzyme mix were obtained from *Thermo Fisher Scientific*. For Gibson Assembly cloning, we used the Gibson Assembly® Cloning Kit (New England Biolabs®). Plasmid DNA was isolated from bacterial cultures using the Presto™ Mini Plasmid Kit (Geneaid Biotech Ltd©).

### 2.5 Cloning

#### 2.5.1 Generation of GFP tagged Constructs

For the creation of C-terminal green fluorescent protein (GFP) tagged enzymes, CrSGD, CrGS, CrGO, CrRedox1, CrRedox2, CrSAT, CrASO, CrDPAS, CrHL1, CrHL2, and

CrCAD2 were amplified using primers 1-24 (Supplementary Table 1) and inserted into pSITE-2CA vectors using Gateway cloning.

### 2.5.2 Generation of BiFC tagged Constructs

We employed a dual-approach strategy to generate Bimolecular Fluorescence Complementation (BiFC) constructs for enzyme-enzyme interaction studies. The BiFC vectors used were pGTQL1221YC and pGTQL1211YN (CD BioSciences), which respectively contain half of a complete mVenus protein. CrSGD, CrGS, CrGO, CrRedox1, CrRedox2, CrASO, CrDPAS, CrHL1, CrHL2, CrCAD2, and NbCAD100 were amplified using primers 1-26 (Supplementary Table 1) and inserted into pGTQL1221YC. CrSGD, CrGS, CrGO, CrRedox1, CrRedox2, CrSAT, CrASO, CrDPAS, CrHL1, CrHL2, and CrCAD2 were amplified using primers 1-26 (Supplementary Table 1) and inserted into pGTQL1211YN. A Gateway cloning system (Thermo Fisher Scientific™) was used to create *N*-terminal fusions of the BiFC tag fragments, while Gibson Assembly (New England Biolabs®) was employed for *C*-terminal fusions. This combinatorial approach allowed for the flexible positioning of BiFC tag fragments, allowing us to position the BiFC fragment on the opposing end of the native protein's subcellular localization sequences when necessary.

### 2.5.3 Subcellular localization markers

The subcellular localization of *C. roseus* CrCAD2, CrSGD, CrGS, CrGO, CrRedox1, CrRedox2, CrSAT, CrASO, CrSAT, CrHL1, and CrHL2 were determined via transgenic expression in *Nicotiana benthamiana* alongside pBIN20+ER-RFP (mCherry, ABRC-CD3-959) or pBIN20+vacuole marker (tonoplast), and pSITE4CA-empty (free RFP).

### 2.5.4 Escherichia coli (*E. coli*) Cloning

*Escherichia coli* Top10 competent cells were initially thawed on ice for 10 minutes, followed by the addition of approximately 100 ng of plasmid DNA, quantified using a ThermoScientific™ Nanodrop™ spectrophotometer. The cell-DNA mixture was gently mixed and incubated on ice for 10 minutes. A heat shock was administered by placing them in a 42°C water bath for 45 seconds, after which the cells were immediately returned to ice for 5 minutes. Post-heat shock, 400 µL of Luria-Bertani (LB) medium (Bio Basic Inc.) was introduced to the transformation mixture, which was then placed in a shaking incubator at 37 °C for 45-90 minutes. The transformed cells were subsequently pelleted by centrifugation at 8000 rcf for 30 seconds and resuspended in 100 µL of LB medium. The concentrated cell suspension was vortexed then plated on LB agar supplemented with the appropriate antibiotic and grown overnight at 37 °C. For mVenus and pBIN20 vectors, LB agar was supplemented with 50 µg/ml kanamycin. For pSITE vectors, LB agar was supplemented with 50 µg/ml spectinomycin. Following overnight incubation, we screened for positive colonies using a colony PCR protocol from *FroggaBio* with 2x Taq Frogga Mix. Amplicons were analyzed by a 10% agarose gel electrophoresis alongside a positive and negative control to confirm the presence of the desired construct. Single positive colonies were used to inoculate overnight LB cultures supplemented with the appropriate antibiotic, then plasmids were isolated and purified using a miniprep kit (*Geneaid Biotech Ltd*©). Overnight cultures were also used to prepare 25% glycerol stocks and stored at -80 °C indefinitely.

### 2.5.5 *Agrobacterium tumefaciens* Transformation

*Agrobacterium tumefaciens* LBA4404 competent cells were thawed on ice for 10 minutes. Approximately 1000 ng of miniprepped plasmid was added and mixed by gently flicking the tube. A heat shock was administered by placing them in a 37 °C water bath for 10 minutes, after which the cells were immediately returned to ice for 5 minutes. Post-heat shock, 400 µL of LB medium (Bio Basic Inc.) was introduced to the transformation mixture, which was then placed in a shaking incubator at 28 °C for three hours. The transformed cells were subsequently pelleted by centrifugation at 8000 rcf for 30 seconds and resuspended in 100 µL of LB medium. The concentrated cell suspension was vortexed then plated on LB agar supplemented with the appropriate antibiotic and incubated for 72 hours at 28 °C. For mVenus and pBIN20 vectors, LB agar was supplemented with 50 µg/ml kanamycin and 30 µl/ml of rifampicin. For pSITE vectors, LB agar was supplemented with 50 µg/ml spectinomycin and 30 µl/ml of rifampicin. Following incubation, we screened for positive colonies using a colony PCR protocol from FroggaBio with 2x Taq Frogga Mix. Amplicons were analyzed by a 10% agarose gel electrophoresis alongside a positive and negative control to confirm the presence of the desired construct. Single positive colonies were used to inoculate overnight LB cultures supplemented with the appropriate antibiotic. Overnight cultures were used to prepare 25% glycerol stocks and stored at -80 °C indefinitely.

## 2.6 Transient gene expression in *Nicotiana benthamiana*

*N. benthamiana* plantlets were subjected to moderate water restriction 24-hours prior to infiltration to enhance transformation efficiency. Liquid *A. tumefaciens* LBA4404 colonies were cultured overnight at 28 °C at 250 rpm in 1 ml of LB medium

supplemented with 30 µl/ml rifampicin and the appropriate plasmid-specific antibiotic (50 µl/ml kanamycin or 50 µl/ml spectinomycin). Cells were harvested by centrifugation at 5000 rcf for 4 minutes, then gently resuspended in infiltration buffer (10 mM MES, 10 mM $MgCl_2$, 0.2 mM acetosyringone, pH5.6) to an $OD_{600}$= 0.8. The resuspended cells were then shaken at 28 °C at 250 rpm for 3 hours.

Cell suspensions were mixed 1:1 or 1:1:1 with additional strains to create the desired combinations. Therefore, each strain was infiltrated at a final concentration of $OD_{600}$ = 0.4 and $OD_{600}$ = 0.27, respectively. The resulting strain mixture was drawn into a needleless syringe and infiltrated into the abaxial surface of *N. benthamiana* leaves. The plants were transferred to a 26 °C growth chamber for a 72-hour incubation period before analysis using confocal scanning laser microscopy (CSLM).

### 2.7 Confocal Scanning Laser Microscopy (CSLM)

#### 2.7.1 Sample Preparation for Confocal Scanning Laser Microscopy

A 5 mm x 5 mm piece of infiltrated leaf was excised and placed onto a 1.5 mm-thick glass microscopy slide with the adaxial side down. Small drops of vacuum grease were placed on the four corners of an 18 mm x 18 mm glass cover slip. A drop of distilled water was placed on the abaxial side of the leaf, then the cover slip was placed over top. Additional distilled water was injected into the space between the cover slip and the leaf. This preparation method was applied to all *N. benthamiana* leaf samples analyzed via confocal scanning laser microscopy (CSLM).

#### 2.7.2 Confocal Scanning Laser Microscopy Fluorescent Imaging

*N. benthamiana* leaves overexpressing mVenus, pSITE2CA, pSITE4CA, and pBIN20 constructs were mounted in water 3-days following the *A. tumefaciens* LBA4404

infiltration. Fluorescent imaging of tobacco leaf samples was performed using a LEICA SP8 Confocal Scanning Laser Microscope equipped with a 25x water immersion objective (Leica) in the Microscopy and Microanalysis Facility at the University of New Brunswick in Fredericton, New Brunswick, Canada. To ensure optimal imaging conditions, a drop of distilled water was applied to the water immersion lens prior to sample visualization, creating a water immersion interface. Samples were imaged using a magnification of 250x, and a zoom of 3x. Images were captured in a single frame using the hybrid detector and Trans detector in sequence, with a minimum spatial resolution of 512 x 512 pixels. The pinhole was set to 1.00 AU.

With excitation from a 488 nm laser at 3.0% of its total possible power (20mW), mVenus emission between 510-530 nm was recorded using a HyD detector and a Smart Gain of 40%. With excitation from a 488 nm laser at 3.0%, GFP emission between 505-525 nm was recorded using a HyD detector and a Smart Gain of 20%. With excitation from a 552 nm laser at 3.0%, mCherry and RFP emission between 570-630 nm was recorded using a HyD detector and a Smart Gain of 40%. Transmitted light images were acquired using a photomultiplier tube (PMT) with a gain of 120.0-170.0 V depending on the thickness of the leaf sample.

### 2.7.3 Processing Images using Fiji

Files obtained from the CSLM were opened in Fiji 2.17.0. To each image, the Lookup Tables tool was used to add colour to each individual channel. mVenus and GFP emissions were changed to Green, mCherry and RFP emissions were changed to Red, and the transmitted light channel was changed to Grays (Image > Lookup Tables > Green/Red/Grays). The Image Type was changed to an RGB Colour (Image > Type >

RGB Colour). Then the channels were stacked using a Z-stack of maximum intensity for images with only two channels, or sum slices for three channels (Image > Stack > Z-project >Maximum Intensity/Sum Slices). A 20 µl scale bar was added to the merged image in the bottom right-hand corner (Analyze > Tools > Scale Bar). The unmerged RGB colour file and the merged Z-project file were both saved as a .tiff (File > Save As > Tiff…). The .tiff files were uploaded to *Microsoft PowerPoint*, then transferred to *BioRender* to create figures displaying multiple BiFC combinations.

## Bibliography 2


(1) Goswami, S.; Ali, A.; Prasad, M. E.; Singh, P. Pharmacological Significance of *Catharanthus Roseus* in Cancer Management: A Review. *Pharmacol. Res. - Mod. Chin. Med.* **2024**, *11*, 100444. https://doi.org/10.1016/j.prmcm.2024.100444.

(2) Little, R.; Wittes, R. E.; Longo, D. L.; Wilson, W. H. Vinblastine for Recurrent Hodgkin's Disease Following Autologous Bone Marrow Transplant. *J. Clin. Oncol. Off. J. Am. Soc. Clin. Oncol.* **1998**, *16* (2), 584–588. https://doi.org/10.1200/JCO.1998.16.2.584.

(3) Palmieri, G.; Lauria, R.; Caponigro, F.; Pagliarulo, C.; Montesarchio, V.; Nuzzo, F.; Gridelli, C.; Bianco, A. R. Salvage Chemotherapy for Non Hodgkin's Lymphoma of Unfavourable Histology with a Combination of CCNU and Vinblastine. *Hematol. Oncol.* **1990**, *8* (4), 179–183. https://doi.org/10.1002/hon.2900080402.

(4) Plimack, E. R.; Hoffman-Censits, J. H.; Viterbo, R.; Trabulsi, E. J.; Ross, E. A.; Greenberg, R. E.; Chen, D. Y. T.; Lallas, C. D.; Wong, Y.-N.; Lin, J.; Kutikov, A.; Dotan, E.; Brennan, T. A.; Palma, N.; Dulaimi, E.; Mehrazin, R.; Boorjian, S. A.; Kelly, W. K.; Uzzo, R. G.; Hudes, G. R. Accelerated Methotrexate, Vinblastine, Doxorubicin, and Cisplatin Is Safe, Effective, and Efficient Neoadjuvant Treatment for Muscle-Invasive Bladder Cancer: Results of a Multicenter Phase II Study with Molecular Correlates of Response and Toxicity. *J. Clin. Oncol. Off. J. Am. Soc. Clin. Oncol.* **2014**, *32* (18), 1895–1901. https://doi.org/10.1200/JCO.2013.53.2465.

(5) Fraschini, G.; Yap, H. Y.; Hortobagyi, G. N.; Buzdar, A.; Blumenschein, G. Five-Day Continuous-Infusion Vinblastine in the Treatment of Breast Cancer. *Cancer* **1985**, *56* (2), 225–229. https://doi.org/10.1002/1097-0142(19850715)56:2%253C225::aid-cncr2820560203%253E3.0.co;2-y.

(6) Grunberg, S. M.; Crowley, J. J.; Livingston, R. B.; Muggia, F. M.; MacDonald, J. S.; Williamson, S. K.; Stephens, R. L. Treatment of Non-Small-Cell Lung Cancer with Vinblastine and Very High-Dose Cisplatin. A Southwest Oncology Group Study. *Cancer Chemother. Pharmacol.* **1991**, *28* (3), 211–213. https://doi.org/10.1007/BF00685511.

(7) Noble, R. L. The Discovery of the Vinca Alkaloids—Chemotherapeutic Agents against Cancer. *Biochem. Cell Biol.* **1990**, *68* (12), 1344–1351. https://doi.org/10.1139/o90-197.

(8) Gao, D.; Liu, T.; Gao, J.; Xu, J.; Gou, Y.; Pan, Y.; Li, D.; Ye, C.; Pan, R.; Huang, L.; Xu, Z.; Lian, J. De Novo Biosynthesis of Vindoline and Catharanthine in *Saccharomyces Cerevisiae*. *BioDesign Res.* **2022**, *2022*, 0002. https://doi.org/10.34133/bdr.0002.

(9) Zhang, J.; Hansen, L. G.; Gudich, O.; Viehrig, K.; Lassen, L. M. M.; Schrübbers, L.; Adhikari, K. B.; Rubaszka, P.; Carrasquer-Alvarez, E.; Chen, L.; D'Ambrosio, V.; Lehka, B.; Haidar, A. K.; Nallapareddy, S.; Giannakou, K.; Laloux, M.; Arsovska, D.; Jørgensen, M. A. K.; Chan, L. J. G.; Kristensen, M.; Christensen, H. B.; Sudarsan, S.; Stander, E. A.; Baidoo, E.; Petzold, C. J.; Wulff, T.; O'Connor, S. E.; Courdavault, V.; Jensen, M. K.; Keasling, J. D. A Microbial Supply Chain for Production of the Anti-Cancer Drug Vinblastine. *Nature* **2022**, *609* (7926), 341–347. https://doi.org/10.1038/s41586-022-05157-3.

# Chapter 3: A BiFC Survey of Core MIA biosynthetic Enzymes in *N. benthamiana* Leaf Epidermal Cells

## 3.1 Interpreting Confocal Microscopy Images

As discussed in Chapter 2, I plan to study PPIs in *C. roseus* by preforming BiFC surveys in *N. benthamiana* epidermal leaf cells via *A. tumefaciens* infiltrations. For visualization of these surveys, I separated emissions into mVenus, mCherry, transmitted light, and merge channels. Notably, I represent mVenus fluorescence as a visual green colour in my figures because when it is overlayed with visual red colour from mCherry subcellular markers, it creates a distinct yellow colour in the merge channel.

However, before using BiFC to identify the localization of PPIs, I had to confirm where these enzymes localize independently. To do this, I use GFP-tagged enzymes (Figure 3.1). I observed results and collected the data in four distinct channels: the GFP channel, which should show the GFP-tagged proteins; the RFP channel, which should show the free RFP and mCherry subcellular makers; the transmitted light channel, which should show the morphology of the epidermal cells in grayscale; and the merge channel, where the previous three channels are overlayed. Notably, when green and red colour are overlayed, they create a yellow colour.

## 3.2 Subcellular Localization of GFP-tagged MIA Biosynthetic Enzymes

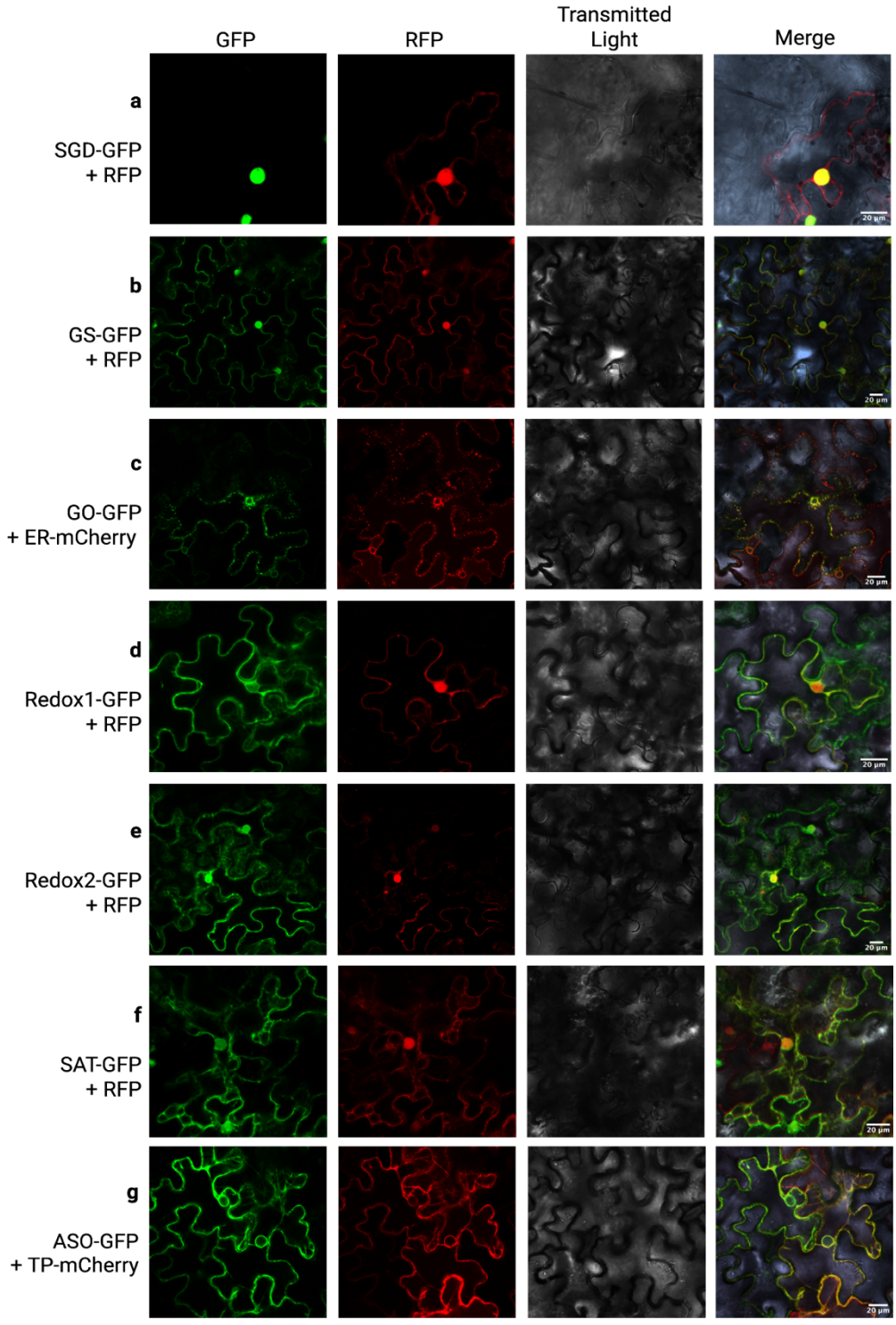
Prior to inspecting protein-protein interactions using BiFC, I generated GFP-tagged proteins to verify their subcellular localization (Figure 3.1). Here, free RFP was used as a cytoplasmic marker (Figure 3.1, a-b, d-f, h-j) but notably exhibited both cytoplasmic and nuclear localization. This is expected, as it is understood that small cytosolic proteins

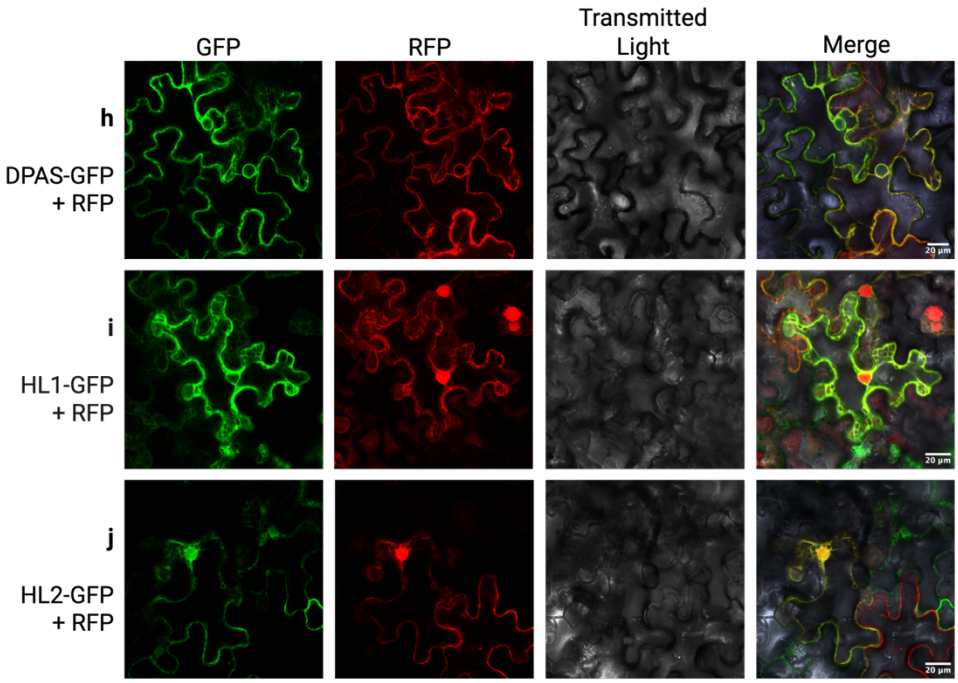
without a localization signal peptide can diffuse into the nucleus through the nuclear pore[1]. Therefore, free RFP can function as subcellular markers for both the cytoplasm and nucleus. We also see that our HDEL-mCherry marker localizes appropriately to the ER, as observed by the fluorescence of the nuclear membrane, and web-like structures in the rest of the cell (Figure 3.1, c). Additionally, we observe our tonoplast marker (TP-mCherry) properly localizing in Figure 3.1, g.

Proceeding to my GFP-tagged pathway proteins, they all behave as previously reported in the literature and act as subcellular controls for the following BiFC surveys. First, SGD, which contains a bipartite C-terminal nuclear targeting signal, localizes to the nucleus as previously established[2] (Figure 3.1, a). Meanwhile, GS, lacking any targeting motif, localizes to the cytoplasm and nucleus, as previously reported[3] (Figure 3.1, b). Here, we importantly observe that an enzyme that is expected to be cytosolic is capable of localizing to the nucleus. This is because it can slowly diffuse inside despite its size. In contrast, we observe that GO, a cytochrome P450 with a ER targeting signal, indeed localizes to the ER as expected[4,5] (Figure 3.1, c).

Conversely, Redox1, Redox2, and SAT all localize to the cytoplasm, along with the expected nuclear localization as well[6] (Figure 3.1, d, e, f). On the other hand ASO, which contains N-terminal secretory signal peptide, localizes to the tonoplast (vacuolar membrane), as previously reported[7] (Figure 3.1, g). Whereas, DPAS, HL1, and HL2 are observed localize to the cytoplasm and nucleus, respectively[8] (Figure 3.1, h, i, j). Notably, all my observations of these GFP-tagged proteins align with results from previous literature reports.

**Figure 3.1: Confocal microscopy of GFP-tagged proteins in N. benthamiana leaves illustrate the subcellular localization of *C. roseus* SGD, GS, GO, Redox1, Redox2, SAT, ASO, DPAS, HL1, and HL2.** Confocal microscopy was used to capture fluorescent signals from tobacco epidermal cells after transient expression of the constructs. **a-j**, C-terminal GFP tags were used to localize the proteins of interest. **a-b, d-f, h-j**, Free RFP was used as cytosolic and nuclear markers; **c**, C-terminal tagged HDEL-mCherry was used as an ER marker; **g**, C-terminal tagged tonoplast-mCherry was used as a tonoplast marker. Visual green colour corresponds to GFP fluorescence, red to RFP fluorescence, yellow to merged GFP and RFP fluorescence, and greyscale for transmitted light. Scale bars indicate 20 μm.


GFP
RFP
Transmitted Light
Merge
a
SGD-GFP + RFP
b
GS-GFP + RFP
c
GO-GFP + ER-mCherry
d
Redox1-GFP + RFP
e
Redox2-GFP + RFP
f
SAT-GFP + RFP
g
ASO-GFP + TP-mCherry
20 µm



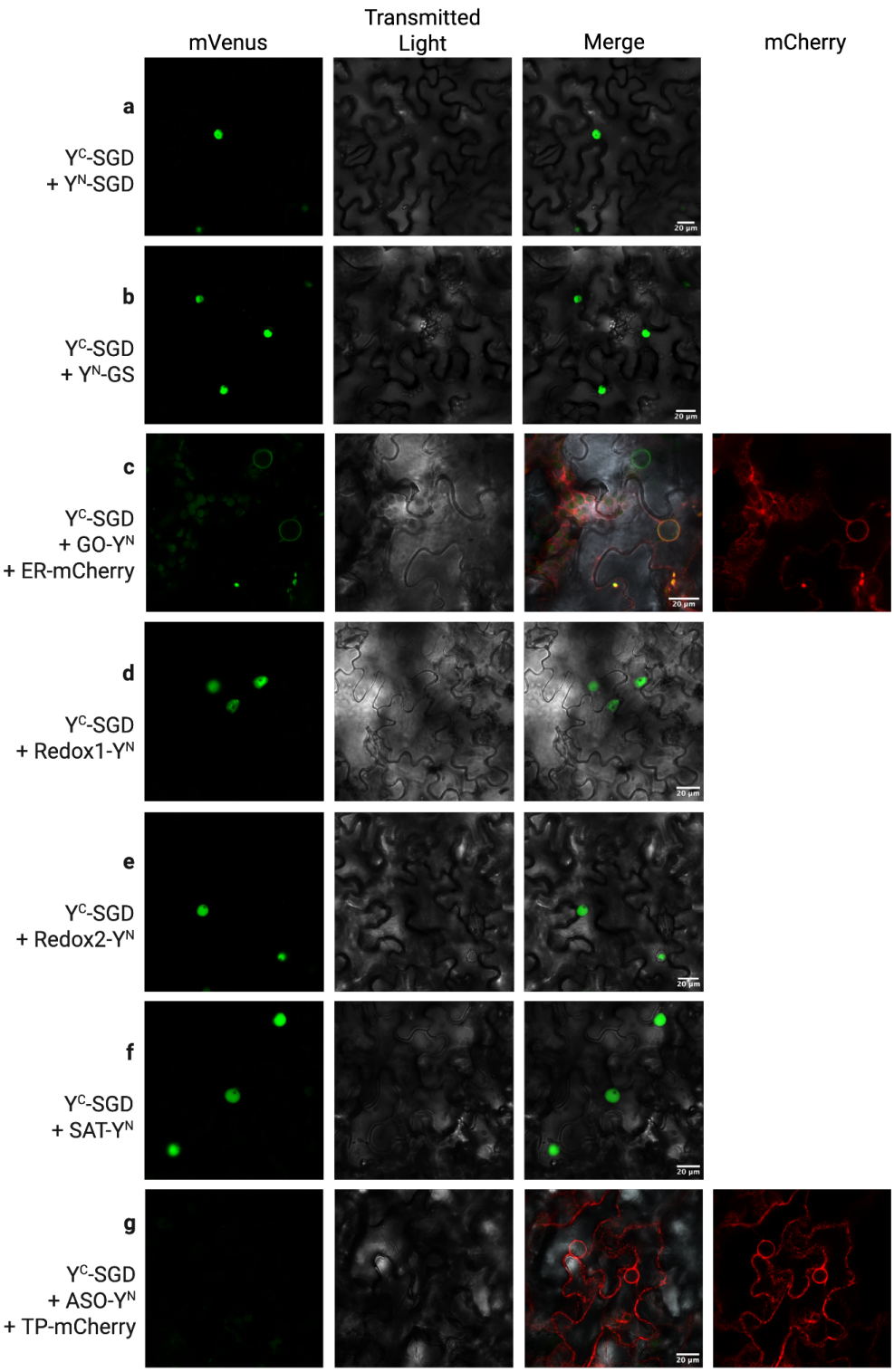

### 3.3 Study of Strictosidine β-D-Glucosidase (SGD) Protein-Protein Interaction

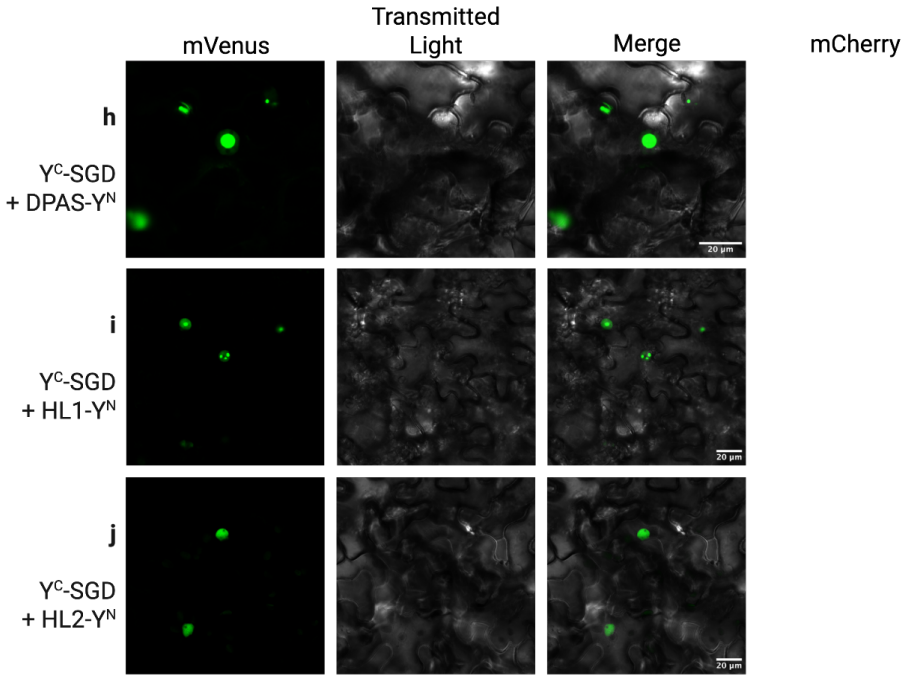
After confirming the subcellular localization of MIA biosynthetic pathway enzymes, I infiltrated the *N. benthamiana* leaves with *A. tumefaciens* carrying various genes fused with complementary mVenus (a YFP variant) tags for BiFC studies. Constructs designated as "$Y^N$/$Y^C$-protein" indicate that the N-terminal or C-terminal fragments of mVenus are fused to the N-terminus of the protein of interest, respectively. Conversely, constructs designated as "protein-$Y^N$/$Y^C$" indicate that the N-terminal or C-terminal fragments of mVenus are fused to the C-terminus of the target proteins. Under confocal microscopy, a yellow fluorescence signal not only indicates a protein-protein interaction (PPI) but allows us to observe the subcellular compartment(s) where these interactions occur.

I began my BiFC surveys with the first enzyme in the biosynthetic pathway, SGD, and tagged it with mVenus$^C$ on its N-terminus (Figure 3.2). These results show that $Y^C$-SGD interacts with itself and all other inspected enzymes in this pathway, except ASO.

The assembly of a mVenus fluorophore was observed in two distinct subcellular compartments: $Y^C$-SGD and $Y^N$-SGD, -GS, -Redox1, -Redox2, -SAT, -DPAS, -HL1, and -HL2 (Figure 3.21, a-b, d-f, h-j) interact in the nucleus; $Y^C$-SGD and GO-$Y^N$ (Figure 3.21, c) interact specifically on the nuclear membrane, which is continuous with the ER.

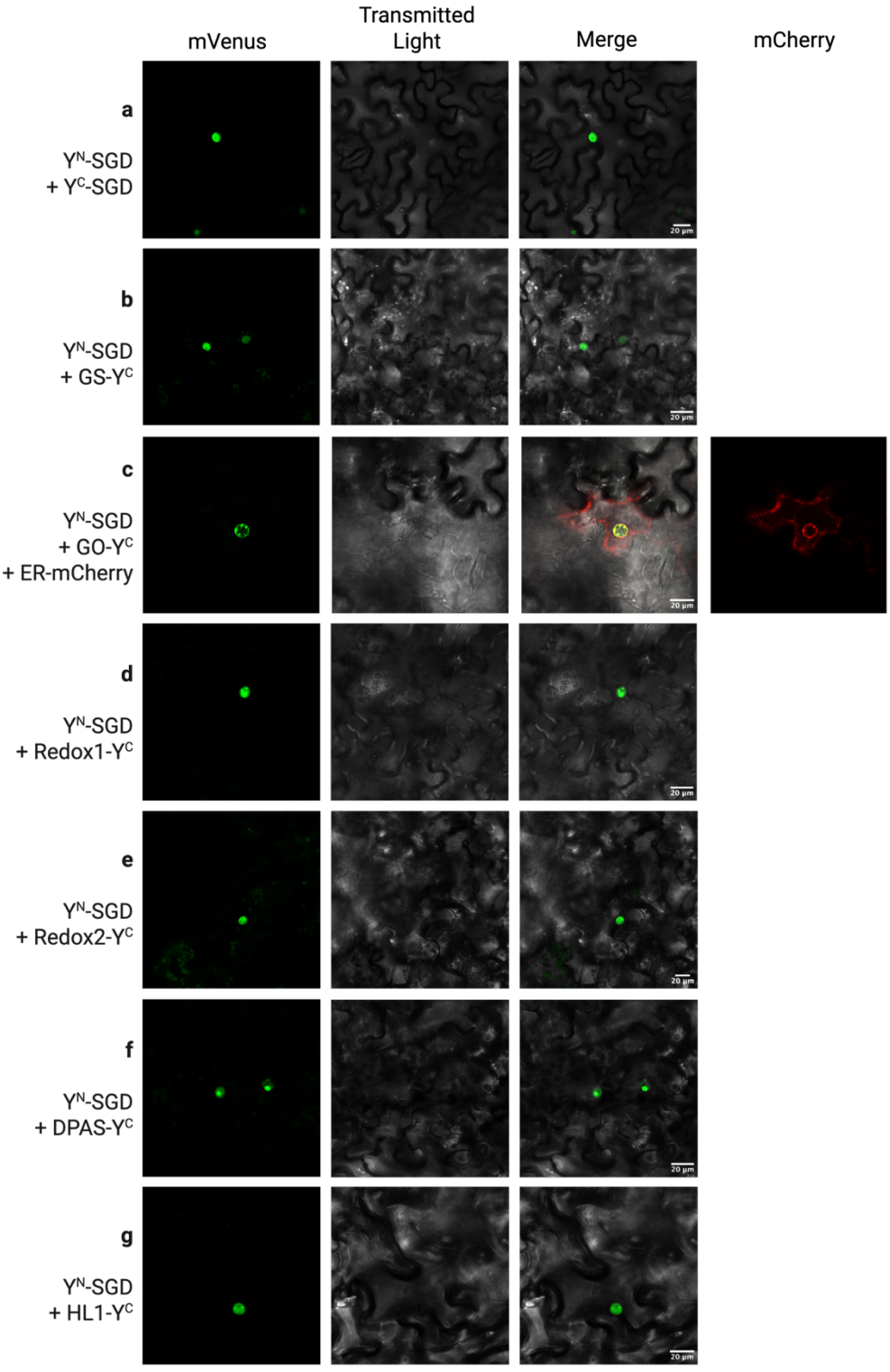
**Figure 3.2: Bimolecular Fluorescence Complementation (BiFC) assay of mVenus$^C$ tagged *C. roseus* SGD and mVenus$^N$ tagged SGD, GS, GO, Redox1, Redox2, SAT, ASO, DPAS, HL1, HL2 in *N. benthamiana* epidermal cells illustrate the subcellular localization of protein-protein interactions.** Confocal microscopy was used to capture fluorescent signals after transient expression of the constructs. mVenus fluorescence is generated when mVenus$^N$ and mVenus$^C$ are brought into proximity through the protein-protein interaction of the fused proteins. **a-j**, mVenus$^C$ was fused to the N-terminus of SGD. **a-b**, mVenus$^N$ is fused to the N-termini of SGD, and GS; **c-j**, mVenus$^N$ was fused to the C-termini of GO, Redox1, Redox2, SAT, ASO, DPAS, HL1, and HL2. Subcellular localization was determined using: **d**, C-terminal tagged HDEL-mCherry as an ER marker; **h**, C-terminal tagged tonoplast-mCherry as a tonoplast marker. Visual green colour corresponds to mVenus fluorescence, red to mCherry fluorescence, yellow to merged mVenus and mCherry fluorescence, and greyscale for transmitted light. Scale bars indicate 20µm.

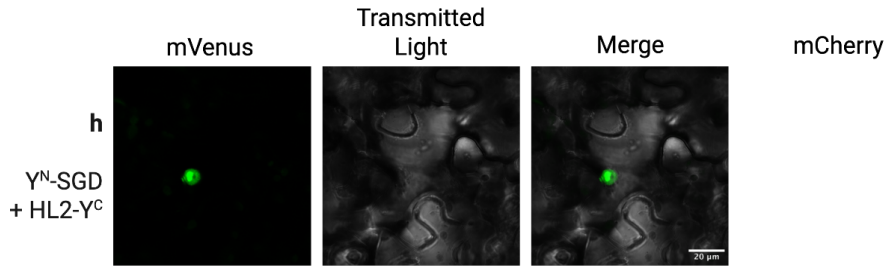

mVenus
Transmitted Light
Merge
mCherry
a
YC-SGD
+ YN-SGD
b
YC-SGD
+ YN-GS
c
YC-SGD
+ GO-YN
+ ER-mCherry
d
YC-SGD
+ Redox1-YN
e
YC-SGD
+ Redox2-YN
f
YC-SGD
+ SAT-YN
g
YC-SGD
+ ASO-YN
+ TP-mCherry
20 µm




Meanwhile, Figure 3.3 contains SGD is tagged with mVenus$^{N}$ on the N-terminus, illustrating the reciprocal nVenus tagging as shown in Figure 3.2. Consistent with Figure 3.2, Figure 3.3 indicates that Y$^{N}$-SGD also interacts with itself and all other enzymes inspected in this pathway. The assembly of a mVenus fluorophore was observed in two distinct subcellular compartments: Y$^{N}$-SGD and -SGD, GS-, Redox1-, Redox2-, DPAS-, HL1-, and HL2-Y$^{C}$ are all observed to interact in the nucleus (Figure 3.3, a-b, d-h); while Y$^{N}$-SGD and GO-Y$^{C}$ are observed to interact on the nuclear membrane, which is continuous with the ER (Figure 3.3, c).

**Figure 3.3: Bimolecular fluorescence (BiFC) assay of mVenus$^{N}$ tagged *C. roseus* SGD and mVenus$^{C}$ tagged SGD, GS, GO, Redox1, Redox2, DPAS, HL1, HL2 in *N. benthamiana* epidermal cells illustrate the subcellular localization of protein-protein interactions.** Confocal microscopy was used to capture fluorescent signals after transient overexpression of the constructs. mVenus fluorescence is generated when mVenus$^{N}$ and mVenus$^{C}$ are brought into proximity through the protein-protein interaction of the fused proteins. **a-h**, mVenus$^{N}$ was fused to the N-terminus of SGD; **a**, mVenus$^{C}$ is fused to the N-terminus of SGD; **b-h**, mVenus$^{C}$ was fused to the C-terminal of GS, GO, Redox1, Redox2, DPAS, HL1, and HL2. **c**, Subcellular localization was determined using C-terminal tagged HDEL-mCherry as an ER marker. Visual green colour corresponds to mVenus fluorescence, red to mCherry fluorescence, yellow to merged mVenus and mCherry fluorescence, and greyscale for transmitted light. Scale bars indicate 20 μm.


mVenus
Transmitted Light
Merge
mCherry
a
$Y^N$-SGD
+ $Y^C$-SGD
b
$Y^N$-SGD
+ GS-$Y^C$
c
$Y^N$-SGD
+ GO-$Y^C$
+ ER-mCherry
d
$Y^N$-SGD
+ Redox1-$Y^C$
e
$Y^N$-SGD
+ Redox2-$Y^C$
f
$Y^N$-SGD
+ DPAS-$Y^C$
g
$Y^N$-SGD
+ HL1-$Y^C$
20 µm




All the reported interaction in Figure 3.3 match those reported in Figure 3.2, increasing their reliability. The SGD PPIs that I have observed here are summarized in Figure 3.4.

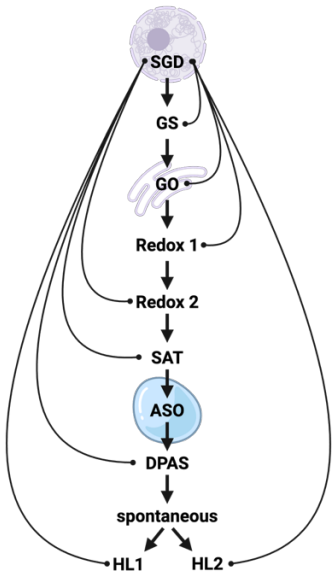



**Figure 3.4: SGD protein-protein interaction map.** Protein-protein interactions (PPIs) are indicated by curved lines between enzymes in the biosynthetic pathway to catharanthine and tabersonine. SGD interacts with GS, GO, Redox1, Redox2, SAT, DPAS, HL1, and HL2. However, it is not observed to interact with ASO.

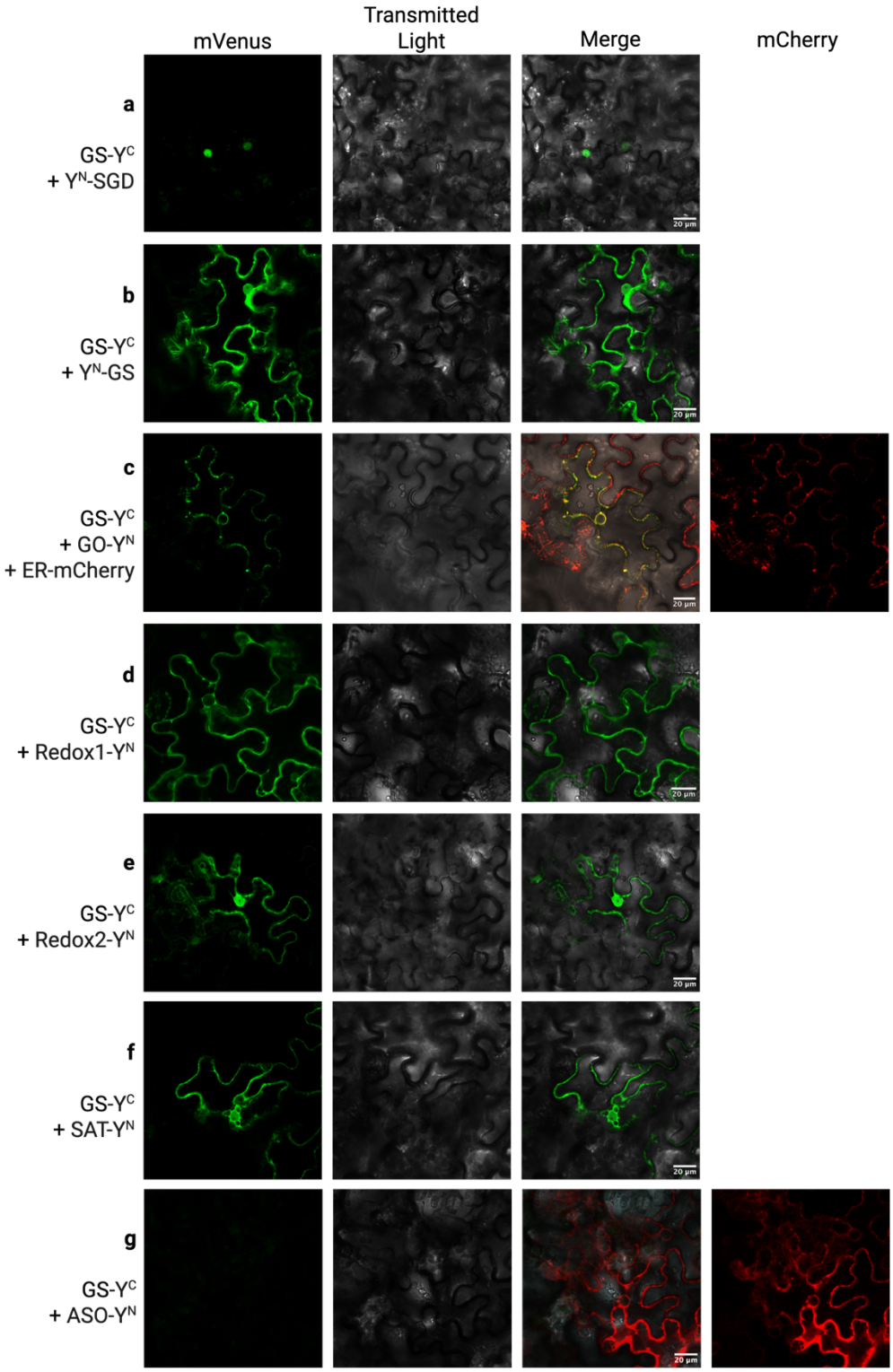
Notably, none of the enzymes in this pathway besides SGD contain a nuclear localization signal. However, in both Figure 3.2 and Figure 3.3, we observe nuclear PPIs with GS, Redox1, Redox2, SAT, DPAS, HL1, and HL2. This indicates that the observed nuclear localization may be simply from passive diffusion through the nuclear pore complex (NPC) or could suggest an underlying mechanism for nuclear transport. Regardless, none of the observed interactions have been previously reported. In contrast,

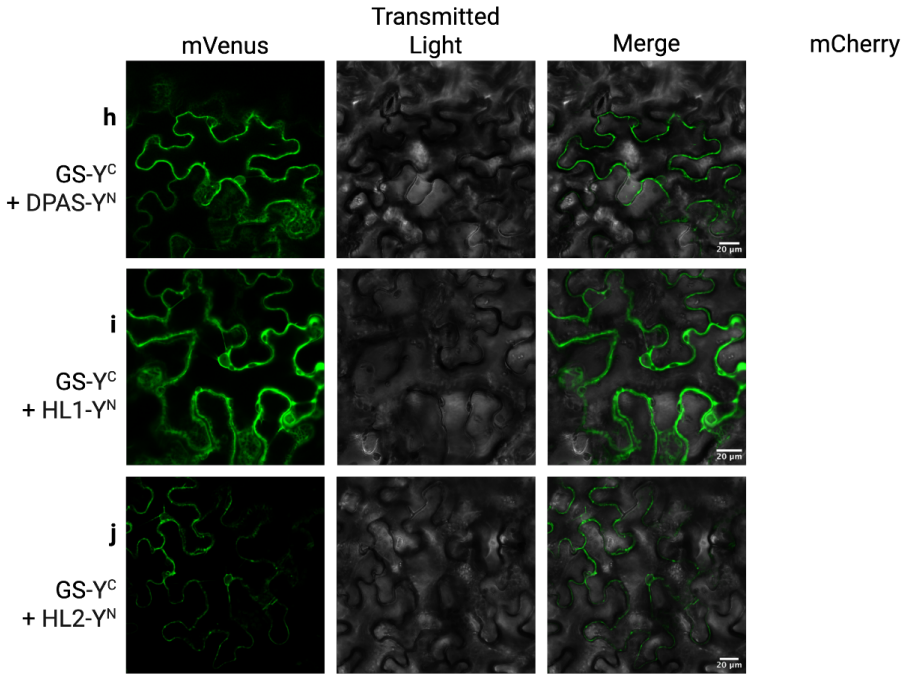
$Y^C$-SGD and ASO-$Y^N$ (Figure 3.2, g) do not produce mVenus fluorescence, and the explanation for why and how this could be happening is discussed in detail in Section 3.9.

### 3.4 Study of Geissoschizine Synthase (GS) Protein-Protein Interactions

Proceeding down the biosynthetic pathway, I then preformed BiFC surveys of GS. First, I tagged GS on the C-terminus with $mVenus^C$ (Figure 3.5). Figure 3.5 shows that GS-$Y^C$ interacts with itself and all other inspected enzymes in this pathway, except for ASO (Figure 3.5, g). The assembly of a mVenus fluorophore was observed in three distinct subcellular compartments: GS-$Y^C$and $Y^N$-SGD interact in the nucleus (Figure 3.5, a); GS-$Y^C$ and $Y^N$-GS, -Redox1, -Redox2, -SAT, -DPAS, -HL1, and -HL2 (Figure 3.5, b, d-f, h-j) interact in the cytoplasm; and GS-$Y^C$ and GO-$Y^N$ interact on the ER (Figure 3.5, c).

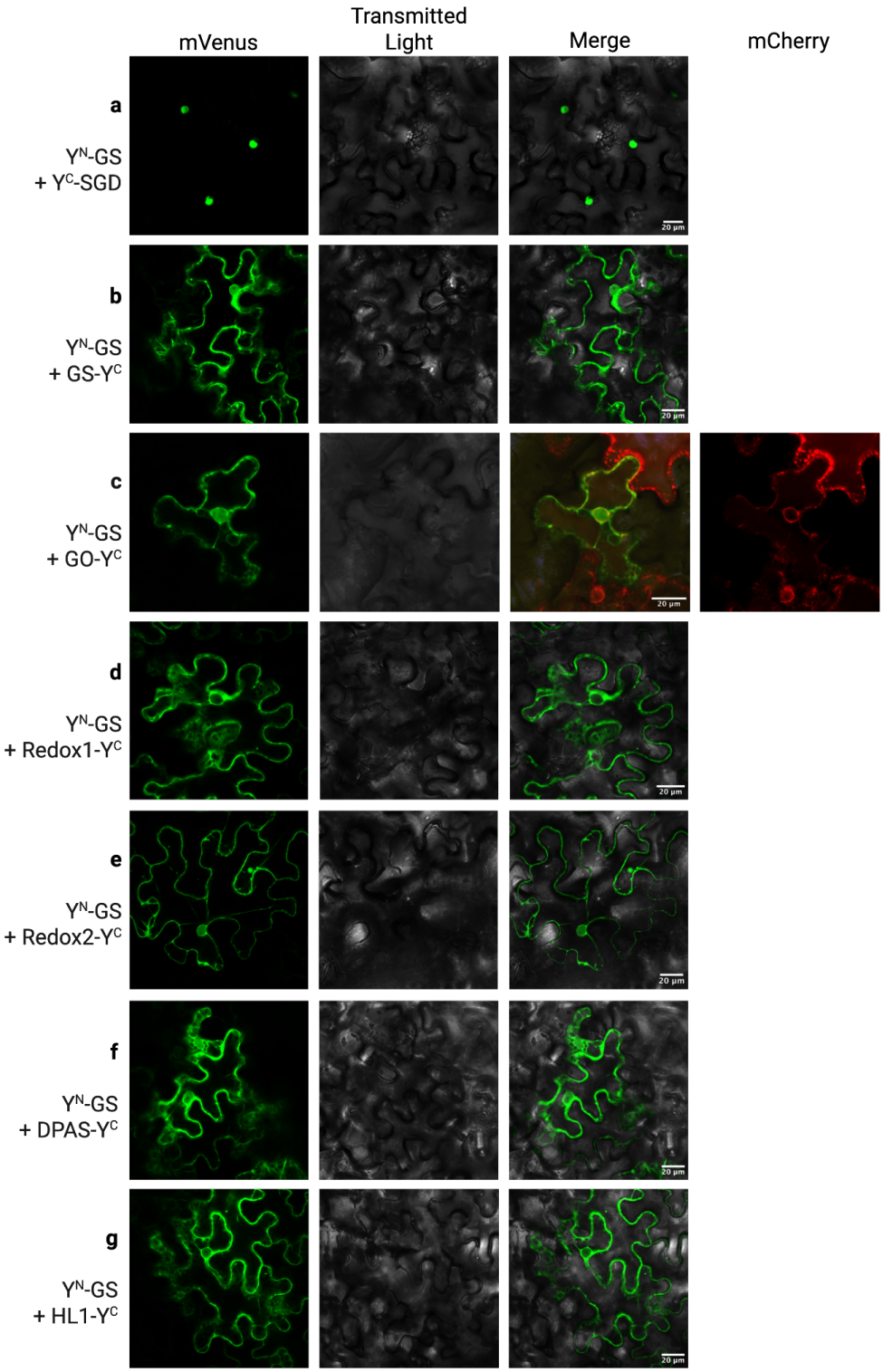
**Figure 3.5: Bimolecular fluorescence (BiFC) assay of $mVenus^C$ tagged *C. roseus* GS and $mVenus^N$ tagged SGD, GS, GO, Redox1, Redox2, SAT, ASO, DPAS, HL1, HL2 in *N. benthamiana* epidermal cells illustrate the subcellular localization of protein-protein interactions.** Confocal microscopy was used to capture fluorescent signals after transient expression of the constructs. mVenus fluorescence is generated when $mVenus^N$ and $mVenus^C$ are brought into proximity through the protein-protein interaction of the fused proteins. **a-j**, $mVenus^C$ was fused to the C-terminus of GS; **a-b**, $mVenus^N$ is fused to the N-termini SGD and GS; **c-j**, $mVenus^N$ was fused to the C-termini of GO, Redox1, Redox2, SAT, ASO, DPAS, HL1, and HL2. Subcellular localization was determined using: **c**, C-terminal tagged HDEL-mCherry as an ER marker; **g**, C-terminal tagged tonoplast-mCherry as a tonoplast marker. Visual green colour corresponds to mVenus fluorescence, red to mCherry fluorescence, yellow to merged mVenus and mCherry fluorescence, and greyscale for transmitted light. Scale bars indicate 20 μm.

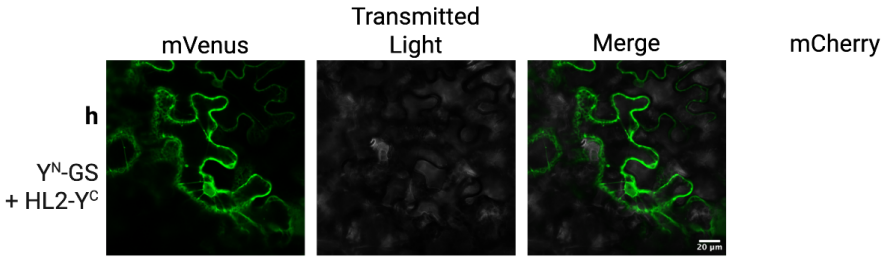

mVenus
Transmitted Light
Merge
mCherry
a
GS-Y^C + Y^N-SGD
b
GS-Y^C + Y^N-GS
c
GS-Y^C + GO-Y^N + ER-mCherry
d
GS-Y^C + Redox1-Y^N
e
GS-Y^C + Redox2-Y^N
f
GS-Y^C + SAT-Y^N
g
GS-Y^C + ASO-Y^N
20 µm




Meanwhile, Figure 3.6 contains GS is tagged with mVenus$^N$ on the N-terminus, illustrating the reciprocal mVenus tagging as shown in Figure 3.5. Consistent with Figure 3.5, Figure 3.6 indicates that Y$^N$-SGD also interacts with itself and all other enzymes inspected in this pathway. The assembly of a mVenus fluorophore was observed in two distinct subcellular compartments: Y$^N$-GS and -SGD interact in the nucleus (Fig. 3.6, a); Y$^N$-GS and Y$^C$-GS, GO-, Redox1-, Redox2-, DPAS-, HL1-, and HL2- are all observed to interact in the cytoplasm (Fig. 3.6, b-h).

**Figure 3.6: Bimolecular fluorescence (BiFC) assay of mVenus$^N$ tagged *C. roseus* GS and mVenus$^C$ tagged SGD, GS, GO, Redox1, Redox2, DPAS, HL1, HL2 in *N. benthamiana* epidermal cells illustrate the subcellular localization of protein-protein interactions.** Confocal microscopy was used to capture fluorescent signals after transient overexpression of the constructs. mVenus fluorescence is generated when mVenus$^N$ and mVenus$^C$ are brought into proximity through the protein-protein interaction of the fused proteins. **a-h**, mVenus$^N$ was fused to the C-terminus of GS; a, mVenus$^C$ is fused to the N-termini of SGD; **b-h**, mVenus$^C$ was fused to the C-termini of GS, GO, Redox1, Redox2, DPAS, HL1, and HL2. **d**, Subcellular localization was determined using C-terminal tagged HDEL-mCherry as an ER marker. Visual green colour corresponds to mVenus fluorescence, red to mCherry fluorescence, yellow to merged mVenus and mCherry fluorescence, and greyscale for transmitted light. Scale bars indicate 20µm.


mVenus
Transmitted Light
Merge
mCherry
a
$Y^N$-GS
+ $Y^C$-SGD
b
$Y^N$-GS
+ GS-$Y^C$
c
$Y^N$-GS
+ GO-$Y^C$
d
$Y^N$-GS
+ Redox1-$Y^C$
e
$Y^N$-GS
+ Redox2-$Y^C$
f
$Y^N$-GS
+ DPAS-$Y^C$
g
$Y^N$-GS
+ HL1-$Y^C$
20 µm




None of these interactions have been reported previously, however they do provide support for all the reported interactions in Figure 3.5, increasing their reliability. The SGD PPIs that I have observed in Figures 3.5 and 3.6 are summarized in Figure 3.7.

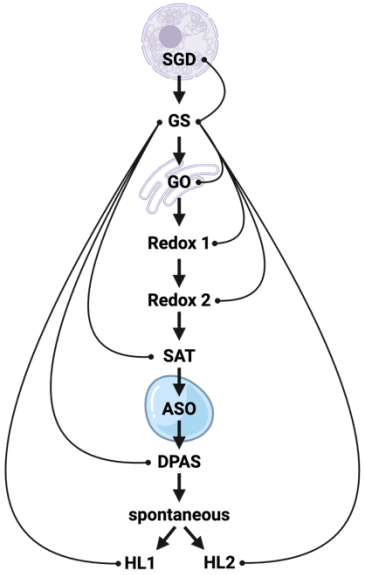



**Figure 3.7: GS BiFC protein-protein interaction map.** PPIs are indicated by curved lines between enzymes in the biosynthetic pathway to catharanthine and tabersonine. GS interacts with SGD, GO, Redox1, Redox2, SAT, DPAS, HL1, and HL2. However, it is not observed to interact with ASO.

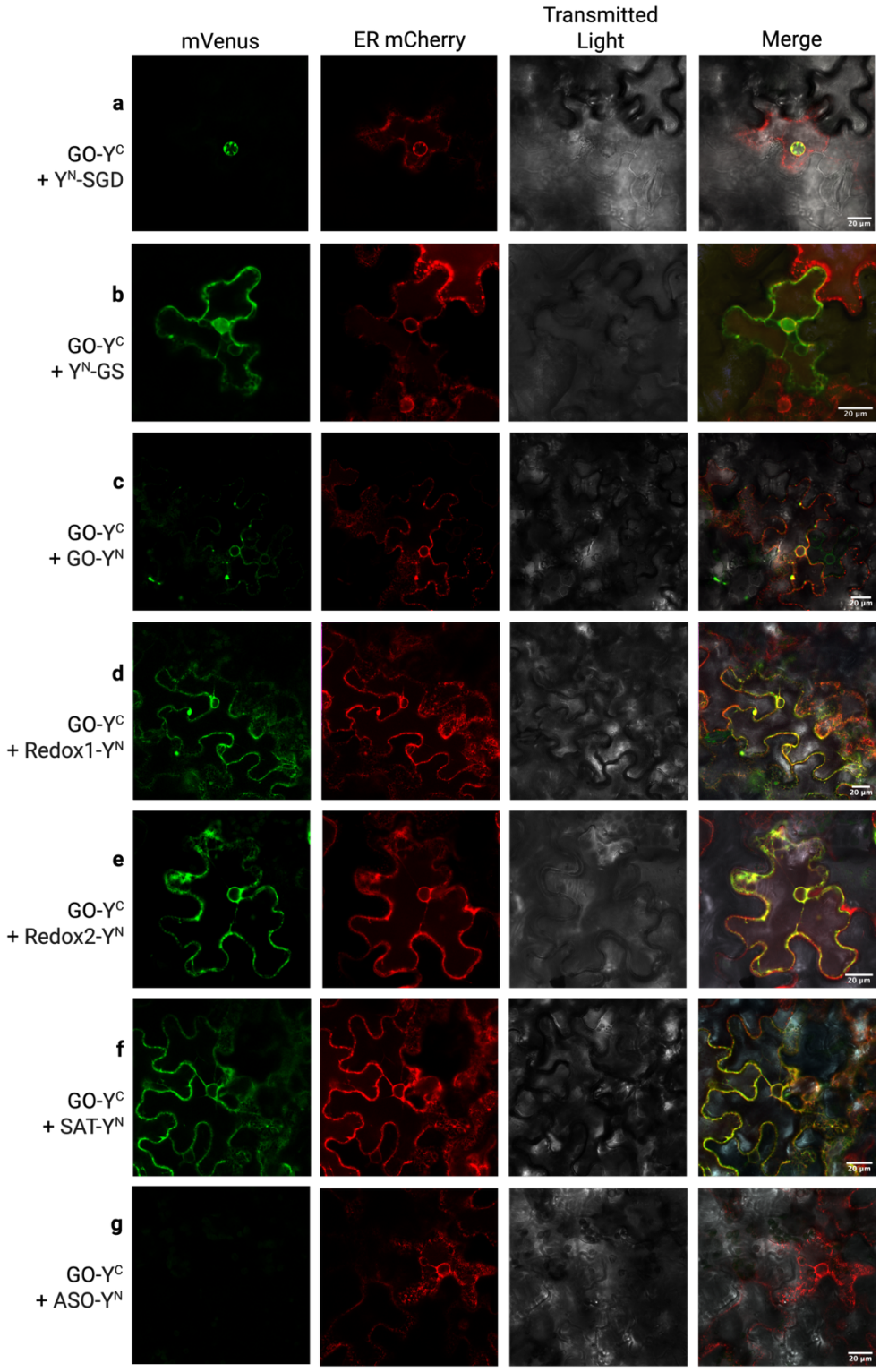
Notably, GS does not contain a nuclear localization signal, unlike SGD, but is localizing inside the nucleus with SGD (Figure 3.5, a; Figure 3.6, a). As discussed in Section 3.2, this change from cytosolic to nuclear location could be happening for several reasons. Additionally, we observe that GS-$Y^C$ and ASO-$Y^N$ (Figure 3.5, g) do not produce mVenus fluorescence, which is discussed in detail in Section 3.9.

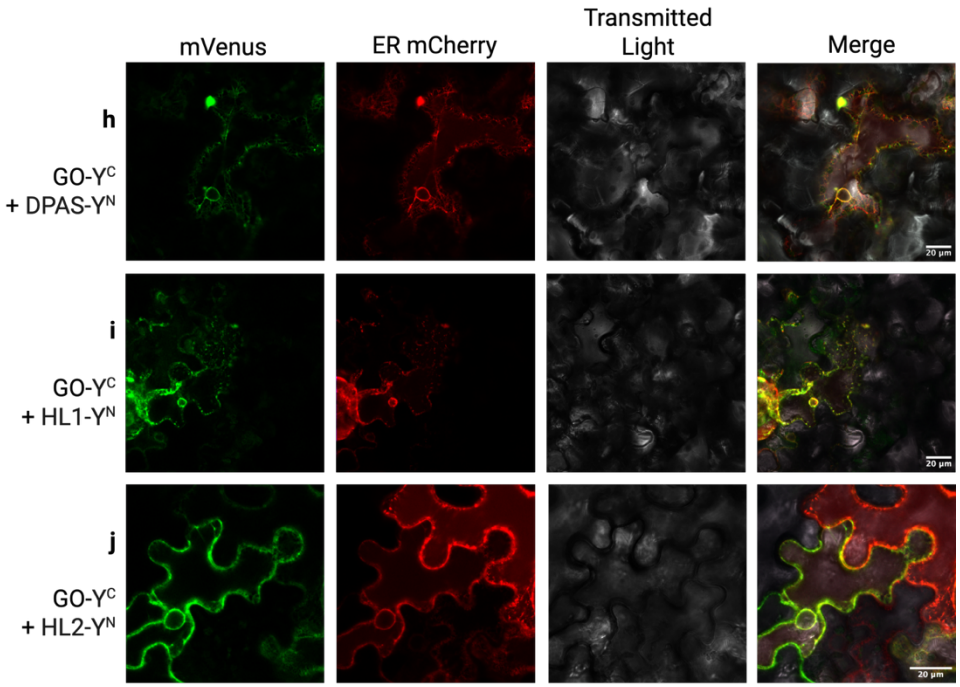
However, an inconsistency is that the interaction between GS and GO occur in different subcellular compartments depending on the orientation of the BiFC tag. With $Y^N$-GS and GO-$Y^C$, fluorescence is clearly on the ER (Figure 3.5, c), while $Y^C$-GS and GO-$Y^N$ fluorescence is found in the cytoplasm (Figure 3.6, c). This could indicate that an underlying mechanism is able to traffic GO from the ER and into the cytoplasm to meet GS. This would be a unique phenomenon, as GO is a Cytochrome P450, and therefore classically found on the ER due to their N-terminal signal peptide, and GS is considered cytosolic enzyme with no localization signal. This conflict in subcellular localization indicates that this interaction can occur in different subcellular localizations and may be spatially dynamic.

### 3.5 *C. roseus* Geissoschizine Oxidase (GO) BiFC in *N. benthamiana*

Next in the biosynthetic pathway is GO. First, I tagged GO with $mVenus^C$ on the C-terminus (Figure 3.8). Figure 3.8 shows that GO-$Y^C$ interacts with itself and all other inspected enzymes in this pathway, except ASO (Figure 3.8, g). The assembly of a mVenus fluorophore was observed in three distinct subcellular compartments: GO-$Y^C$ and $Y^N$-SGD interact on the nuclear membrane, which is considered continuous with the ER (Figure 3.8, a); GO-$Y^C$ and $Y^N$-GS interact in the cytoplasm (Figure 3.8, b); and GO-$Y^C$ and GO-$Y^N$, -Redox1, -Redox2, -SAT, -DPAS, -HL1, and -HL2 interact on the ER (Figure 3.8, c-f, h-j). Additionally, GO-$Y^C$ and ASO-$Y^N$ (Figure 3.8, g) do not produce mVenus fluorescence. This could be a result of no protein interaction, or unfavourable fluorescent tag geometry that prevents a positive BiFC result (discussed in further detail in Section 3.9).

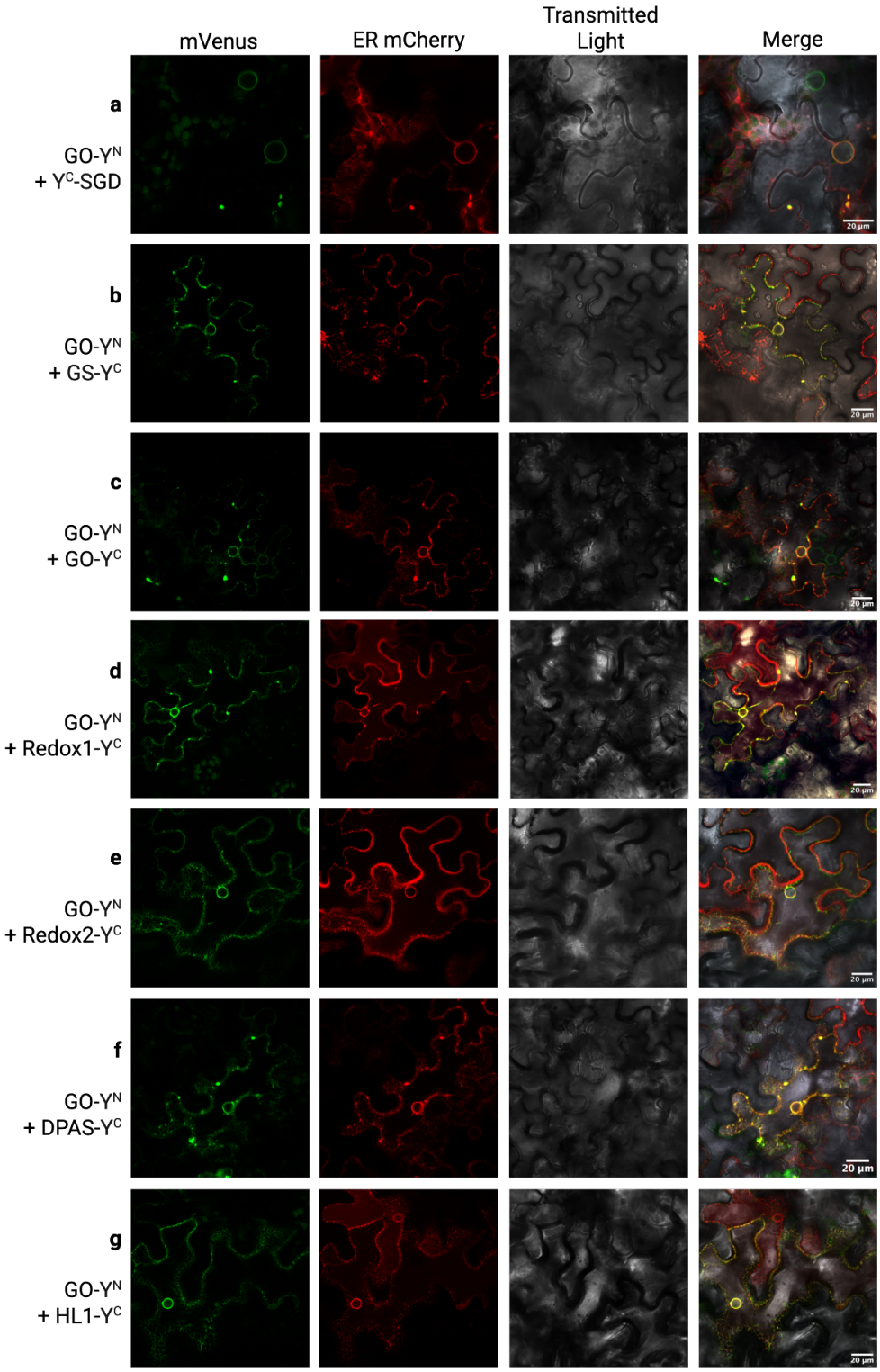
**Figure 3.8: Bimolecular fluorescence (BiFC) assay of mVenus$^{C}$ tagged *C. roseus* GO and mVenus$^{N}$ tagged SGD, GS, GO, Redox1, Redox2, SAT, ASO, DPAS, HL1, HL2 in *N. benthamiana* epidermal cells illustrate protein-protein interactions.** Confocal microscopy was used to capture fluorescent signals after transient expression of the constructs. mVenus fluorescence is generated when mVenus$^{N}$ and mVenus$^{C}$ are brought into proximity through the protein-protein interaction of the fused proteins. a-j, mVenus$^{C}$ was fused to the C-terminus of GO; a-b, mVenus$^{N}$ is fused to the N-termini of SGD and GS; c-j, mVenus$^{N}$ was fused to the C-termini of GO, Redox1, Redox2, SAT, ASO, DPAS, HL1, and HL2. Subcellular localization was determined using: c, C-terminal tagged HDEL-mCherry as an ER marker; g, C-terminal tagged tonoplast-mCherry as a tonoplast marker. Visual green colour corresponds to mVenus fluorescence, red to mCherry fluorescence, yellow to merged mVenus and mCherry fluorescence, and greyscale for transmitted light. Scale bars indicate 20 μm.

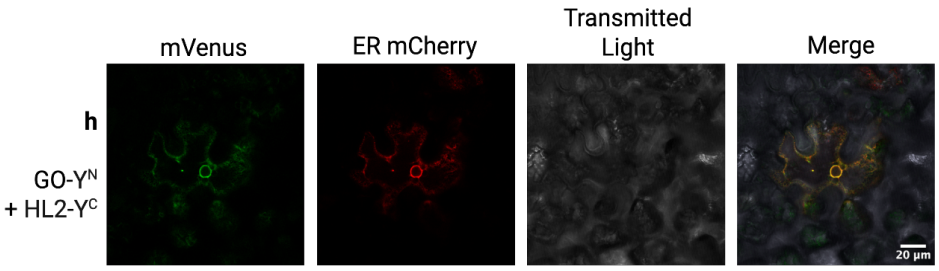

mVenus
ER mCherry
Transmitted Light
Merge
a
GO-Y^C + Y^N-SGD
b
GO-Y^C + Y^N-GS
c
GO-Y^C + GO-Y^N
d
GO-Y^C + Redox1-Y^N
e
GO-Y^C + Redox2-Y^N
f
GO-Y^C + SAT-Y^N
g
GO-Y^C + ASO-Y^N
20 µm




Then we preformed BiFC surveys with mVenus$^{N}$ on the C-terminus of GO (Figure 3.9), importantly demonstrating the opposite mVenus tagging as Figure 3.8. In alignment with Figure 3.8, Figure 3.9 indicates that GO-Y$^{N}$ also interacts with itself and all other enzymes inspected in this pathway. The assembly of a mVenus fluorophore was observed in two distinct subcellular compartments: GO-Y$^{N}$ and Y$^{C}$-SGD interact on the nuclear membrane (Figure 3.9, a); and GO-Y$^{N}$ and Y$^{C}$-GS, GO-, Redox1-, Redox2-, DPAS-, HL1-, and HL2- are all observed to interact on the ER (Figure 3.9, b-h).

**Figure 3.9: Bimolecular fluorescence (BiFC) assay of mVenus$^{N}$ tagged *C. roseus* GO and mVenus$^{C}$ tagged SGD, GS, GO, Redox1, Redox2, DPAS, HL1, HL2 in *N. benthamiana* epidermal cells illustrate protein-protein interactions.** Confocal microscopy was used to capture fluorescent signals after transient overexpression of the constructs. mVenus fluorescence is generated when mVenus$^{N}$ and mVenus$^{C}$ are brought into proximity through the protein-protein interaction of the fused proteins. a-h, mVenus$^{N}$ was fused to the C-terminus of GO; a, mVenus$^{C}$ is fused to the N-termini of SGD; b-h, mVenus$^{C}$ was fused to the C-termini of GS, GO, Redox1, Redox2, DPAS, HL1, and HL2. d, Subcellular localization was determined using C-terminal tagged HDEL-mCherry as an ER marker. Visual green colour corresponds to mVenus fluorescence, red to mCherry fluorescence, yellow to merged mVenus and mCherry fluorescence, and greyscale for transmitted light. Scale bars indicate 20 µm.


mVenus
ER mCherry
Transmitted Light
Merge
a
GO-Y^N + Y^C-SGD
b
GO-Y^N + GS-Y^C
c
GO-Y^N + GO-Y^C
d
GO-Y^N + Redox1-Y^C
e
GO-Y^N + Redox2-Y^C
f
GO-Y^N + DPAS-Y^C
g
GO-Y^N + HL1-Y^C
20 µm




Importantly, I observe that GO interacts with GO (Figure 3.8, c), which confirms it forms homodimers (Figure 3.8, c; Figure 3.9, c). This is consistent with the literature consensus, as Cytochrome P450s have been shown to form homodimers and high-order oligomers on the ER[9]. Meanwhile, I observe that SGD and GO interact specifically on the nuclear membrane (Figure 3.8, a; Figure 3.9, a). This indicates that SGD is not exiting the nucleus, and GO is not entering the nucleus and is instead remaining on the ER. I hypothesize that SGD and GO may interact across the nuclear membrane, although I cannot speculate how this interaction is occurring.

Aligning with Section 3.4, we again observe interactions between GO-$Y^C$ and $Y^N$-GS in the cytoplasm (Figure 3.8, c) and GO-$Y^N$ and $Y^C$-GS on the ER (Figure 3.9, c). Explanations as to why this is occurring is briefly discussed in Section 3.4. Further, we recognize that Redox1, Redox2, SAT, DPAS, HL1, and HL2 do not contain an ER signal peptide, yet they are observed to localize on the ER with GO (Figure 3.8 d-f, h-j; Figure 3.9 d-h). This could indicate an underlying mechanism which directs these enzymes onto the ER to meet GO, or that GO is outwardly facing on the ER membrane and able to interact with cytosolic enzymes. Regardless, these interactions are notable and have not been previously reported. The GO PPIs that I have observed in Figures 3.8 and 3.9 are summarized in Figure 3.10.

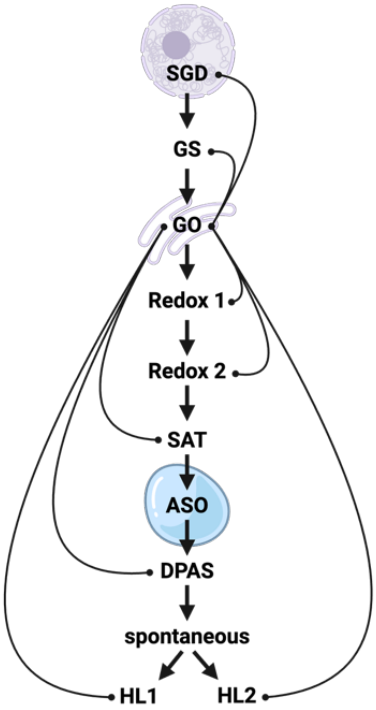
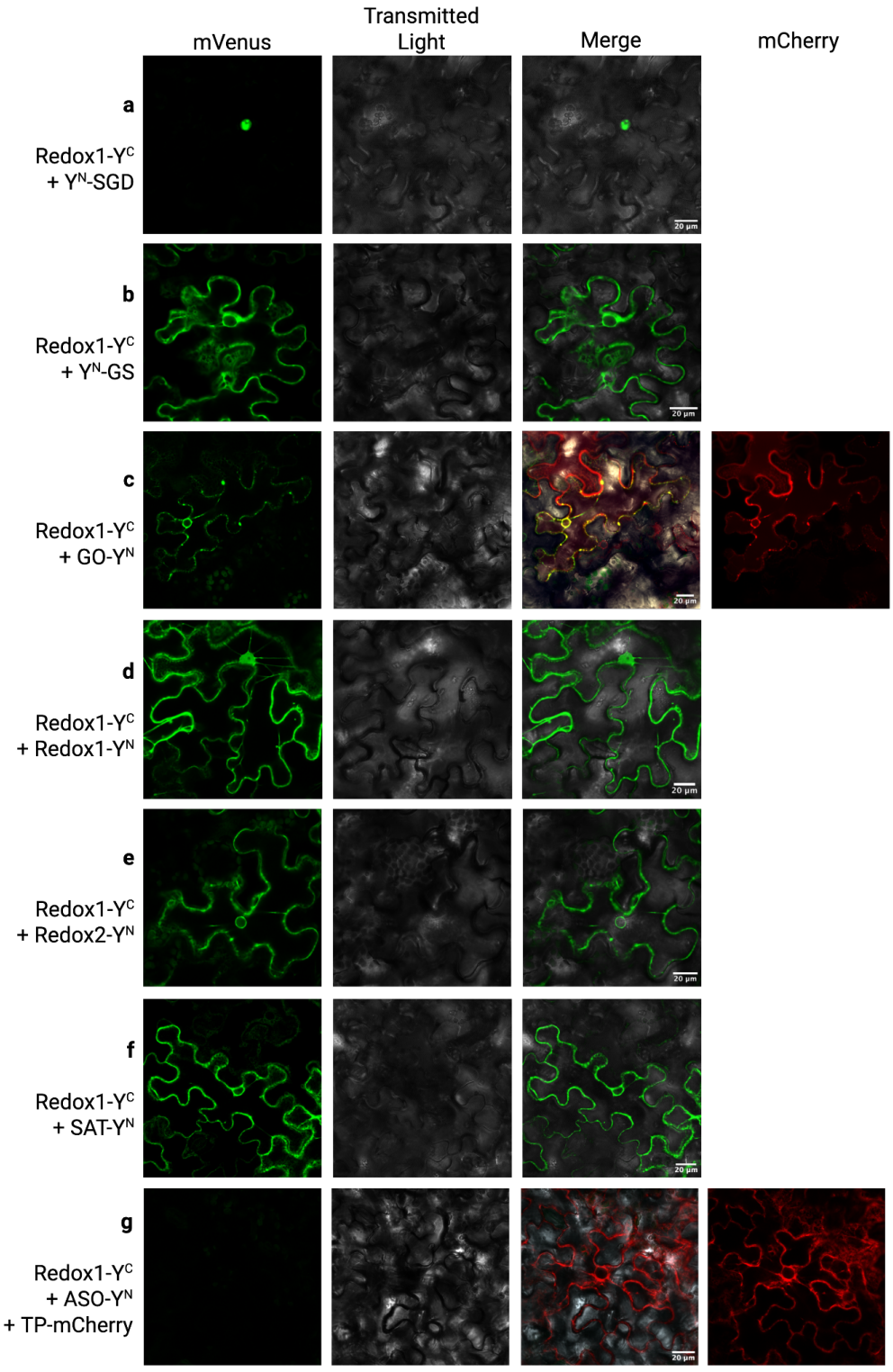


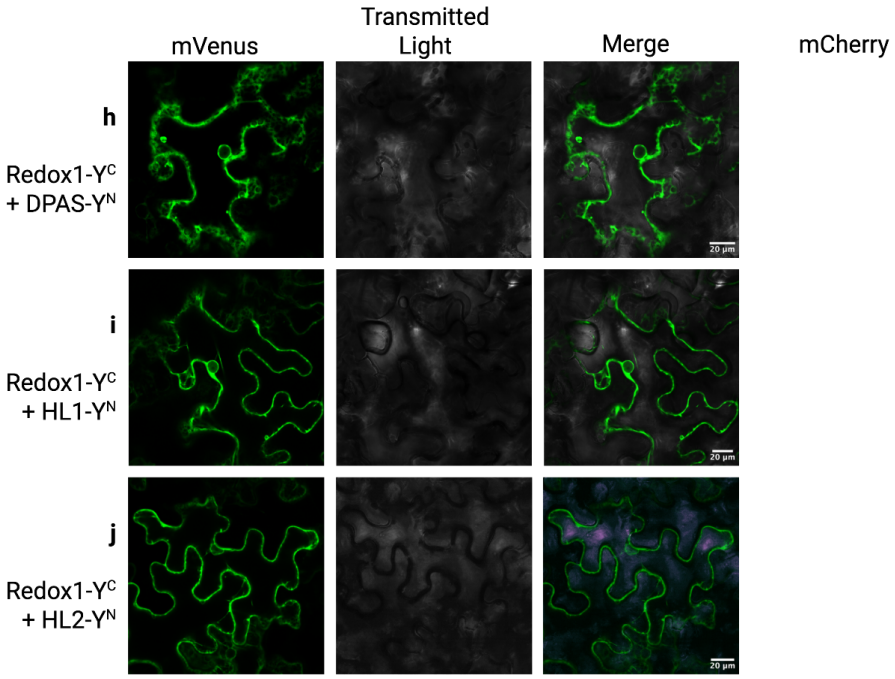

**Figure 3.10: GO BiFC protein-protein interaction map.** PPIs are indicated by curved lines between enzymes in the biosynthetic pathway to catharanthine and tabersonine. GO interacts with SGD, GS, Redox1, Redox2, SAT, DPAS, HL1, and HL2. However, it is not observed to interact with ASO.

### 3.6 *C. roseus* Oxidoreductase I (Redox1) BiFC in *N. benthamiana*

Moving down the biosynthetic pathway is Redox1. I began with tagging Redox1 with mVenus$^{C}$ on the C-terminus (Figure 3.11). Figure 3.11 shows that Redox1-Y$^{C}$ interacts with itself and all other inspected enzymes in this pathway, except ASO (Figure 3.11, g). The assembly of a mVenus fluorophore was observed in three distinct subcellular compartments: Redox1-Y$^{C}$ and Y$^{N}$-SGD interact in the nucleus (Figure 3.11, a); Redox1-Y$^{C}$ and Y$^{N}$-GS, -Redox1, -Redox2, -SAT, -DPAS, -HL1, and -HL2 (Figure 3.11, b, d-f, h-j) interact in the cytoplasm; and Redox1-Y$^{C}$ and GO-Y$^{N}$ interact on the ER (Figure 3.11, c).

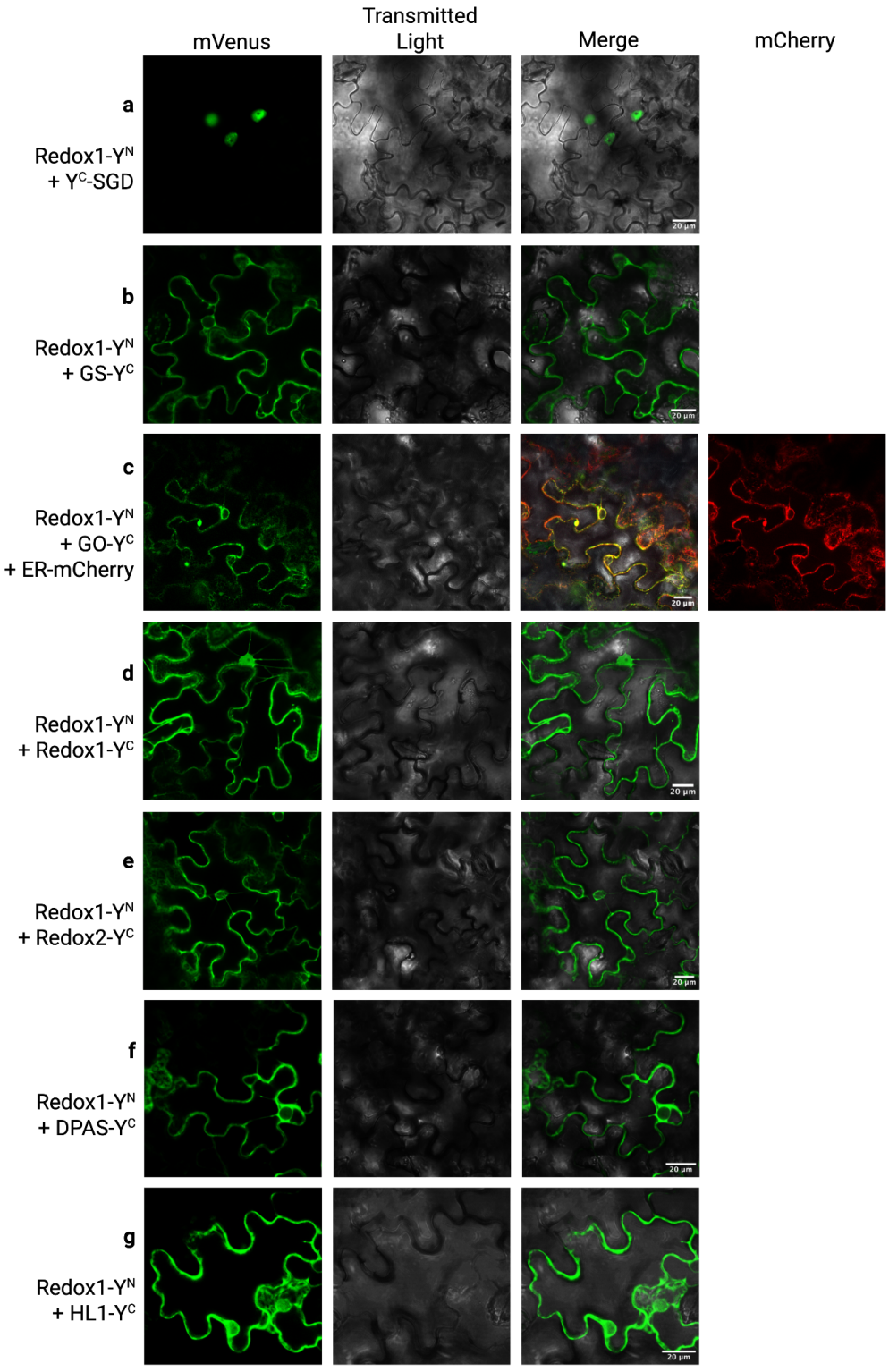
**Figure 3.11: Bimolecular fluorescence (BiFC) assay of mVenus$^{C}$ tagged *C. roseus* Redox1 and mVenus$^{N}$ tagged SGD, GS, GO, Redox1, Redox2, SAT, ASO, DPAS, HL1, HL2 in *N. benthamiana* epidermal cells illustrates protein-protein interactions.** Confocal microscopy was used to capture fluorescent signals after transient expression of the constructs. mVenus fluorescence is generated when mVenus$^{N}$ and mVenus$^{C}$ are brought into proximity through the protein-protein interaction of the fused proteins. **a-j**, mVenus$^{C}$ was fused to the C-terminus of Redox1; **a-b**, mVenus$^{N}$ is fused to the N-termini of SGD and GS; **c-j**, mVenus$^{N}$ was fused to the C-termini of GO, Redox1, Redox2, SAT, ASO, DPAS, HL1, and HL2. Subcellular localization was determined using: **c**, C-terminal tagged HDEL-mCherry as an ER marker; **g**, C-terminal tagged tonoplast-mCherry as a tonoplast marker. Visual green colour corresponds to mVenus fluorescence, red to mCherry fluorescence, yellow to merged mVenus and mCherry fluorescence, and greyscale for transmitted light. Scale bars indicate 20 μm.

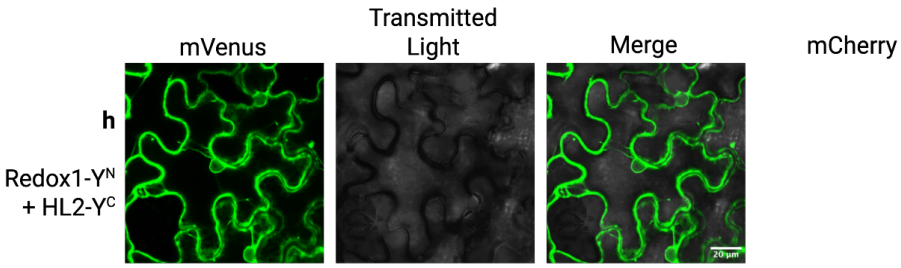

mVenus
Transmitted Light
Merge
mCherry
a
Redox1-Y^C + Y^N-SGD
b
Redox1-Y^C + Y^N-GS
c
Redox1-Y^C + GO-Y^N
d
Redox1-Y^C + Redox1-Y^N
e
Redox1-Y^C + Redox2-Y^N
f
Redox1-Y^C + SAT-Y^N
g
Redox1-Y^C + ASO-Y^N + TP-mCherry
20 µm




Sequentially, BiFC surveys with mVenus$^{N}$ on the C-terminus of Redox1 were preformed (Figure 3.12) which illustrates the reciprocal mVenus tagging as shown in Figure 3.11. Consistent with Figure 3.11, Figure 3.12 indicates that Redox1- $Y^{N}$ also interacts with itself and all other enzymes inspected in this pathway. The assembly of a mVenus fluorophore was observed in two distinct subcellular compartments: Redox1-$Y^{N}$ and $Y^{C}$-SGD interact in the nucleus (Fig. 3.12, a); Redox1-$Y^{N}$and $Y^{C}$-GS, Redox1-, Redox2-, DPAS-, HL1-, and HL2- are all observed to interact in the cytoplasm (Fig. 3.6, b-h); and Redox1- $Y^{N}$ and GO-$Y^{C}$ interact on the ER.

**Figure 3.12: Bimolecular fluorescence (BiFC) assay of mVenus$^{N}$ tagged *C. roseus* Redox1 and mVenus$^{C}$ tagged SGD, GS, GO, Redox1, Redox2, DPAS, HL1, HL2 in *N. benthamiana* epidermal cells illustrates protein-protein interactions.** Confocal microscopy was used to capture fluorescent signals after transient overexpression of the constructs. mVenus fluorescence is generated when mVenus$^{N}$ and mVenus$^{C}$ are brought into proximity through the protein-protein interaction of the fused proteins. **a-h**, mVenus$^{N}$ was fused to the C-terminus of Redox1; **a-b**, mVenus$^{N}$ is fused to the N-termini of SGD and GS; **c-h**, mVenus$^{N}$ was fused to the C-termini of GO, Redox1, Redox2, DPAS, HL1, and HL2. **c**, Subcellular localization was determined using C-terminal tagged HDEL-mCherry as an ER marker. Visual green colour corresponds to mVenus fluorescence, red to mCherry fluorescence, yellow to merged mVenus and mCherry fluorescence, and greyscale for transmitted light. Scale bars indicate 20 μm.


mVenus
Transmitted Light
Merge
mCherry
a
Redox1-Y^N + Y^C-SGD
b
Redox1-Y^N + GS-Y^C
c
Redox1-Y^N + GO-Y^C + ER-mCherry
d
Redox1-Y^N + Redox1-Y^C
e
Redox1-Y^N + Redox2-Y^C
f
Redox1-Y^N + DPAS-Y^C
g
Redox1-Y^N + HL1-Y^C
20 µm




The observed interactions with SGD in the nucleus (Figure 3.11, a; Figure 3.12, a) are discussed in Section 3.2. Additionally, the cytosolic Redox1 clearly interacts with GO on the ER (Figure 3.11, c; Figure 3.12, c), which is further discussed in Section 3.5. In contrast, Redox1 and ASO (Figure 3.11, g) do not produce mVenus fluorescence, which is examined in Section 3.9. The observed Redox1 PPIs from Figures 3.11 and 3.12 are summarized in Figure 3.13.

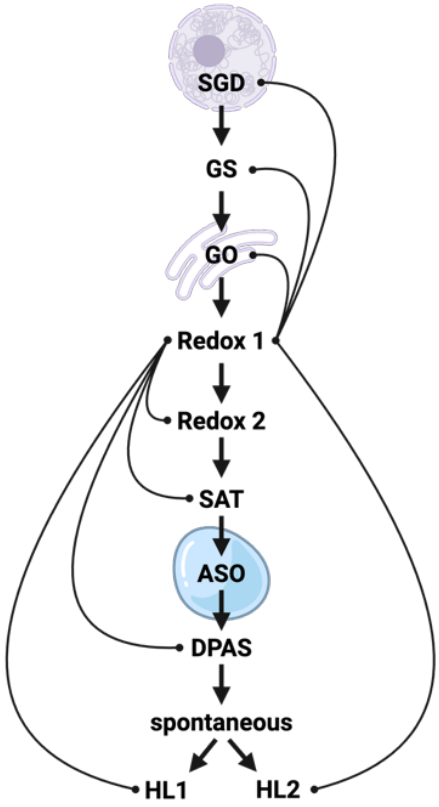
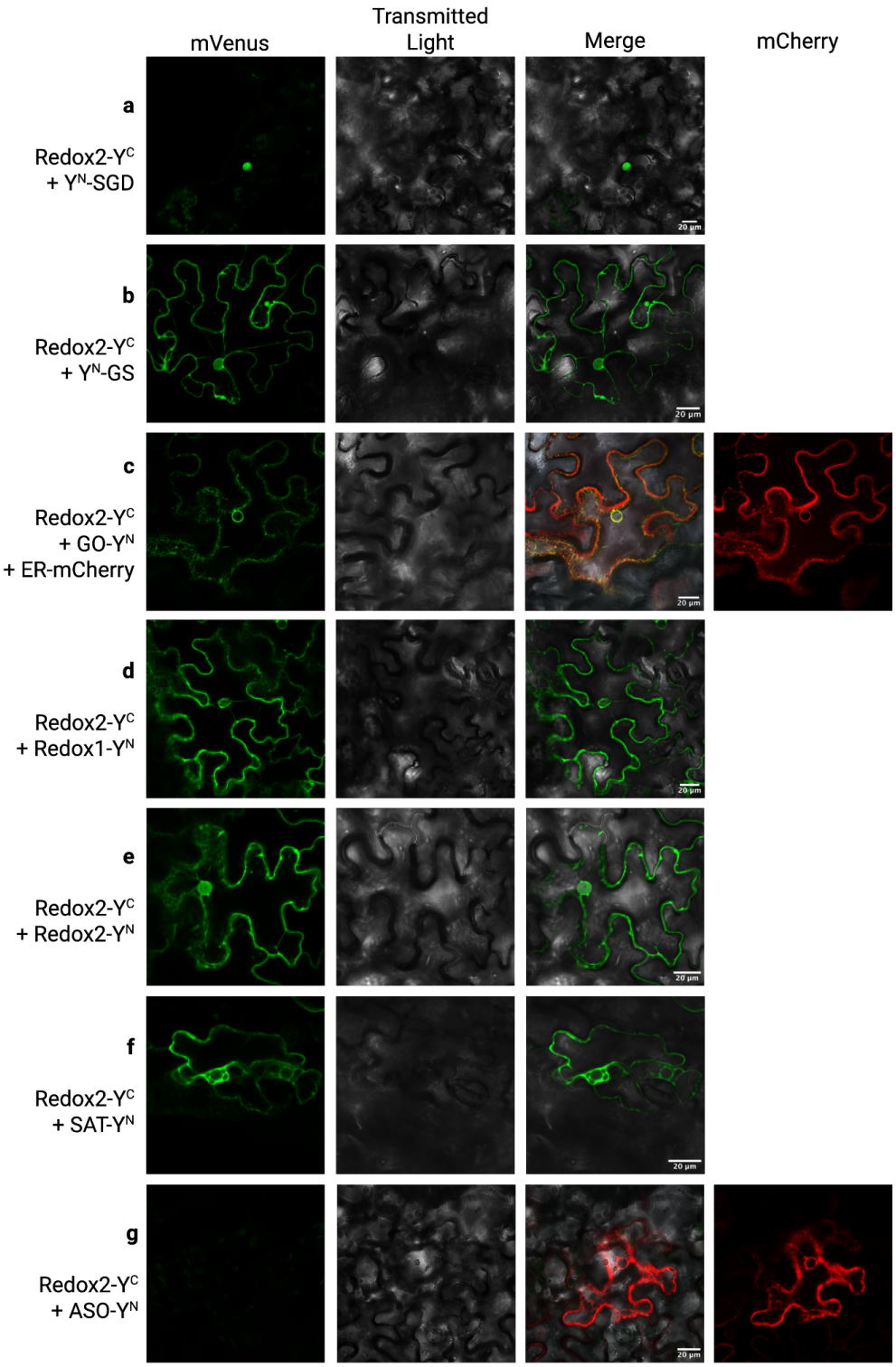


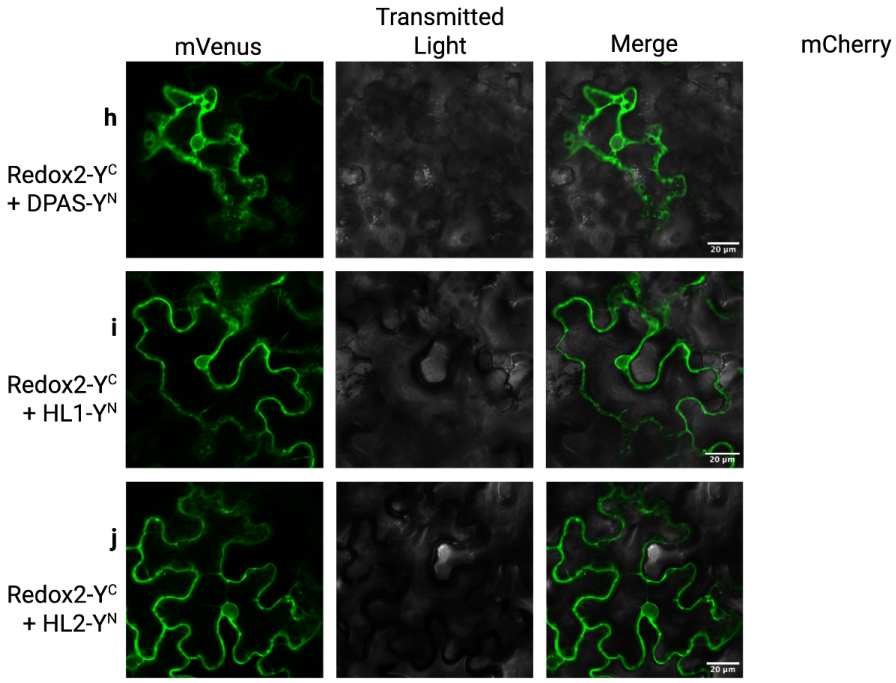

**Figure 3.13: Redox1 BiFC protein-protein interaction map.** PPIs are indicated by curved lines between enzymes in the biosynthetic pathway to catharanthine and tabersonine. Redox1 interacts with SGD, GS, GO, Redox2, SAT, DPAS, HL1, and HL2. However, it is not observed to interact with ASO.

### 3.7 *C. roseus* Oxidoreductase II (Redox2) BiFC in *N. benthamiana*

The next enzyme in the biosynthetic pathway is Redox2. I began with tagging Redox2 with mVenus$^{C}$ on the C-terminus (Figure 3.14). Figure 3.14 shows that Redox2-Y$^{C}$ interacts with itself and all other inspected enzymes in this pathway, except ASO (Figure 3.14, g). The assembly of a mVenus fluorophore was observed in three distinct subcellular compartments: Redox2-Y$^{C}$ and Y$^{N}$-SGD interact in the nucleus (Figure 3.14, a); Redox2-Y$^{C}$ and Y$^{N}$-GS, -Redox1, -Redox2, -SAT, -DPAS, -HL1, and -HL2 (Figure 3.14, b, d-f, h-j) interact in the cytoplasm; and Redox2-Y$^{C}$ and GO-Y$^{N}$ interact on the ER (Figure 3.14, c).

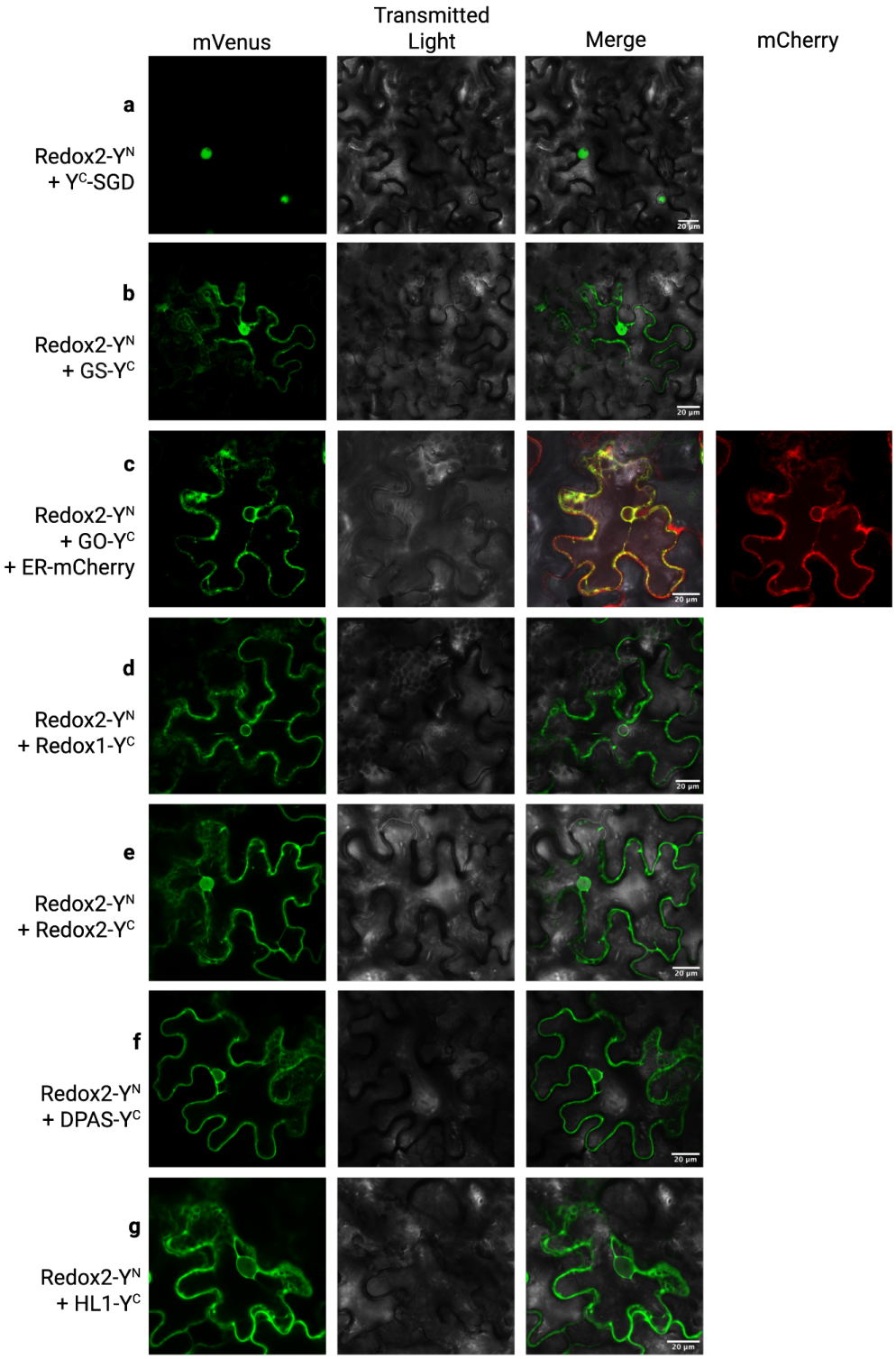
**Figure 3.14: Bimolecular fluorescence (BiFC) assay of mVenus$^{C}$ tagged *C. roseus* Redox2 and mVenus$^{N}$ tagged SGD, GS, GO, Redox1, Redox2, SAT, ASO, DPAS, HL1, HL2 in N. benthamiana epidermal cells illustrates protein-protein interactions.** Confocal microscopy was used to capture fluorescent signals after transient expression of the constructs. mVenus fluorescence is generated when mVenusN and mVenusC are brought into proximity through the protein-protein interaction of the fused proteins. **a-j**, mVenusC was fused to the C-terminus of Redox2; **a-b**, mVenusN is fused to the N-termini of SGD, and GS; **c-j**, mVenusN was fused to the C-termini of GO, Redox1, Redox2, SAT, ASO, DPAS, HL1, and HL2. Subcellular localization was determined using: **c**, C-terminal tagged HDEL-mCherry as an ER marker; **g**, C-terminal tagged tonoplast-mCherry as a tonoplast marker. Visual green colour corresponds to mVenus fluorescence, red to mCherry fluorescence, yellow to merged mVenus and mCherry fluorescence, and greyscale for transmitted light. Scale bars indicate 20 μm.

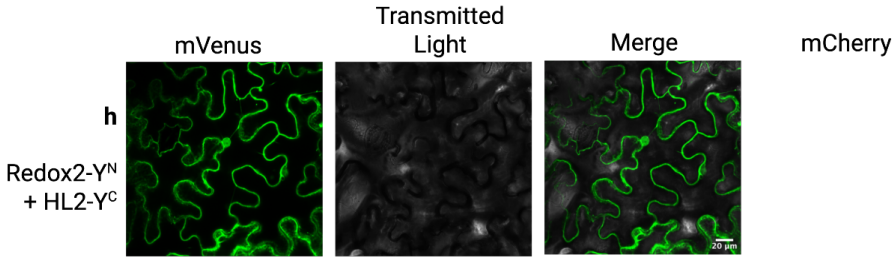

mVenus
Transmitted Light
Merge
mCherry
a
Redox2-Y^C + Y^N-SGD
b
Redox2-Y^C + Y^N-GS
c
Redox2-Y^C + GO-Y^N + ER-mCherry
d
Redox2-Y^C + Redox1-Y^N
e
Redox2-Y^C + Redox2-Y^N
f
Redox2-Y^C + SAT-Y^N
g
Redox2-Y^C + ASO-Y^N
20 µm




Then, I preformed BiFC surveys with mVenus$^{N}$ on the C-terminus of Redox2 (Figure 3.15) which illustrates the reciprocal mVenus tagging than shown in Figure 3.14. Consistent with Figure 3.14, Figure 3.15 indicates that Redox2-Y$^{N}$ also interacts with itself and all other enzymes inspected in this pathway. The assembly of a mVenus fluorophore was observed in three distinct subcellular compartments: Redox2-Y$^{N}$ and Y$^{C}$-SGD interact in the nucleus (Figure 3.15, a); Redox2-Y$^{N}$ and Y$^{C}$-GS, Redox1-, Redox2-, DPAS-, HL1-, and HL2- are all observed to interact in the cytoplasm (Figure 3.15, b, d-h); and Redox2- Y$^{N}$ and GO-Y$^{C}$ interact on the ER (Figure 3.15, c).

**Figure 3.15: Bimolecular fluorescence (BiFC) assay of mVenus$^{N}$ tagged *C. roseus* Redox2 and mVenus$^{C}$ tagged SGD, GS, GO, Redox1, Redox2, DPAS, HL1, HL2 in *N. benthamiana* epidermal cells illustrate protein-protein interactions.** Confocal microscopy was used to capture fluorescent signals after transient overexpression of the constructs. mVenus fluorescence is generated when mVenus$^{N}$ and mVenus$^{C}$ are brought into proximity through the protein-protein interaction of the fused proteins. a-h, mVenus$^{N}$ was fused to the C-terminus of Redox2; a, mVenus$^{C}$ is fused to the N-terminus of SGD; b-h, mVenus$^{C}$ was fused to the C-termini of GS, GO, Redox1, Redox2, DPAS, HL1, and HL2. c, Subcellular localization was determined using C-terminal tagged HDEL-mCherry as an ER marker. Visual green colour corresponds to mVenus fluorescence, red to mCherry fluorescence, yellow to merged mVenus and mCherry fluorescence, and greyscale for transmitted light. Scale bars indicate 20 µm.


mVenus
Transmitted Light
Merge
mCherry
a
Redox2-YN + YC-SGD
b
Redox2-YN + GS-YC
c
Redox2-YN + GO-YC + ER-mCherry
d
Redox2-YN + Redox1-YC
e
Redox2-YN + Redox2-YC
f
Redox2-YN + DPAS-YC
g
Redox2-YN + HL1-YC
20 µm




The observed Redox2 interactions with SGD in the nucleus (Figure 3.14, a; Figure 3.15, a) are discussed in Section 3.2. Additionally, the cytosolic Redox2 clearly interacts with GO on the ER (Figure 3.14, c; Figure 3.15, c), which is further discussed in Section 3.5. In contrast, Redox2 and ASO (Figure 3.14, g) do not produce mVenus fluorescence, which is examined in Section 3.9. Importantly, none of these interactions in Figure 3.14 and Figure 3.15 have been reported previously and are summarized in Figure 3.16.

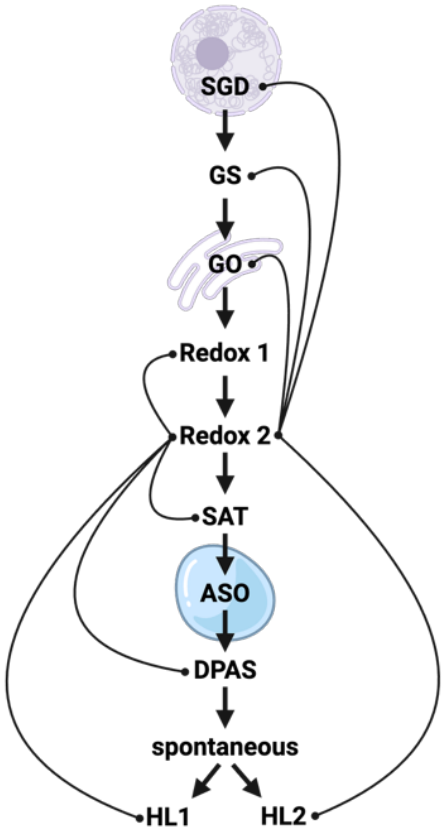
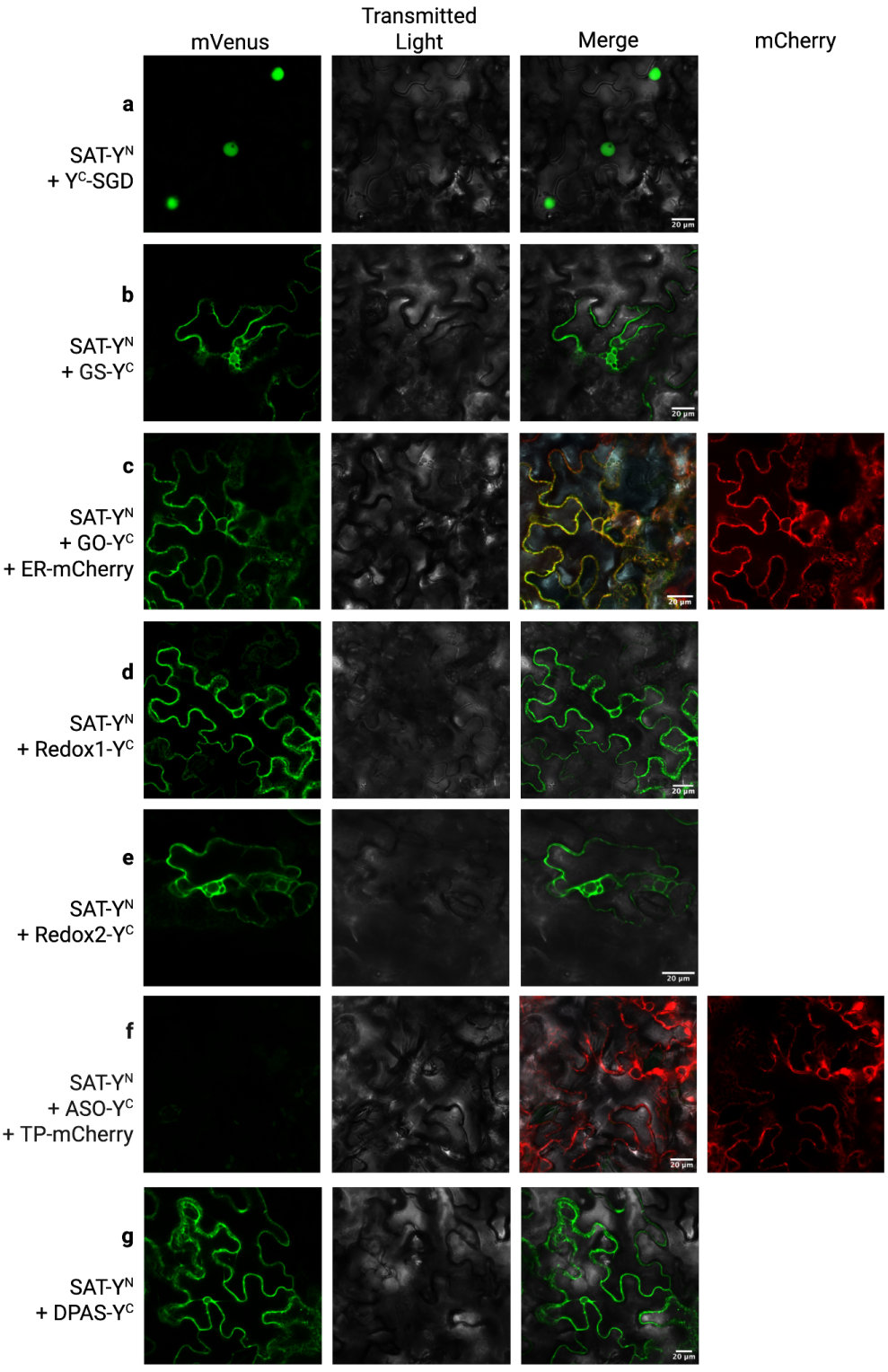


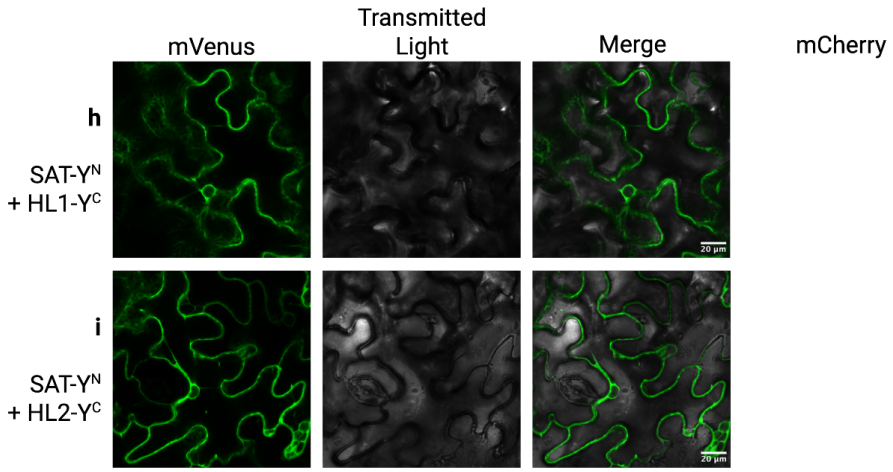

**Figure 3.16: Redox2 BiFC protein-protein interaction map.** PPIs are indicated by curved lines between enzymes in the biosynthetic pathway to catharanthine and tabersonine. Redox2 interacts with SGD, GS, GO, Redox1, SAT, DPAS, HL1, and HL2. However, it is not observed to interact with ASO.

### 3.8 *C. roseus* Stemmadenine Acetyltransferase (SAT) BiFC in *N. benthamiana*

The next enzyme in the biosynthetic pathway is SAT, and I tagged it with mVenus$^{N}$ on its C-terminus (Figure 3.17). The results in Figure 3.17 show that SAT-Y$^{N}$ interacts with itself and all other inspected enzymes in this pathway, except ASO. The assembly of a mVenus fluorophore was observed in three distinct subcellular compartments: SAT-Y$^{N}$ and Y$^{C}$-SGD interact in the nucleus (Figure 3.17, a); SAT-Y$^{N}$ and GS-, Redox1-, Redox2-, SAT-, DPAS-, HL1-, and HL2- (Figure 3.17, b, d-e, g-i) interact in the cytoplasm; and SAT-Y$^{N}$ and GO-Y$^{C}$ interact on the ER (Figure 3.17, c).

**Figure 3.17: Bimolecular fluorescence (BiFC) assay of mVenus$^{N}$ tagged *C. roseus* SAT and mVenus$^{C}$ tagged SGD, GS, GO, Redox1, Redox2, ASO, DPAS, HL1, HL2 in *N. benthamiana* epidermal cells illustrates protein-protein interactions.** Confocal microscopy was used to capture fluorescent signals after transient overexpression of the constructs. mVenus fluorescence is generated when mVenus$^{N}$ and mVenus$^{C}$ are brought into proximity through the protein-protein interaction of the fused proteins. **a-i**, mVenus$^{N}$ was fused to the C-terminus of SAT; **a**, mVenus$^{C}$ is fused to the N-terminus of SGD; **b-i**, mVenus$^{C}$ was fused to the C-termini of GS, GO, Redox1, Redox2, ASO, DPAS, HL1, and HL2. Subcellular localization was determined using: **c**, C-terminal tagged HDEL-mCherry as an ER marker; **g**, C-terminal tagged tonoplast-mCherry as a tonoplast marker. Visual green colour corresponds to mVenus fluorescence, red to mCherry fluorescence, yellow to merged mVenus and mCherry fluorescence, and greyscale for transmitted light. Scale bars indicate 20 μm.


mVenus
Transmitted Light
Merge
mCherry
a
SAT-YN + YC-SGD
b
SAT-YN + GS-YC
c
SAT-YN + GO-YC + ER-mCherry
d
SAT-YN + Redox1-YC
e
SAT-YN + Redox2-YC
f
SAT-YN + ASO-YC + TP-mCherry
g
SAT-YN + DPAS-YC
20 µm




Critically, none of the observed SAT interactions in Figure 3.17 have been reported previously. The observed interaction of SAT and SGD in the nucleus (Figure 3.17, a) is discussed in Section 3.2. Additionally, the cytosolic SAT clearly interacts with GO on the ER (Figure 3.17, c) which is further discussed in Section 3.5. In contrast, SAT and ASO (Figure 3.17, f) do not produce mVenus fluorescence, which is examined in Section 3.9. The observations from Figure 3.17 have been summarized in Figure 3.18.

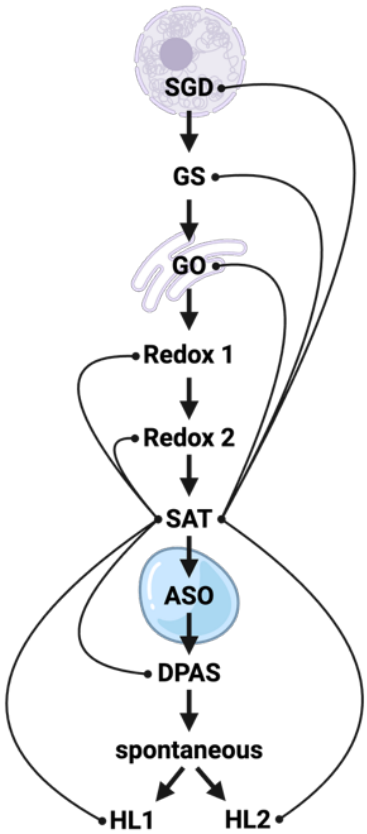
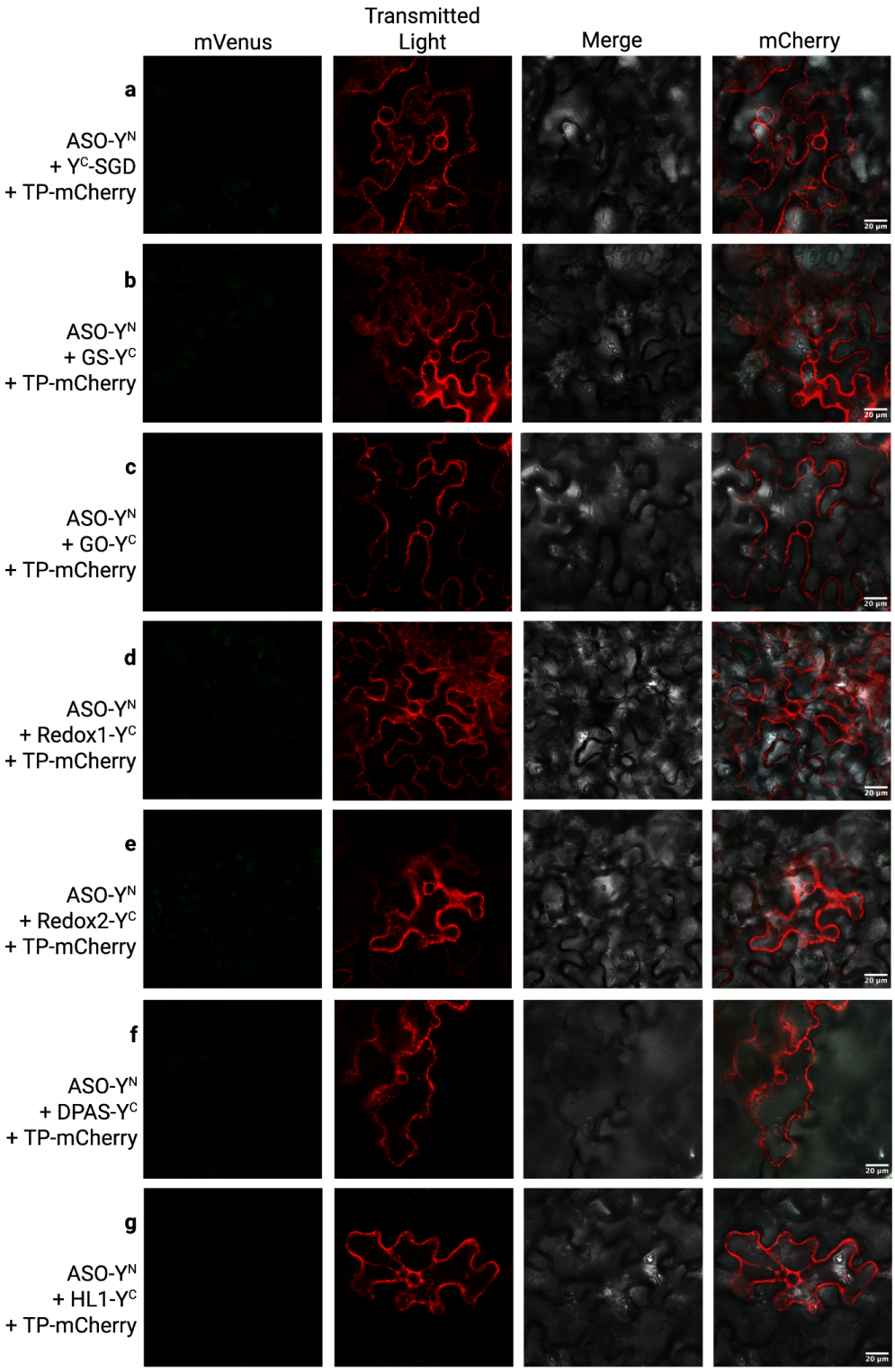


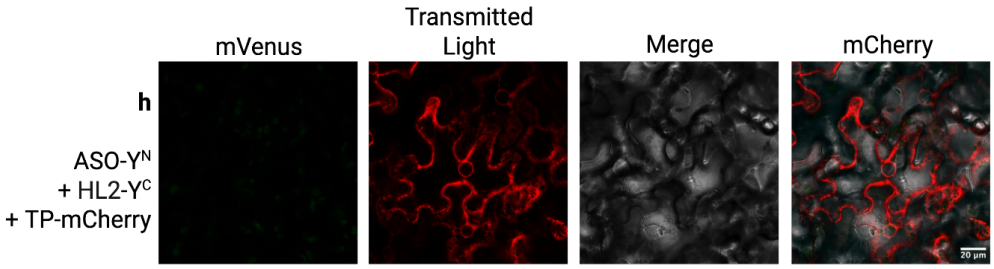

**Figure 3.18: SAT BiFC protein-protein interaction map.** PPIs are indicated by curved lines between enzymes in the biosynthetic pathway to catharanthine and tabersonine. SAT interacts with SGD, GS, GO, Redox1, Redox 2, DPAS, HL1, and HL2. However, it is not observed to interact with ASO.

### 3.9 *C. roseus* O-acetylstemmadenine oxidase (ASO) BiFC in *N. benthamiana*

Following SAT, the next enzymatic step is ASO. I tagged ASO with mVenus$^{N}$ on its C-terminus (ASO-Y$^{C}$) and did not observe any interactions with enzymes in the expected (Figure 3.19). The assembly of a mVenus fluorophore was not observed in any subcellular location.

**Figure 3.19: Bimolecular fluorescence (BiFC) assay of mVenus$^{N}$ tagged *C. roseus* ASO and mVenus$^{C}$ tagged SGD, GS, GO, Redox1, Redox2, DPAS, HL1, HL2 in *N. benthamiana* epidermal cells illustrates protein-protein interactions.** Confocal microscopy was used to capture fluorescent signals after transient overexpression of the constructs. mVenus fluorescence is generated when mVenus$^{N}$ and mVenus$^{C}$ are brought into proximity through the protein-protein interaction of the fused proteins. **a-h**, mVenus$^{N}$ was fused to the C-terminus of ASO; **a**, mVenus$^{C}$ is fused to the N-terminus of SGD; **b-h,** mVenus$^{C}$ was fused to the C-termini of GS, GO, Redox1, Redox2, DPAS, HL1, and HL2. **a-h,** Subcellular localization was determined using a C-terminal tagged tonoplast-mCherry as a tonoplast marker. Visual green colour corresponds to mVenus fluorescence, red to mCherry fluorescence, yellow to merged mVenus and mCherry fluorescence, and greyscale for transmitted light. Scale bars indicate 20 μm.


mVenus
Transmitted Light
Merge
mCherry
a
ASO-YN + YC-SGD + TP-mCherry
b
ASO-YN + GS-YC + TP-mCherry
c
ASO-YN + GO-YC + TP-mCherry
d
ASO-YN + Redox1-YC + TP-mCherry
e
ASO-YN + Redox2-YC + TP-mCherry
f
ASO-YN + DPAS-YC + TP-mCherry
g
ASO-YN + HL1-YC + TP-mCherry
20 µm




Intriguingly, ASO is the only enzyme of the ones we tested that does not show any PPIs. To speculate why ASO does not exhibit PPIs, we must recognize what makes the enzyme unique compared to others: its vacuolar localization. To elaborate, ASO is predicted to encode a N-terminal secretory signal peptide which directs the protein through the well-characterized secretory pathway into ER lumen and Golgi, where the protein is folded properly and glycosylated. Instead of being secreted to the apoplast as many secretory glycoproteins, ASO is sorted to the tonoplast, the membrane of the plant vacuole.

Because ASO interacts with the tonoplast membrane, it is possible that the orientation of the protein's interaction with the membrane may shield the $Y^N$ fragment from any potential interactions. For example, how the protein embeds in the membrane could result in the $Y^N$ fragment projecting into the vacuole, blocking it from interacting with the $Y^C$ fragment of the fusion proteins in the cytosol.

In contrast, how proteins are being trafficked around the cell (*i.e.* secretory system) from the Golgi apparatus may pose an additional issue; however, this notably is not an issue with the ER-localized GO or GFP-tagged ASO. The first step of the secretory system is the ER, as the protein (ex: ASO) is translated by the ribosomes located here. The ER is also a critical checkpoint for correct protein folding and assembly, acting as a stringent quality control enforcer[10]. Misfolded proteins are

recognized by molecular chaperons in the ER and retained in the lumen to attempt proper re-folding[11]. However, if there are repeatedly misfolded proteins, they are transported to the cytoplasm and degraded by the plant's proteosome system[12]. First, it is possible that the topology of the $Y^C$ fragment may not favour the reconstruction of a mVenus fluorophore, and therefore, results in negative BiFC in all tested combinations. Second, it is possible that the $Y^N$ tag is causing the ASO fusion protein to misfold repeatedly, and it is therefore its being sent to the cytosol to be degraded by the plant's ubiquitin proteosome system (UPS). Inherently, this means that the ASO-$Y^N$ would not actually be present in the cells and is therefore why no mVenus signal is present in any of the assays (Figure 3.19, a-h).

Another explanation is that ASO-$Y^N$ is being folded correctly, however the C-terminal $Y^N$ tag is interfering with ASO's C-terminal vacuolar signal peptide. As previously described, the ER is the first step of the secretory pathway and where proteins are folded. Proteins that are to be secreted (i.e. ASO), contain a hydrophobic ER signal sequence of 20-25 amino acids on their N-terminus. Importantly, this hydrophobic signal sequence will insert into the ER membrane and will be cleaved by ER signal peptidases. This removes the N-terminal signal sequence on secreted proteins. For this reason, it is important that we do not put the $Y^N$ tag on the N-terminus of the fusion protein as it will lead to the loss of this tag, as the secretory signal peptide will by cleaved when the glycoproteins are fully matured during the secretory pathway modification[13]. However, it is possible that we construct the ASO construct in such a way where the $Y^N$ tag is embedded between the N-terminal secretory peptide and the remaining ASO protein,

however, this will need to be experimentally tested because it could cause protein misfolding.

Continuing the second step of the secretory system, the protein will be transported from the ER to the Golgi via Coat Protein Complex II (COPII) vesicles, the major sorting station of the cell[14]. Here, it is possible that the C-terminal $Y^N$ tag may be interfering with the Golgi's recognition of the Vacuolar Sorting Determinants (VSDs) on the protein's C-terminus. Without the recognition of the VSD motif, the protein may be secreted to the surface of the cell[15]. However, this is unlikely as I did observe the GFP C-terminal tag on ASO in the tonoplast (Fig. 3.1, g).

Alternatively, the Golgi may recognize ASO's VSD and will secrete the protein to the vacuole. Here, C-terminal VSDs are commonly cleaved by vacuolar proteases after protein maturation and vacuolar sorting, which could possibly interfere or remove the $Y^N$ tag from ASO[16]. Essentially, vacuolar proteins have a signal peptide on both their N-terminus and C-terminus, critical to their proper secretion, and are both cleaved by proteases at different points in the secretion system[13]. Naturally, this complicates fluorescent tagging at either end of the protein. However, this is not an issue for GFP-tagged ASO (Figure 3.1, g), meaning these interactions could be true negatives. Finally, this brings us to the final option, where the reality is that ASO simply does not interact with any of the inspected enzymes in the pathway. Summarized in Figure 3.20 below is a visual representation of the lack of PPIs observed in Figure 3.19.

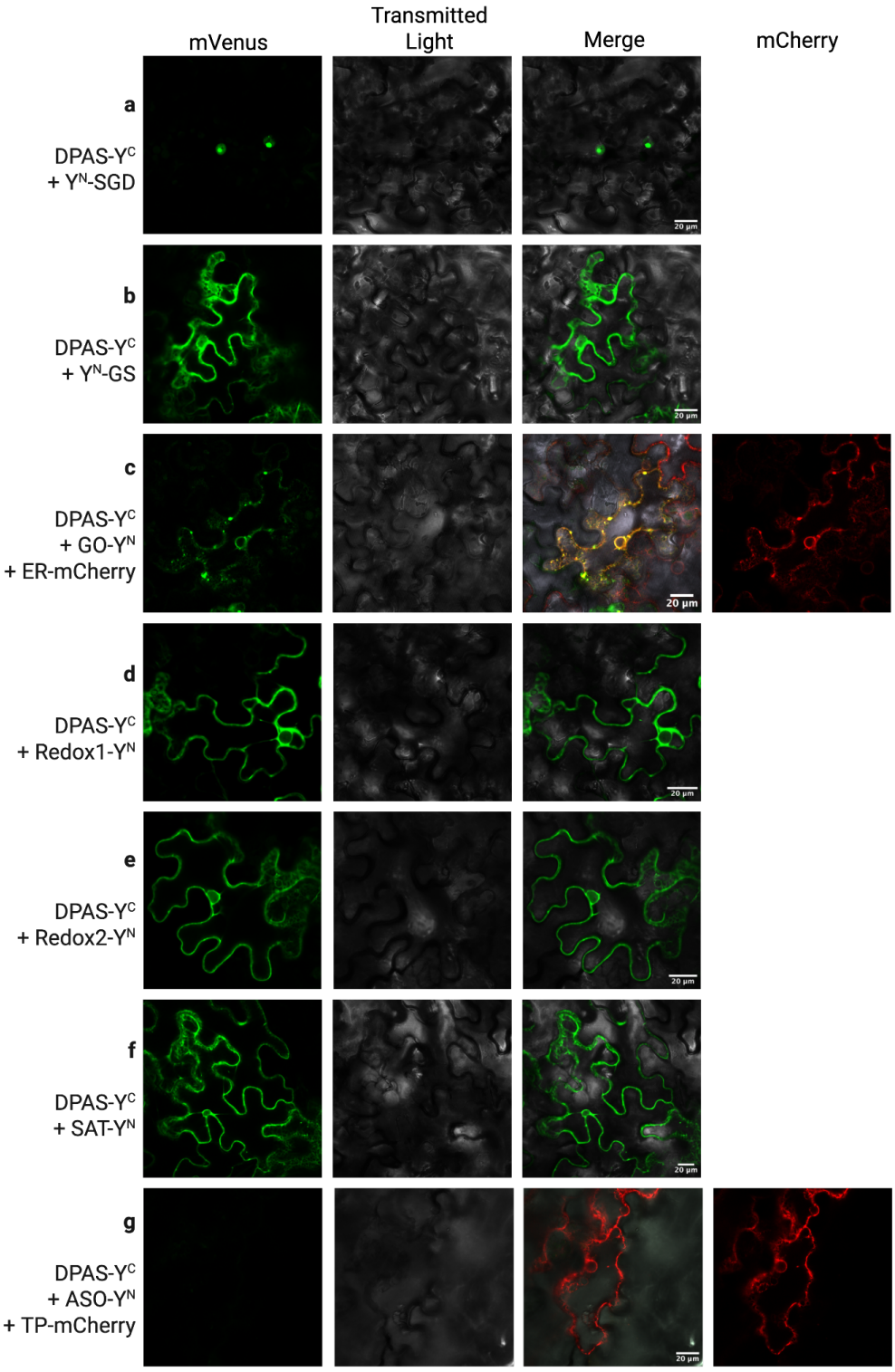


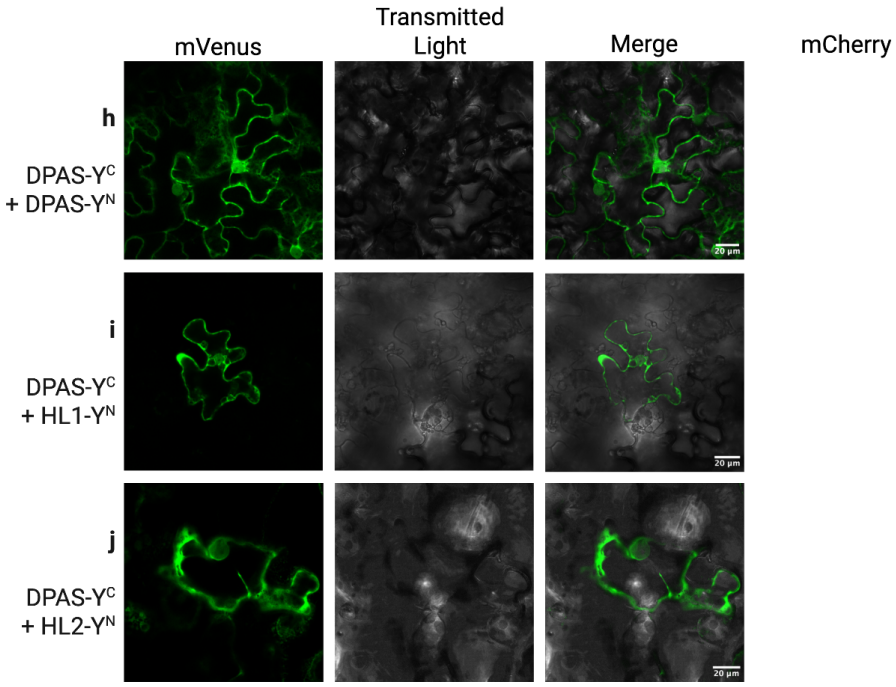

**Figure 3.20: ASO BiFC protein-protein interaction map.** ASO does not interact with any of the enzymes inspected in the pathway.

### 3.10 *C. roseus* Dihydroprecondylocarpine Acetate Synthase (DPAS) BiFC in *N. benthamiana*

Following ASO, the next enzyme in the biosynthetic pathway is DPAS. Notably, DPAS was recently discovered to interact with HL1 and HL2[8], and would expect to see that replicated in my studies. I began by tagging DPAS on its C-terminus with $mVenus^C$. Figure 3.21 shows that DPAS-$Y^C$ interacts with itself and all other inspected enzymes in this pathway, except ASO. The assembly of a mVenus fluorophore was observed in three distinct subcellular compartments: DPAS-$Y^C$ and $Y^N$-SGD interact in the nucleus (Figure 3.21, a); DPAS-$Y^C$ and $Y^N$-GS, Redox1-, Redox2-, SAT-, DPAS-, HL1-, and HL2- (Figure 3.21, b, d-f, h-j) interact in the cytoplasm; and DPAS-$Y^C$ and GO-$Y^N$ interact on the ER (Figure 3.21, c).

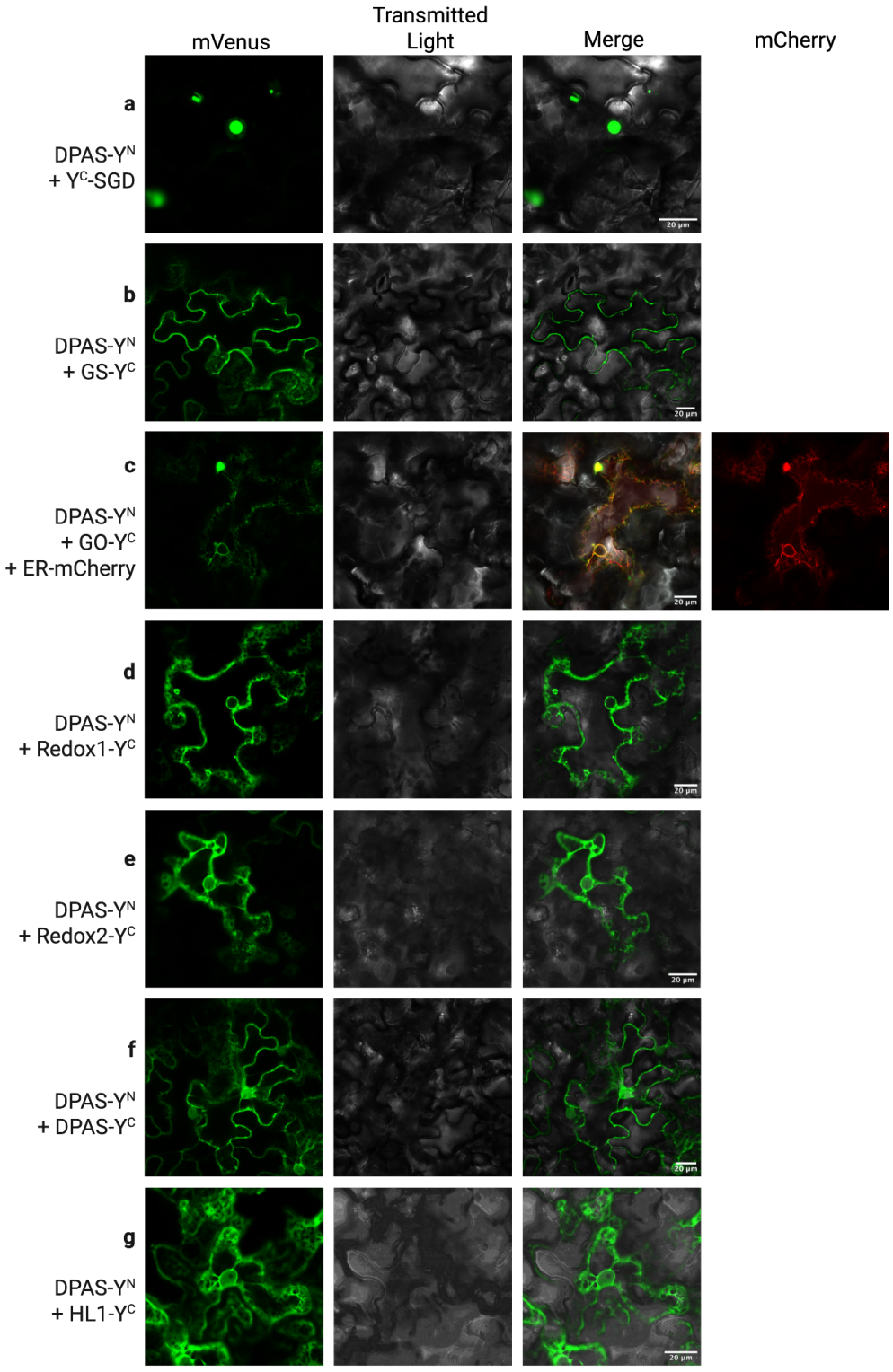
**Figure 3.21: Bimolecular fluorescence (BiFC) assay of $mVenus^C$ tagged *C. roseus* DPAS and $mVenus^N$ tagged SGD, GS, GO, Redox1, Redox2, SAT, ASO, DPAS, HL1, HL2 in *N. benthamiana* epidermal cells illustrate protein-protein interactions**. Confocal microscopy was used to capture fluorescent signals after transient expression of the constructs. mVenus fluorescence is generated when $mVenus^N$ and $mVenus^C$ are brought into proximity through the protein-protein interaction of the fused proteins. **a-j**, $mVenus^C$ was fused to the C-terminus of DPAS; **a-b**, $mVenus^N$ is fused to the N-termini of SGD and GS; **c-j**, $mVenus^N$ was fused to the C-termini of GO, Redox1, Redox2, SAT, ASO, DPAS, HL1, and HL2. Subcellular localization was determined using: **c**, C-terminal tagged HDEL-mCherry as an ER marker; **g**, C-terminal tagged tonoplast-mCherry as a tonoplast marker. Visual green colour corresponds to mVenus fluorescence, red to mCherry fluorescence, yellow to merged mVenus and mCherry fluorescence, and greyscale for transmitted light. Scale bars indicate 20 μm.

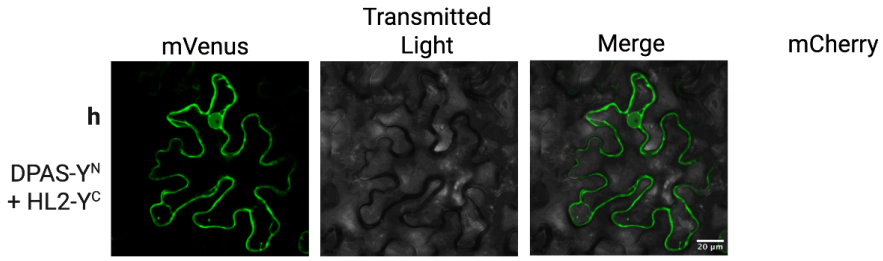

mVenus
Transmitted Light
Merge
mCherry
a
DPAS-Y^C + Y^N-SGD
b
DPAS-Y^C + Y^N-GS
c
DPAS-Y^C + GO-Y^N + ER-mCherry
d
DPAS-Y^C + Redox1-Y^N
e
DPAS-Y^C + Redox2-Y^N
f
DPAS-Y^C + SAT-Y^N
g
DPAS-Y^C + ASO-Y^N + TP-mCherry
20 µm




Then, I preformed BiFC surveys with mVenus$^N$ on the C-terminus of DPAS (Figure 3.22) which illustrates the reciprocal mVenus tagging as Figure 3.21. In alignment with Figure 3.21, Figure 3.22 indicates that DPAS-Y$^N$ also interacts with itself and all other enzymes inspected in this pathway. The assembly of a mVenus fluorophore was observed in two distinct subcellular compartments: DPAS-Y$^N$ and Y$^C$-SGD interact in the nucleus (Figure 3.22, a); DPAS-Y$^N$ and GS-, Redox1-, Redox2-, DPAS-, HL1-, and HL2-Y$^C$ are all observed to interact in the cytoplasm (Figure 3.22, b, d-h); and Redox1- Y$^N$ and GO-Y$^C$ interact on the ER (Figure 3.22, c).

**Figure 3.22: Bimolecular fluorescence (BiFC) assay of mVenus$^{N}$ tagged *C. roseus* DPAS and mVenus$^{C}$ tagged SGD, GS, GO, Redox1, Redox2, DPAS, HL1, HL2 in *N. benthamiana* epidermal cells illustrate protein-protein interactions.** Confocal microscopy was used to capture fluorescent signals after transient overexpression of the constructs. mVenus fluorescence is generated when mVenus$^{N}$ and mVenus$^{C}$ are brought into proximity through the protein-protein interaction of the fused proteins. **a-h**, mVenus$^{N}$ was fused to the C-terminus of DPAS; **a**, mVenus$^{C}$ is fused to the N-termini of SGD; **b-h**, mVenus$^{C}$ was fused to the C-termini of GS, GO, Redox1, Redox2, DPAS, HL1, and HL2. **c**, Subcellular localization was determined using C-terminal tagged HDEL-mCherry as an ER marker. Visual green colour corresponds to mVenus fluorescence, red to mCherry fluorescence, yellow to merged mVenus and mCherry fluorescence, and greyscale for transmitted light. Scale bars indicate 20 μm.


mVenus
Transmitted Light
Merge
mCherry
a
DPAS-YN + YC-SGD
b
DPAS-YN + GS-YC
c
DPAS-YN + GO-YC + ER-mCherry
d
DPAS-YN + Redox1-YC
e
DPAS-YN + Redox2-YC
f
DPAS-YN + DPAS-YC
g
DPAS-YN + HL1-YC
20 µm




Critically, we confirm that DPAS interacts with HL1 (Figure 3.21, i; Figure 3.22, g) and HL2 (Figure 3.21, j; Figure 3.22, h), as previously reported using split-luciferase assays[8]. Other than this, none of the observed interactions in Figure 3.21 and Figure 3.22 have been previously reported. The observed interaction of DPAS and SGD in the nucleus (Figure 3.21, a; Figure 3.22, a) is discussed in Section 3.2. Additionally, the cytosolic DPAS clearly interacts with GO on the ER (Figure 3.21, c; Figure 3.22, c) which is further discussed in Section 3.5. In contrast, DPAS and ASO (Figure 3.21, g) do not produce mVenus fluorescence, which is examined in Section 3.9. The observed DPAS PPIs from Figures 3.21 and 3.22 are summarized in Figure 3.23.

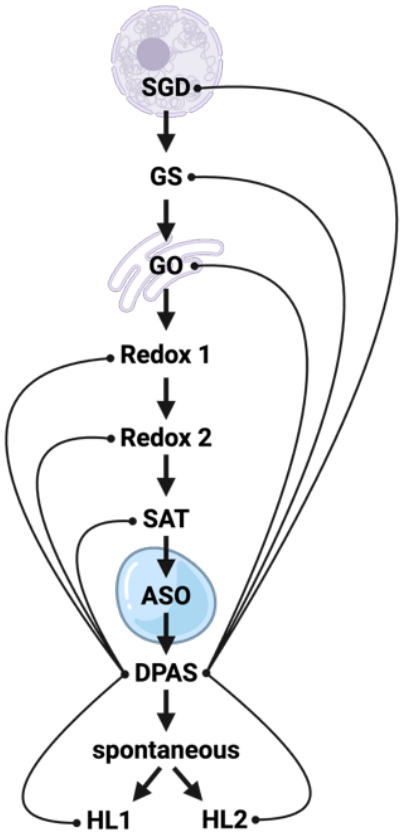
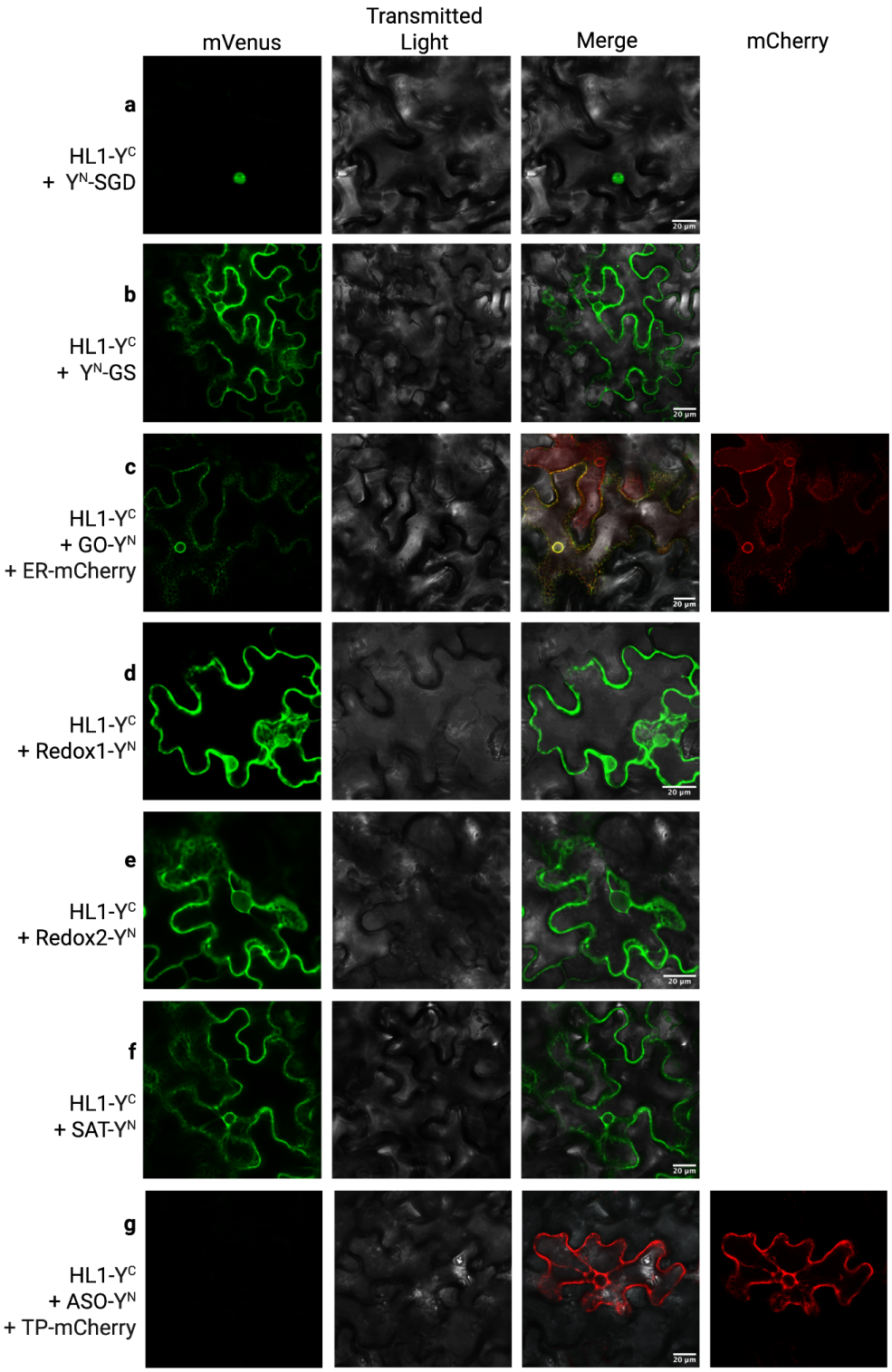


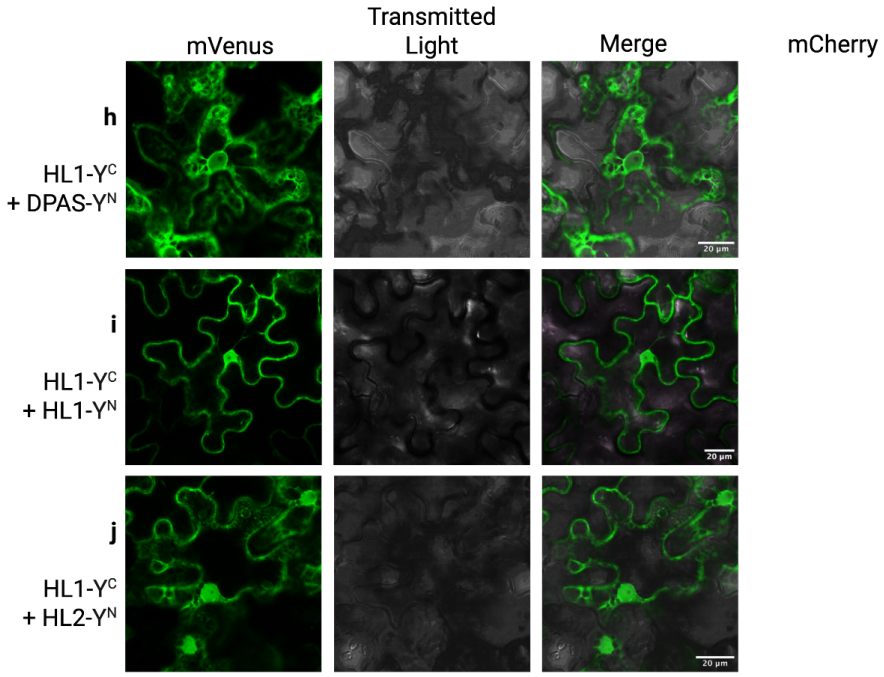

**Figure 3.23: DPAS BiFC protein-protein interaction map.** PPIs are indicated by curved lines between enzymes in the biosynthetic pathway to catharanthine and tabersonine. DPAS interacts with SGD, GS, GO, Redox1, Redox 2, SAT, HL1, and HL2. However, it is not observed to interact with ASO.

### 3.11 *C. roseus* Tabersonine Synthase (HL1) BiFC in *N. benthamiana*

After DPAS converts *O*-precondylcarpine acetate to dehydrosecodine, the pathway splits into two: HL1 will create catharanthine, while HL2 will create tabersonine (which will be further converted to vindoline prior to dimerization with catharanthine). First, I began investigating HL1 PPIs by tagging it with $mVenus^C$ on its C-terminus. Figure 3.24 shows that HL1-$Y^C$ interacts with itself and all other inspected enzymes in this pathway, except ASO. The assembly of a mVenus fluorophore was observed in three distinct subcellular compartments: HL1-$Y^C$ and $Y^N$-SGD interact in the nucleus (Figure 3.24, a); HL1-$Y^C$ and -GS, Redox1-, Redox2-, SAT-, DPAS-, HL1-, and HL2-$Y^N$ (Figure 3.24, b, d-f, h-j) interact in the cytoplasm; and HL1-$Y^C$ and GO-$Y^N$ interact on the ER (Figure 3.24, c).

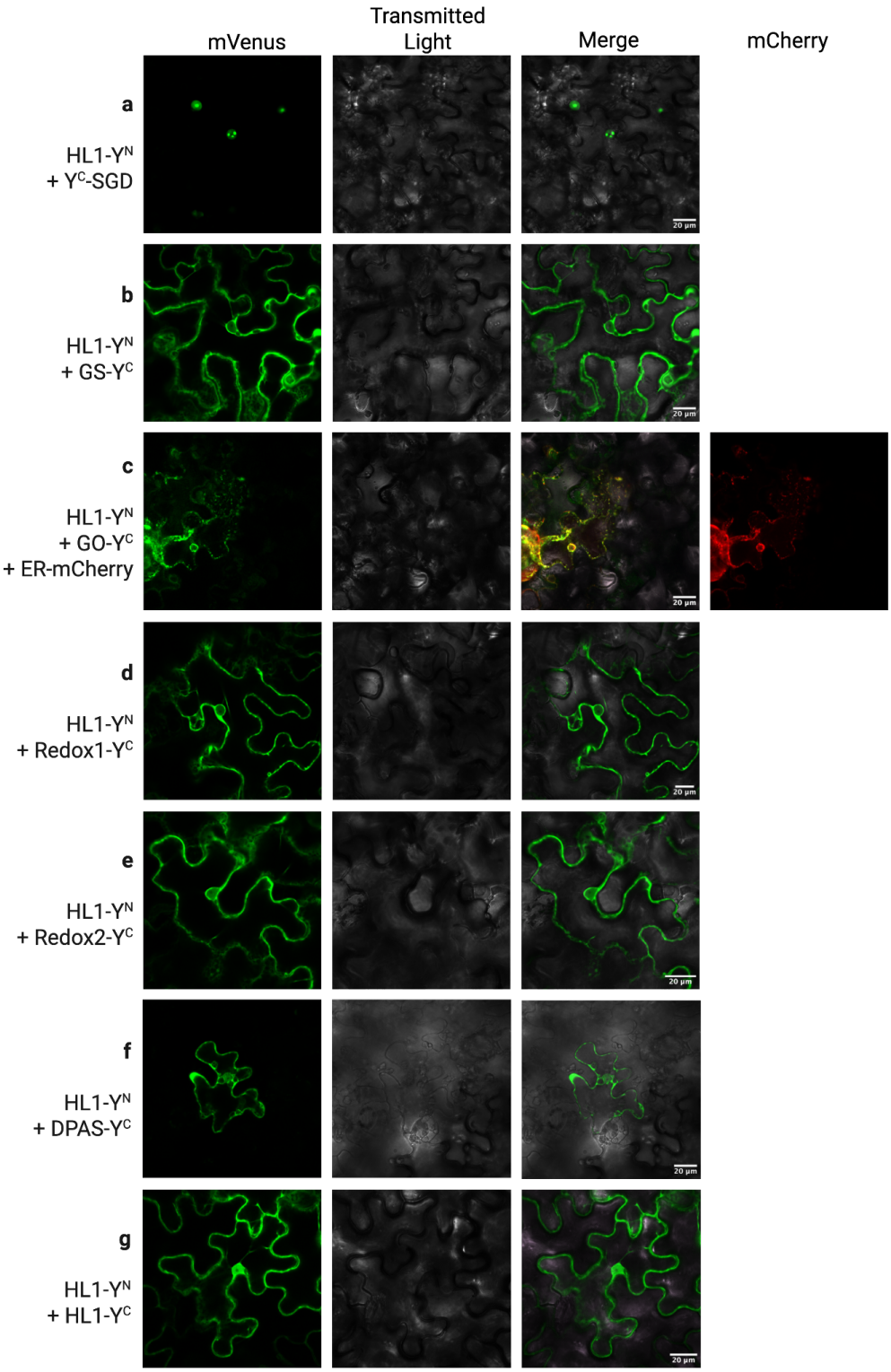
**Figure 3.24: Bimolecular fluorescence (BiFC) assay of $mVenus^C$ tagged *C. roseus* HL1 and $mVenus^N$ tagged CAD2, SGD, GS, GO, Redox1, Redox2, SAT, ASO, DPAS, HL1, HL2 in *N. benthamiana* epidermal cells illustrates protein-protein interactions.** Confocal microscopy was used to capture fluorescent signals after transient expression of the constructs. mVenus fluorescence is generated when $mVenus^N$ and $mVenus^C$ are brought into proximity through the protein-protein interaction of the fused proteins. **a-j**, $mVenus^C$ was fused to the C-terminus of HL1; **a-b**, $mVenus^N$ is fused to the N-termini of SGD, and GS; **c-j**, $mVenus^N$ was fused to the C-termini of GO, Redox1, Redox2, SAT, ASO, DPAS, HL1, and HL2. Subcellular localization was determined using: **c**, C-terminal tagged HDEL-mCherry as an ER marker; **g**, C-terminal tagged tonoplast-mCherry as a tonoplast marker. Visual green colour corresponds to mVenus fluorescence, red to mCherry fluorescence, yellow to merged mVenus and mCherry fluorescence, and greyscale for transmitted light. Scale bars indicate 20 μm.

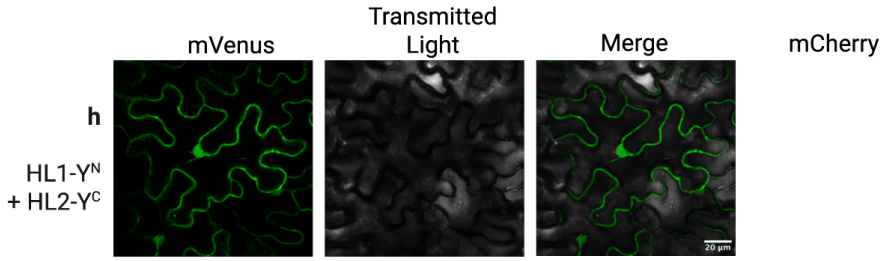

mVenus
Transmitted Light
Merge
mCherry
a
HL1-YC + YN-SGD
b
HL1-YC + YN-GS
c
HL1-YC + GO-YN + ER-mCherry
d
HL1-YC + Redox1-YN
e
HL1-YC + Redox2-YN
f
HL1-YC + SAT-YN
g
HL1-YC + ASO-YN + TP-mCherry
20 µm




Then, I preformed BiFC surveys with mVenus$^{N}$ on the C-terminus of HL1 (Figure 3.25) which illustrates the reciprocal mVenus tagging as Figure 3.24. Consistent with Figure 3.24, Figure 3.25 indicates that HL1-Y$^{N}$ also interacts with itself and all other enzymes inspected in this pathway. The assembly of a mVenus fluorophore was observed in three distinct subcellular compartments: HL1-Y$^{N}$ and Y$^{C}$-SGD interact in the nucleus (Figure 3.25, a); HL1-Y$^{N}$ and GS-, Redox1-, Redox2-, DPAS-, HL1-, and HL2-Y$^{C}$ are all observed to interact in the cytoplasm (Figure 3.25, b, d-h); and HL1-Y$^{N}$ and GO-Y$^{C}$ interact on the ER (Figure 3.25, c).

**Figure 3.25: Bimolecular fluorescence (BiFC) assay of mVenus$^{N}$ tagged *C. roseus* HL1 and mVenus$^{C}$ tagged SGD, GS, GO, Redox1, Redox2, DPAS, HL1, HL2 in *N. benthamiana* epidermal cells via *Agrobacterium*-mediated infiltration.** Confocal microscopy was used to capture fluorescent signals after transient overexpression of the constructs. mVenus fluorescence is generated when mVenus$^{N}$ and mVenus$^{C}$ are brought into proximity through the protein-protein interaction of the fused proteins. **a-h**, mVenus$^{N}$ was fused to the C-terminus of HL1; **a**, mVenus$^{C}$ is fused to the N-terminus of SGD; **c-h**, mVenus$^{C}$ was fused to the C-termini of GS, GO, Redox1, Redox2, DPAS, HL1, and HL2. **c**, Subcellular localization was determined using C-terminal tagged HDEL-mCherry as an ER marker. Visual green colour corresponds to mVenus fluorescence, red to mCherry fluorescence, yellow to merged mVenus and mCherry fluorescence, and greyscale for transmitted light. Scale bars indicate 20 μm.


mVenus
Transmitted Light
Merge
mCherry
a
HL1-YN + YC-SGD
b
HL1-YN + GS-YC
c
HL1-YN + GO-YC + ER-mCherry
d
HL1-YN + Redox1-YC
e
HL1-YN + Redox2-YC
f
HL1-YN + DPAS-YC
g
HL1-YN + HL1-YC
20 µm




Critically, we confirm that HL1 interacts with DPAS (Figure 3.24, h; Figure 3.25, f) as recently discovered[8]. However, here I also observe cytosolic interactions between HL1 and HL2, which has not been previously reported and was not investigated in Carr et al.[8] The observed interaction of HL1 and SGD in the nucleus (Figure 3.24, a; Figure 3.25, a) is discussed in Section 3.2. Additionally, the cytosolic HL1 clearly interacts with GO on the ER (Figure 3.24, c; Figure 3.25, c) which is further discussed in Section 3.5. In contrast, HL1 and ASO (Figure 3.24, g) do not produce mVenus fluorescence, which is examined in Section 3.9. The observed HL1 PPIs from Figures 3.24 and 3.25 are summarized in Figure 3.26.

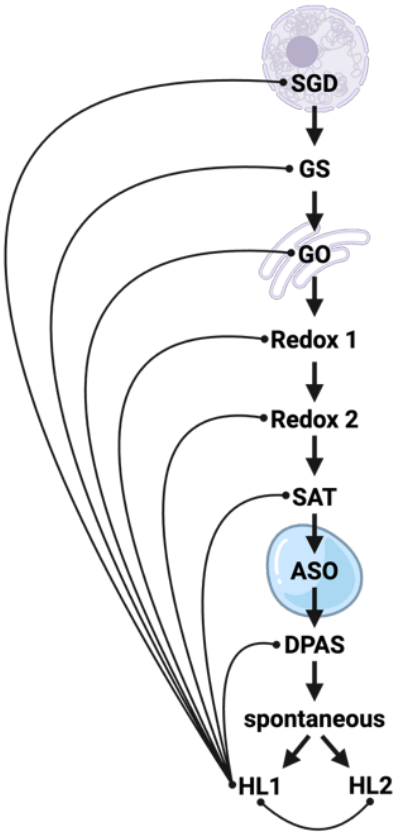
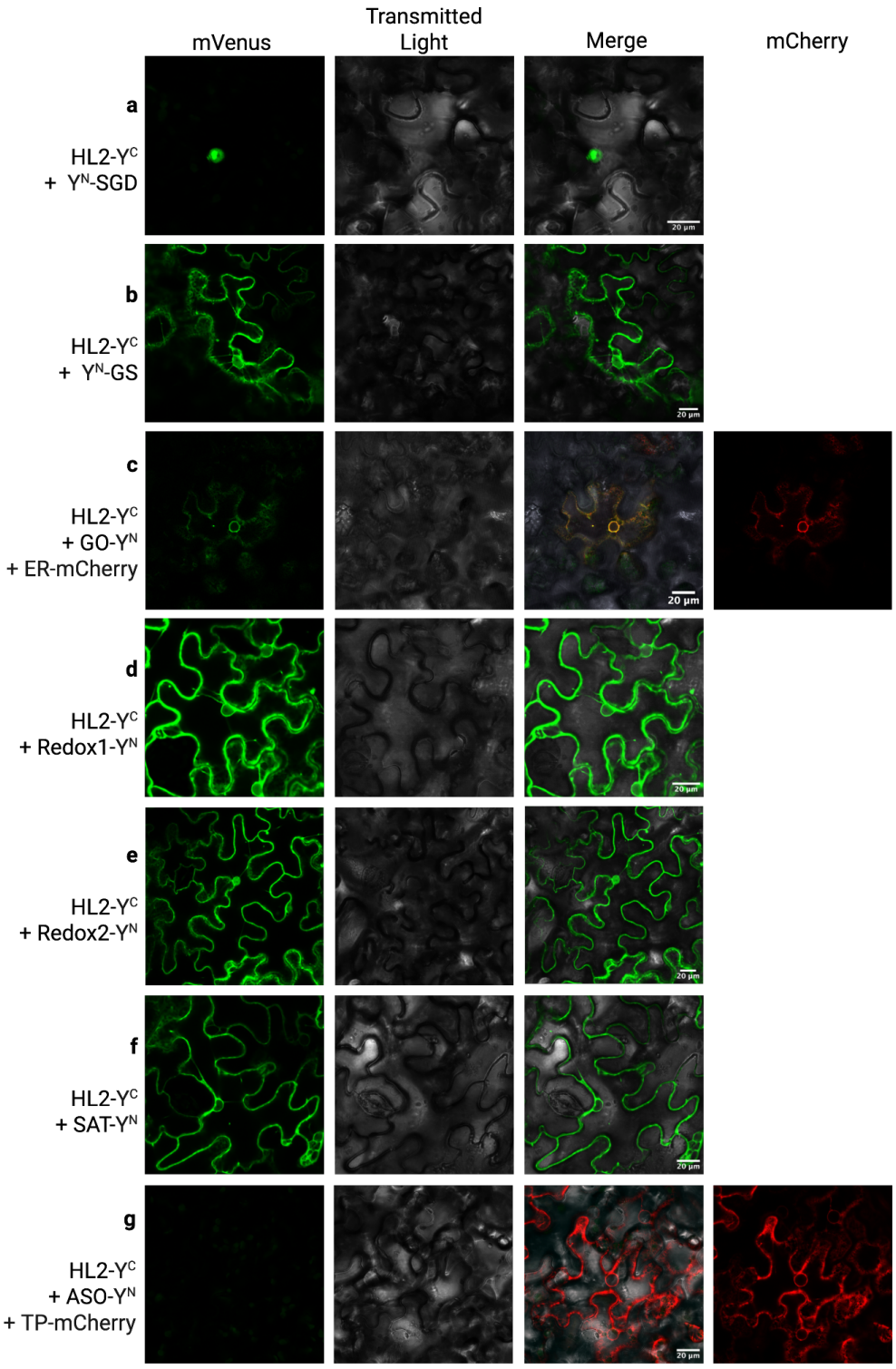


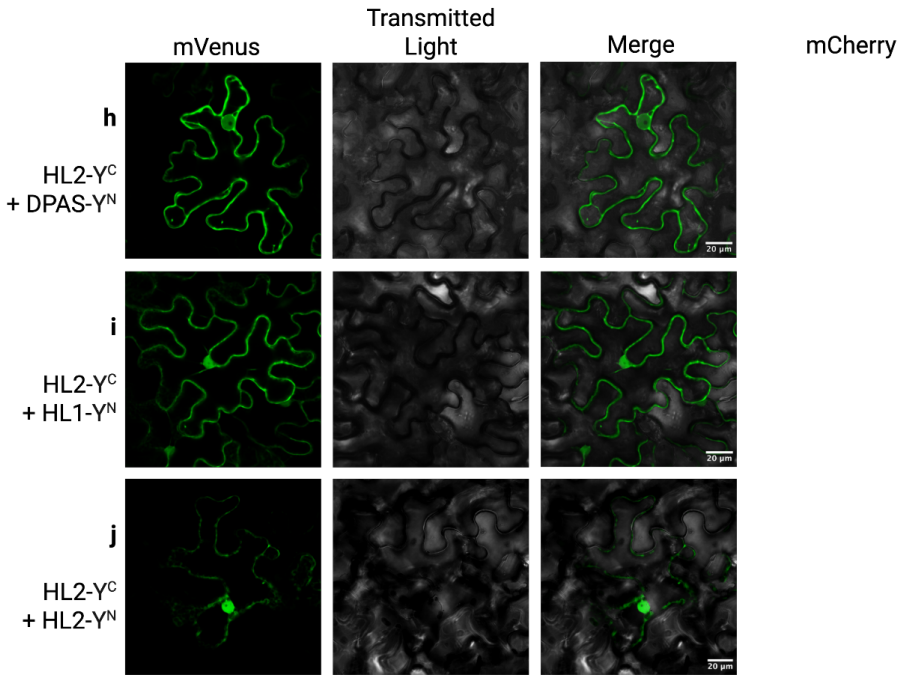

**Figure 3.26: HL1 BiFC protein-protein interaction map.** PPIs are indicated by curved lines between enzymes in the biosynthetic pathway to catharanthine and tabersonine. HL1 interacts with SGD, GS, GO, Redox1, Redox 2, SAT, DPAS, and HL2. However, it is not observed to interact with ASO.

### 3.12 *C. roseus* Catharanthine Synthase (HL2) BiFC in *N. benthamiana*

In contrast to HL1, the opposing step following DPAS is HL2. I began by first tagging HL2 on its C-terminus with mVenus$^{C}$. Figure 3.27 shows that HL2-Y$^{C}$ interacts with itself and all other inspected enzymes in this pathway, except ASO. The assembly of a mVenus fluorophore was observed in three distinct subcellular compartments: HL2-Y$^{C}$ and Y$^{N}$-SGD interact in the nucleus (Figure 3.27, a); HL2-Y$^{C}$ and -GS, Redox1-, Redox2-, SAT-, DPAS-, HL1-, and HL2-Y$^{N}$ (Figure 3.27, b, d-f, h-j) interact in the cytoplasm; and HL2-Y$^{C}$ and GO-Y$^{N}$ interact on the ER (Figure 3.27, c).

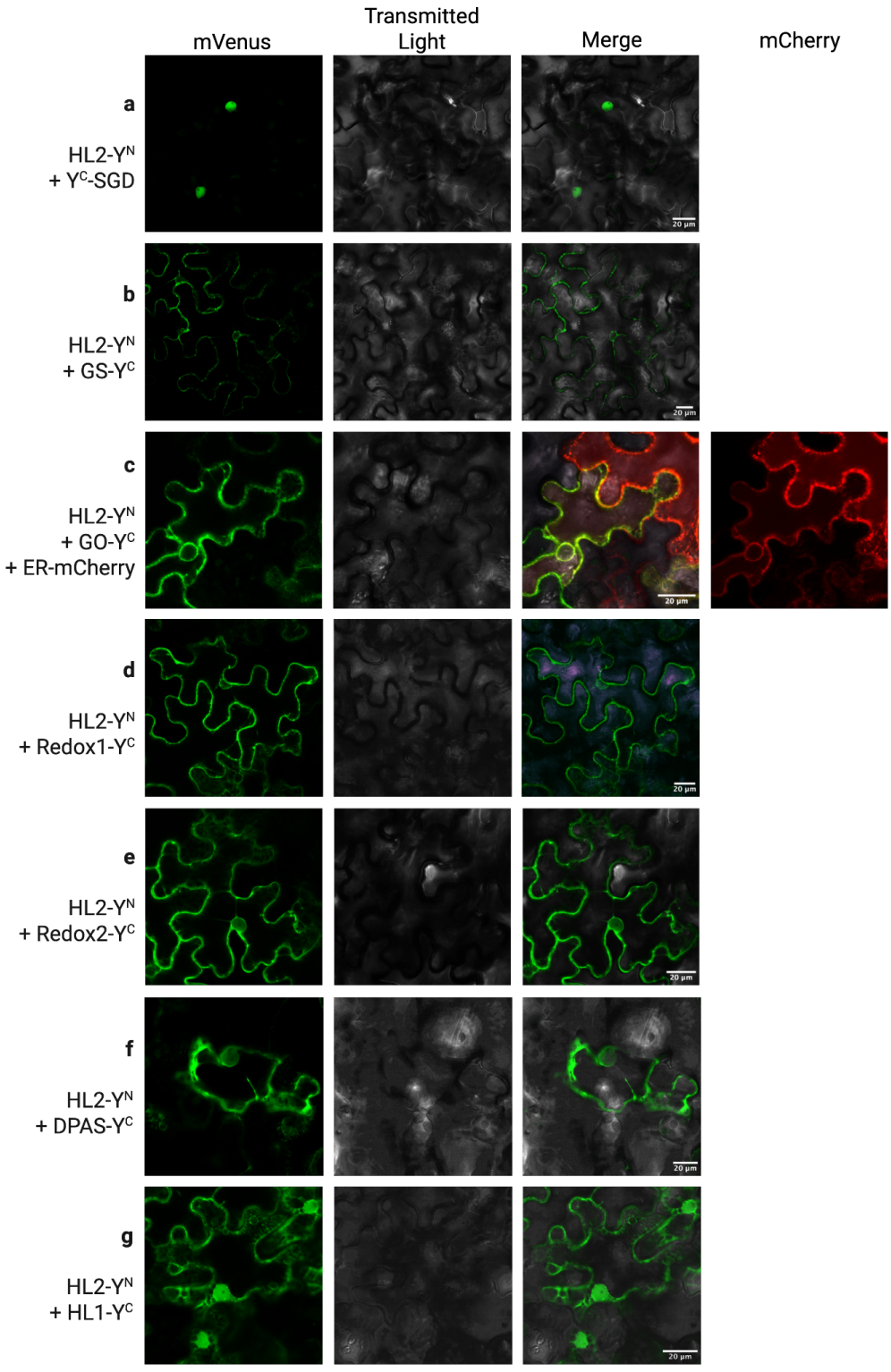
**Figure 3.27: Bimolecular fluorescence (BiFC) assay of mVenus$^{C}$ tagged *C. roseus* HL2 and mVenus$^{N}$ tagged SGD, GS, GO, Redox1, Redox2, SAT, ASO, DPAS, HL1, HL2 in *N. benthamiana* epidermal cells illustrate protein-protein interactions.** Confocal microscopy was used to capture fluorescent signals after transient expression of the constructs. mVenus fluorescence is generated when mVenus$^{N}$ and mVenus$^{C}$ are brought into proximity through the protein-protein interaction of the fused proteins. **a-j**, mVenus$^{C}$ was fused to the C-terminus of HL2; **a-b**, mVenus$^{N}$ is fused to the N-termini of SGD, and GS; **c-j**, mVenus$^{N}$ was fused to the C-termini of GO, Redox1, Redox2, SAT, ASO, DPAS, HL1, and HL2. Subcellular localization was determined using: **c**, C-terminal tagged HDEL-mCherry as an ER marker; **g**, C-terminal tagged tonoplast-mCherry as a tonoplast marker. Visual green colour corresponds to mVenus fluorescence, red to mCherry fluorescence, yellow to merged mVenus and mCherry fluorescence, and greyscale for transmitted light. Scale bars indicate 20 μm.

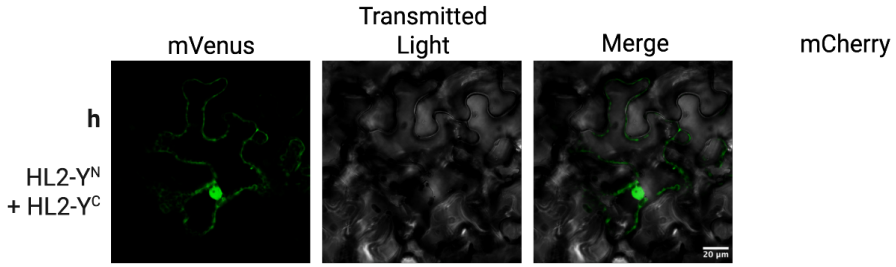

mVenus
Transmitted Light
Merge
mCherry
a
HL2-Y^C + Y^N-SGD
b
HL2-Y^C + Y^N-GS
c
HL2-Y^C + GO-Y^N + ER-mCherry
d
HL2-Y^C + Redox1-Y^N
e
HL2-Y^C + Redox2-Y^N
f
HL2-Y^C + SAT-Y^N
g
HL2-Y^C + ASO-Y^N + TP-mCherry
20 µm




Then, I tagged HL2 with mVenus$^N$ on its C-terminus (Figure 3.28), illustrating the reciprocal mVenus tagging as Figure 3.27. Consistent with Figure 3.27, Figure 3.28 indicates that HL2-Y$^N$ also interacts with itself and all other enzymes inspected in this pathway. The assembly of a mVenus fluorophore was observed in three distinct subcellular compartments: HL2-Y$^N$ and Y$^C$-SGD interact in the nucleus (Figure 3.28, a); HL2-Y$^N$ and GS-, Redox1-, Redox2-, DPAS-, HL1-, and HL2-Y$^C$ are all observed to interact in the cytoplasm (Figure 3.28, b, d-h); and HL2-Y$^N$ and GO-Y$^C$ interact on the ER (Figure 3.28, c).

**Figure 3.28: Bimolecular fluorescence (BiFC) assay of mVenus$^{N}$ tagged *C. roseus* HL2 and mVenus$^{C}$ tagged SGD, GS, GO, Redox1, Redox2, DPAS, HL1, HL2 in *N. benthamiana* epidermal cells via *Agrobacterium*-mediated infiltration.** Confocal microscopy was used to capture fluorescent signals after transient overexpression of the constructs. mVenus fluorescence is generated when mVenus$^{N}$ and mVenus$^{C}$ are brought into proximity through the protein-protein interaction of the fused proteins. **a-h**, mVenus$^{N}$ was fused to the C-terminus of HL2; **a**, mVenus$^{C}$ is fused to the N-termini of SGD; **b-h**, mVenus$^{C}$ was fused to the C-termini of GS, GO, Redox1, Redox2, DPAS, HL1, and HL2. **c**, Subcellular localization was determined using C-terminal tagged HDEL-mCherry as an ER marker. Visual green colour corresponds to mVenus fluorescence, red to mCherry fluorescence, yellow to merged mVenus and mCherry fluorescence, and greyscale for transmitted light. Scale bars indicate 20 μm.


mVenus
Transmitted Light
Merge
mCherry
a
HL2-YN + YC-SGD
b
HL2-YN + GS-YC
c
HL2-YN + GO-YC + ER-mCherry
d
HL2-YN + Redox1-YC
e
HL2-YN + Redox2-YC
f
HL2-YN + DPAS-YC
g
HL2-YN + HL1-YC
20 µm




Critically, we confirm that HL2 interacts with DPAS (Figure 3.27, h; Figure 3.28, f) as recently discovered[8]. However, here I also observe cytosolic interactions between HL2 and HL1, which has not been previously reported and was not investigated in Carr et al.[8] The observed interaction of HL2 and SGD in the nucleus (Figure 3.27, a; Figure 3.28, a) is discussed in Section 3.2. Additionally, the cytosolic HL2 clearly interacts with GO on the ER (Figure 3.27, c; Figure 3.28, c) which is further discussed in Section 3.5. In contrast, HL2 and ASO (Figure 3.27, g) do not produce mVenus fluorescence, which is examined in Section 3.9. The observed HL2 PPIs from Figures 3.27 and 3.28 are summarized below in Figure 3.29.

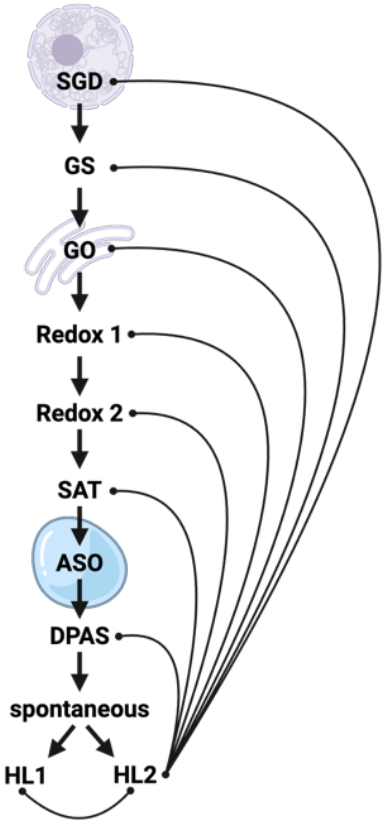



**Figure 3.29: HL2 BiFC protein-protein interaction map.** PPIs are indicated by curved lines between enzymes in the biosynthetic pathway to catharanthine and tabersonine. HL2 interacts with SGD, GS, GO, Redox1, Redox 2, SAT, DPAS, and HL1. However, it is not observed to interact with ASO.

### 3.13 Investigation of the Influence of Native Cinnamyl Alcohol Dehydrogenase

From these results, we speculate that there may be an underlying mechanism facilitating many of the interactions observed in the *N. benthamiana* cells—something that is common to all plants: cinnamyl alcohol dehydrogenases (CADs). CADs are a class of enzymes conserved across all terrestrial plants that participate in the synthesis of lignin, a structural component of the cell wall. CADs catalyze the final step in monolignol biosynthesis in the cytoplasm, reducing cinnamyl aldehydes to cinnamyl alcohols. In our unpublished study, we highlight that *C. roseus* CAD2 is in the GS BGC, consisting of GS, THAS2, ASO, an ASO homolog, CAD1, CAD2, and 8-

hydroxygernaiol oxidoreductase (8HGO) and its homologs, indicating that enzymes specific to MIA biosynthesis may be co-regulated with the CADs that work to produce monolignol[17]. Most importantly, our unpublished study demonstrates that CrCAD2 acts as a scaffold protein for SGD and GS, and its expression in a vindoline and catharanthine producing yeast strain increased MIA yields by nearly 1000x. Critically, *C. roseus* and *N. benthamiana* both contain native CADs in the cytosol, meaning that doing BiFC studies in *N. benthamiana* may naturally influence our observed BiFC interactions.

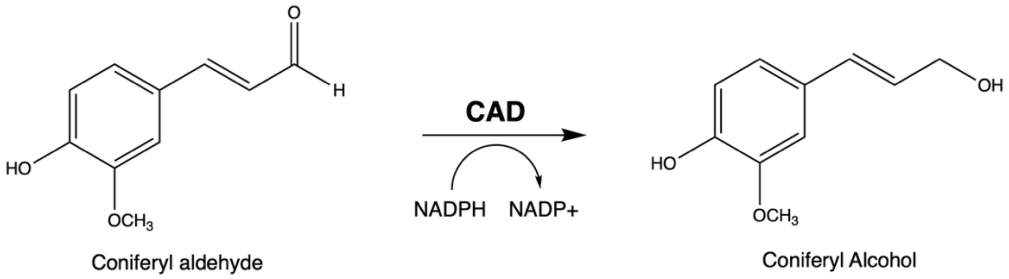



**Figure 3.31:** Reduction of coniferyl aldehyde to coniferyl alcohol by a cinnamyl alcohol dehydrogenase (CAD).

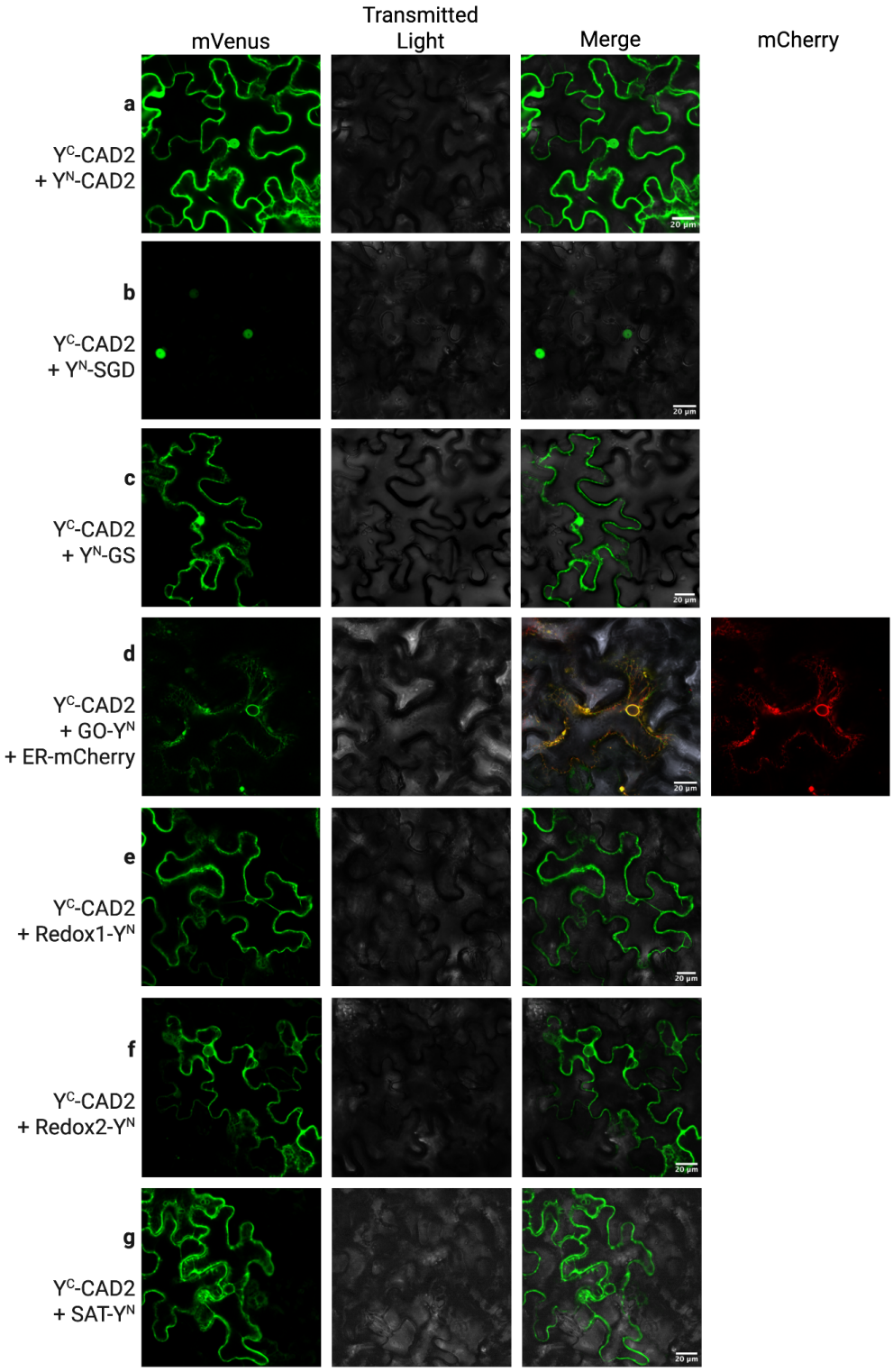
Therefore, I postulate that CADs influence on MIA producing enzymes extends beyond SGD and GS. I hypothesize that the native CrCAD in *C. roseus* facilitates protein-protein interactions in this pathway, and my BiFC results are being influenced by its homolog, NbCAD100, in *N. benthamiana*. To test this theory, I decided to perform BiFC of both CrCAD2 and NbCAD100 with the pathway enzymes in *N. benthamiana*. Notably, this does not remove the native CAD background in the *N. benthamiana* plant, however my priority was to identify the subcellular localization of these interactions in a plant cell. If I was able to completely remove the native CAD background, I would instead preform these assays in yeast. While yeast are eukaryotes, they do not have the same organelles or morphology as plant cells[18], which are integral for correctly

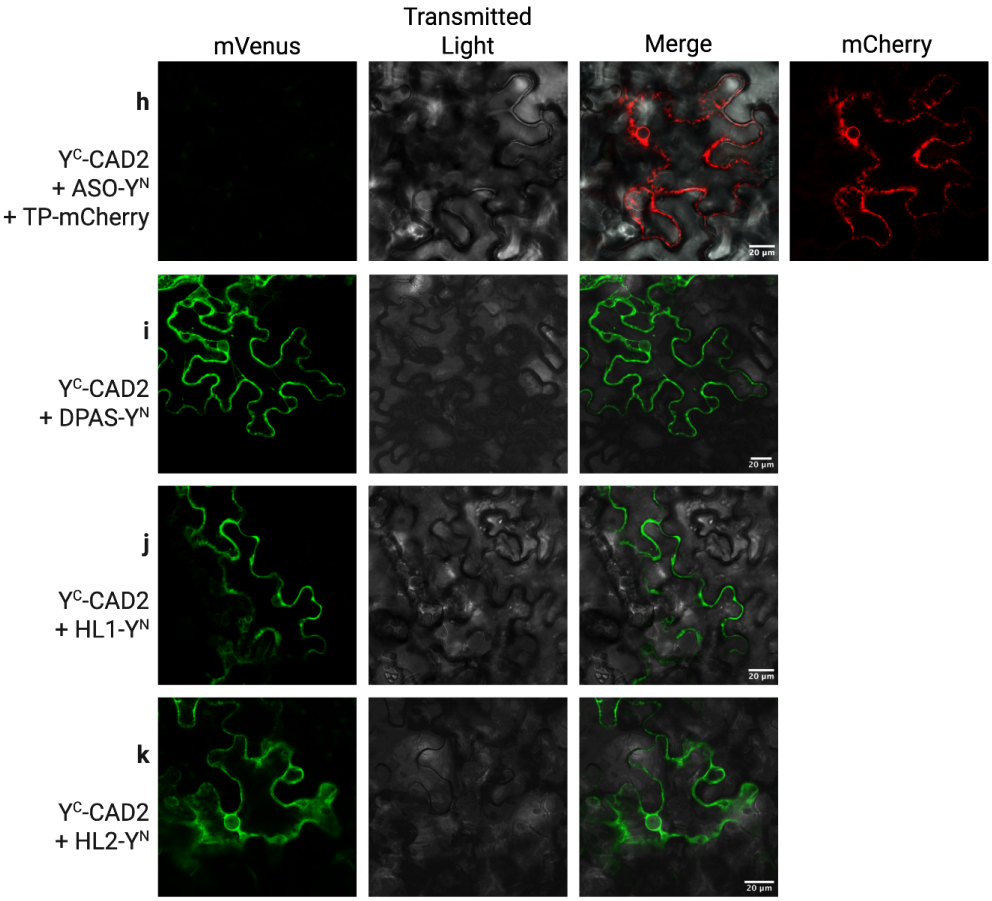
identifying subcellular localization. Additionally, yeast cells are very small, making them difficult to view under the microscope[19].

### 3.14 *C. roseus* Cinnamyl Alcohol Dehydrogenase II (CAD2) BiFC in *N. benthamiana*

CADs are known to form homodimers in the cytoplasm[20], so I will first infiltrate a control of $Y^C$-CAD2 + $Y^N$-CAD2 to ensure my constructs are working as expected. Because GS, Redox1, and DPAS are CAD-like enzymes, I also predict these enzymes will form homodimers with CAD2 in the cytoplasm. To start, I tagged CAD2 with $mVenus^C$ on its N-terminus. Figure 3.32 shows that CAD2 interacts with itself and all other inspected enzymes in this pathway, except ASO. The assembly of a mVenus fluorophore was observed in three distinct subcellular compartments: $Y^C$-CAD2 and $Y^N$-SGD interact in the nucleus (Figure 3.32, b); $Y^C$-CAD2 and -CAD2, -GS, Redox1-, Redox2-, SAT-, DPAS-, HL1-, and HL2-$Y^N$ interact in the cytoplasm (Figure 3.32, a, c, e-g, i-k); and $Y^C$-CAD2 and GO-$Y^N$ interact on the ER (Figure 3.32, d).

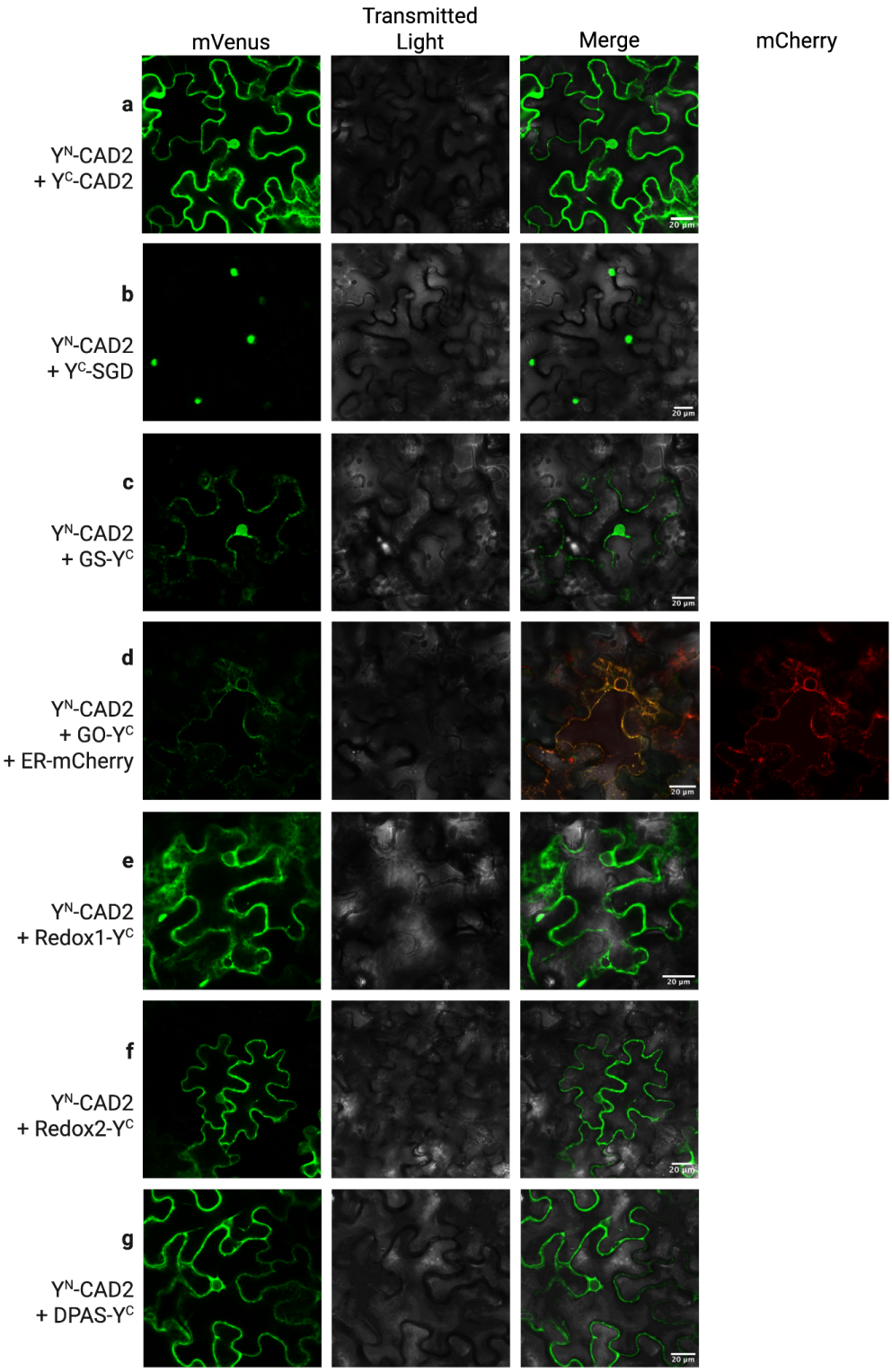
**Figure 3.32: Bimolecular fluorescence (BiFC) assay of $mVenus^C$ tagged *C. roseus* CAD2 and $mVenus^N$ tagged CAD2, SGD, GS, GO, Redox1, Redox2, SAT, ASO, DPAS, HL1, HL2 in *N. benthamiana* epidermal cells via *Agrobacterium*-mediated infiltration illustrates protein-protein interactions.** Confocal microscopy was used to capture fluorescent signals after transient expression of the constructs. mVenus fluorescence is generated when $mVenus^N$ and $mVenus^C$ are brought into proximity through the protein-protein interaction of the fused proteins. **a-k**, $mVenus^C$ was fused to the N-terminus of CAD2; **a-c**, $mVenus^N$ is fused to the N-termini of CAD2, SGD, and GS; **d-k**, $mVenus^N$ was fused to the C-termini of GO, Redox1, Redox2, SAT, ASO, DPAS, HL1, and HL2. Subcellular localization was determined using: **d**, C-terminal tagged HDEL-mCherry as an ER marker; **h**, C-terminal tagged tonoplast-mCherry as a tonoplast marker. Visual green colour corresponds to mVenus fluorescence, red to mCherry fluorescence, yellow to merged mVenus and mCherry fluorescence, and greyscale for transmitted light. Scale bars indicate 20 μm.

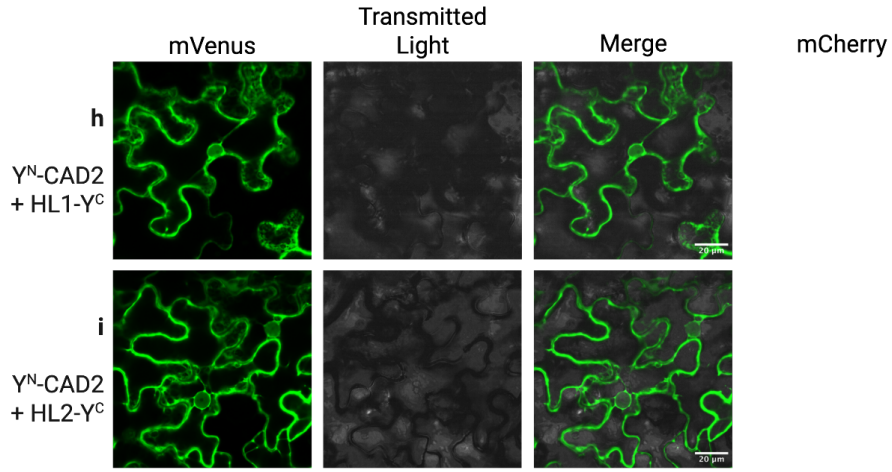

mVenus
Transmitted Light
Merge
mCherry
a
YC-CAD2 + YN-CAD2
b
YC-CAD2 + YN-SGD
c
YC-CAD2 + YN-GS
d
YC-CAD2 + GO-YN + ER-mCherry
e
YC-CAD2 + Redox1-YN
f
YC-CAD2 + Redox2-YN
g
YC-CAD2 + SAT-YN
20 µm




Then, I investigated CAD2 with mVenusN tagged on its N-terminus (Figure 3.33), which importantly illustrates the reciprocal mVenus tagging as Figure 3.32. Consistent with Figure 3.32, Figure 3.33 indicates that $Y^N$-CAD2 also interacts with itself and all other enzymes inspected in this pathway (ASO and SAT not tested here). The assembly of a mVenus fluorophore was observed in three distinct subcellular compartments: $Y^N$-CAD2 and $Y^C$-SGD interact in the nucleus (Figure 3.33, b); $Y^N$-CAD2 and -CAD2, GS-, Redox1-, Redox2-, DPAS-, HL1-, and HL2-$Y^C$ are all observed to interact in the cytoplasm (Figure 3.33, a, c, e-i); and $Y^N$-CAD2 and GO-$Y^C$ interact on the ER (Figure 3.33, d).

**Figure 3.33: Bimolecular fluorescence complementation (BiFC) assay of mVenus$^{N}$ tagged *C. roseus* CAD2 and mVenus$^{C}$ tagged CAD2, SGD, GS, GO, Redox1, Redox2, DPAS, HL1, HL2 in *N. benthamiana* epidermal cells via *Agrobacterium*-mediated infiltration illustrate PPIs.** Confocal microscopy was used to capture fluorescent signals after transient overexpression of the constructs. mVenus fluorescence is generated when mVenus$^{N}$ and mVenus$^{C}$ are brought into proximity through the protein-protein interaction of the fused proteins. **a-i**, mVenus$^{N}$ was fused to the N-terminal of CAD2; **a-b**, mVenus$^{C}$ is fused to the N-termini of CAD2 and SGD; **c-i**, mVenus$^{C}$ was fused to the C-termini of GS, GO, Redox1, Redox2, SAT, ASO, DPAS, HL1, and HL2. **d**, Subcellular localization was determined using C-terminal tagged HDEL-mCherry as an ER marker. Visual green colour corresponds to mVenus fluorescence, red to mCherry fluorescence, yellow to merged mVenus and mCherry fluorescence, and greyscale for transmitted light. Scale bars indicate 20 μm.


mVenus
Transmitted Light
Merge
mCherry
a
YN-CAD2 + YC-CAD2
b
YN-CAD2 + YC-SGD
c
YN-CAD2 + GS-YC
d
YN-CAD2 + GO-YC + ER-mCherry
e
YN-CAD2 + Redox1-YC
f
YN-CAD2 + Redox2-YC
g
YN-CAD2 + DPAS-YC
20 µm




Intriguingly, we observe in Figure 3.32 and Figure 3.33 that CAD2 from *C. roseus* interacts with all enzymes in our inspected biosynthetic pathway except ASO. However, as previously discussed in Section 3.9, we may not observe BiFC with ASO (Figure 3.32, h) for multiple reasons[13]. Despite this, none of the other interactions have been previously reported in the literature, however our lab has recently established that CAD2 is capable of acting as a scaffold to bring SGD and GS together in the nucleus. Importantly, we see these interactions visualized here, with interactions between SGD and CAD2 (Figure 3.32, b; Figure 3.33, b) in the nucleus and GS and CAD2 (Figure 3.32, c; Figure 3.33, c) in the cytoplasm.

Unlike SGD, CAD2 does not contain a nuclear localization signal. This indicates that the observed nuclear localization (Figure 3.32, b; Figure 3.33, c) may be simply from passive diffusion through the nuclear pore complex (NPC) or could suggest an underlying mechanism for nuclear transport. In addition, CAD2 does not contain an ER signal peptide, yet clearly interacts with GO on the ER (Figure 3.32, d; Figure 3.33, d). This could indicate an underlying mechanism which directs CAD2 onto the ER to meet GO, or that GO is outwardly facing on the ER membrane and able to interact with this cytosolic enzyme, discussed further in Section 3.5. Overall, here we observe that CAD2 can

interact with many different enzyme classes, not just CAD-like enzymes as predicted. Remarkably, this promiscuity indicates that CAD-mediated interactions in plant specialized metabolism may be more widespread than previously thought. The interactions observed in Figure 3.32 and 3.33 are summarized in Figure 3.34.

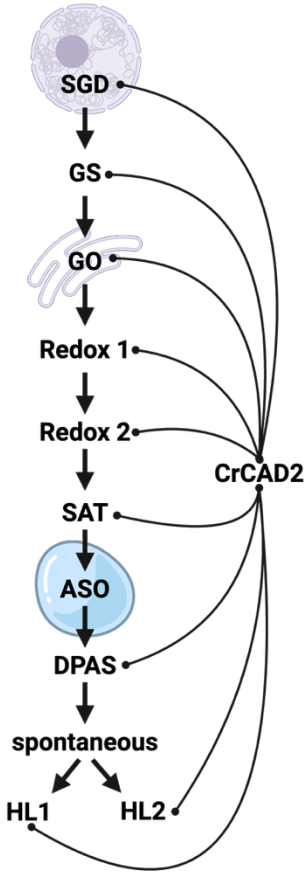



**Figure 3.34: CAD2 BiFC protein-protein interaction map.** PPIs are indicated by curved lines between enzymes in the biosynthetic pathway to catharanthine and tabersonine. CAD2 interacts with SGD, GS, GO, Redox1, Redox 2, SAT, DPAS, HL1, and HL2. However, it is not observed to interact with ASO.

### 3.15 Summarized BiFC Results

These BiFC assays in *N. benthamiana* enabled me to identify a complex network of PPIs in the *C. roseus* biosynthetic pathway from strictosidine to catharanthine and tabersonine. All these interactions can be visualized in Figure 3.30, while Table 3.1 indicates their respective subcellular localizations. To summarize concisely, everything interacts with everything except ASO, which interacts with none of the enzymes tested. More specifically, SGD interacts with everything but GO and ASO in the nucleus, because its interaction with GO is on the nuclear membrane, and it is not observed to interact with ASO. Meanwhile, GS/Redox1/Redox2/SAT/DPAS/HL1/HL2 interact with everything but SGD, GO, and ASO in the cytoplasm. This is because they interact with SGD in the nucleus, GO in the ER, and they were not observed to interact with ASO. Further, GO interacts with everything on the ER except SGD, GS, and ASO, because its interaction with SGD is on the nuclear membrane, its interaction with GS was observed to be cytosolic or ER depending on the orientation of the BiFC tag, and it was not observed to interact with ASO. Finally, ASO is not observed to interact with anything.

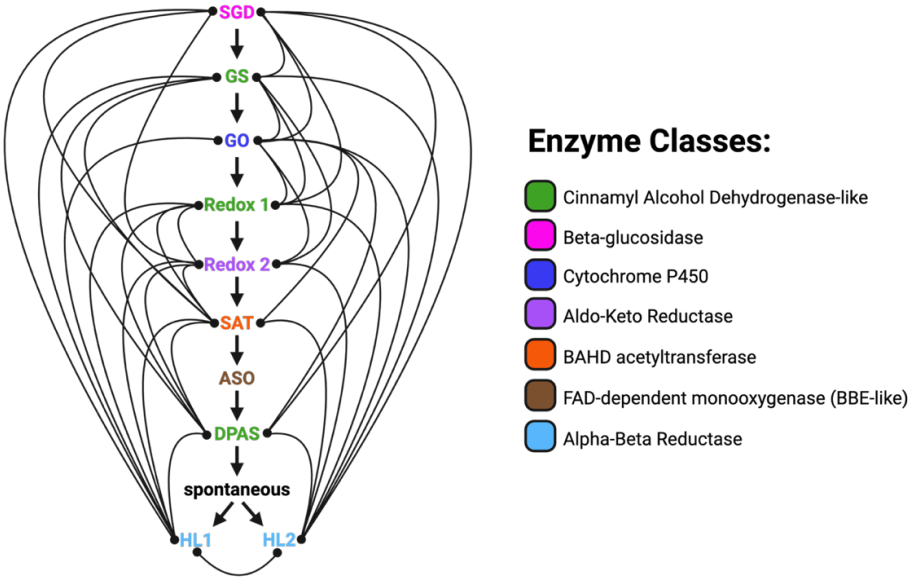



**Figure 3.35:** Overall BiFC protein-protein interaction map of inspected enzymes in the *C. roseus* biosynthetic pathway from strictosidine to catharanthine and vindoline.

**Table 3.1:** BiFC subcellular fluorescence of inspected enzymes in the *C. roseus* biosynthetic pathway from strictosidine to catharanthine and vindoline.

| mVenus$^C$ \ mVenus$^N$ | SGD | GS | GO | Redox1 | Redox2 | SAT | ASO | DPAS | HL1 | HL2 |
|---|---|---|---|---|---|---|---|---|---|---|
| SGD | | | | | | | | | | |
| GS | | | | | | | | | | |
| GO | | | | | | | | | | |
| Redox1 | | | | | | | | | | |
| Redox2 | | | | | | | | | | |
| SAT | | | | | | | | | | |
| ASO | | | | | | | | | | |
| DPAS | | | | | | | | | | |
| HL1 | | | | | | | | | | |
| HL2 | | | | | | | | | | |

| Florescence Localization |
|---|
| Nucleus |
| Nuclear Membrane |
| ER |
| Cytoplasm |
| No fluorescence |

In Table 3.1, I highlight that GO-$Y^C$ and $Y^N$-GS are observed to interact in the cytoplasm, while GO-$Y^N$ and GS-$Y^C$ are observed to interact on the ER. This difference in subcellular localization, either depending on the orientation of the BiFC tags or the time when being observed, may indicate a spatially dynamic interaction between these two enzymes. Critically, GS and GO are two consecutive steps in this pathway, and

independently localize to the cytoplasm (Figure 3.1, b) and ER (Figure 3.1, c), respectively.

Additionally, in Section 3.14 we observe that CAD2 from *C. roseus* interacts with all enzymes in the inspected pathway except ASO. A currently unpublished study in our lab provides strong evidence that CAD2 acts as a scaffold for SGD and GS to mediate MIA metabolic flux in *C. roseus*. However, the data in Figure 3.33 and Figure 3.34 supports the existence of a large network of interactions with CAD2, which was previously uninvestigated and therefore undiscovered.

# Bibliography 3


(1) Lisitsyna, O. M.; Kurnaeva, M. A.; Arifulin, E. A.; Shubina, M. Y.; Musinova, Y. R.; Mironov, A. A.; Sheval, E. V. Origin of the Nuclear Proteome on the Basis of Pre-Existing Nuclear Localization Signals in Prokaryotic Proteins. *Biol. Direct* **2020**, *15* (1), 9. https://doi.org/10.1186/s13062-020-00263-6.

(2) Guirimand, G.; Courdavault, V.; Lanoue, A.; Mahroug, S.; Guihur, A.; Blanc, N.; Giglioli-Guivarc'h, N.; St-Pierre, B.; Burlat, V. Strictosidine Activation in Apocynaceae: Towards a "Nuclear Time Bomb"? *BMC Plant Biol.* **2010**, *10*, 182. https://doi.org/10.1186/1471-2229-10-182.

(3) Tatsis, E. C.; Carqueijeiro, I.; Dugé de Bernonville, T.; Franke, J.; Dang, T.-T. T.; Oudin, A.; Lanoue, A.; Lafontaine, F.; Stavrinides, A. K.; Clastre, M.; Courdavault, V.; O'Connor, S. E. A Three Enzyme System to Generate the Strychnos Alkaloid Scaffold from a Central Biosynthetic Intermediate. *Nat. Commun.* **2017**, *8* (1), 316. https://doi.org/10.1038/s41467-017-00154-x.

(4) Stavrinides, A.; Tatsis, E. C.; Foureau, E.; Caputi, L.; Kellner, F.; Courdavault, V.; O'Connor, S. E. Unlocking the Diversity of Alkaloids in *Catharanthus Roseus*: Nuclear Localization Suggests Metabolic Channeling in Secondary Metabolism. *Chem. Biol.* **2015**, *22* (3), 336–341. https://doi.org/10.1016/j.chembiol.2015.02.006.

(5) Stavrinides, A.; Tatsis, E. C.; Caputi, L.; Foureau, E.; Stevenson, C. E. M.; Lawson, D. M.; Courdavault, V.; O'Connor, S. E. Structural Investigation of Heteroyohimbine Alkaloid Synthesis Reveals Active Site Elements That Control Stereoselectivity. *Nat. Commun.* **2016**, *7* (1), 12116. https://doi.org/10.1038/ncomms12116.

(6) Qu, Y.; Easson, M. E. A. M.; Simionescu, R.; Hajicek, J.; Thamm, A. M. K.; Salim, V.; De Luca, V. Solution of the Multistep Pathway for Assembly of Corynanthean, Strychnos, Iboga, and Aspidosperma Monoterpenoid Indole Alkaloids from 19E-Geissoschizine. *Proc. Natl. Acad. Sci.* **2018**, *115* (12), 3180–3185. https://doi.org/10.1073/pnas.1719979115.

(7) Qu, Y.; Safonova, O.; De Luca, V. Completion of the Canonical Pathway for Assembly of Anticancer Drugs Vincristine/Vinblastine in Catharanthus Roseus. *Plant J.* **2019**, *97* (2), 257–266. https://doi.org/10.1111/tpj.14111.

(8) Carr, S. C.; McDonald, A.; Langley, C.; Grabe, V.; Gase, K.; O'Connor, S. E. Protein–Protein Interactions Modulate a Key Branch Point in Monoterpene Indole Alkaloid Biosynthesis. *ACS Chem. Biol.* **2026**, *21* (1), 8–13. https://doi.org/10.1021/acschembio.5c00485.

(9) Davydov, D. R.; Davydova, N. Y.; Sineva, E. V.; Halpert, J. R. Interactions among Cytochromes P450 in Microsomal Membranes. *J. Biol. Chem.* **2015**, *290* (6), 3850–3864. https://doi.org/10.1074/jbc.M114.615443.

(10) Claessen, J. H. L.; Kundrat, L.; Ploegh, H. L. Protein Quality Control in the ER: Balancing the Ubiquitin Checkbook. *Trends Cell Biol.* **2012**, *22* (1), 22–32. https://doi.org/10.1016/j.tcb.2011.09.010.

(11) Liu, J.-X.; Howell, S. H. Endoplasmic Reticulum Protein Quality Control and Its Relationship to Environmental Stress Responses in Plants. *Plant Cell* **2010**, *22* (9), 2930–2942. https://doi.org/10.1105/tpc.110.078154.

(12) Ellgaard, L.; Helenius, A. Quality Control in the Endoplasmic Reticulum. *Nat. Rev. Mol. Cell Biol.* **2003**, *4* (3), 181. https://doi.org/10.1038/nrm1052.
(13) Xiang, L.; Etxeberria, E.; Ende, W. V. den. FEBS Press. https://doi.org/10.1111/febs.12092.
(14) Jensen, D.; Schekman, R. COPII-Mediated Vesicle Formation at a Glance. *J. Cell Sci.* **2011**, *124* (1), 1–4. https://doi.org/10.1242/jcs.069773.
(15) Craddock, C. P.; Hunter, P. R.; Szakacs, E.; Hinz, G.; Robinson, D. G.; Frigerio, L. Lack of a Vacuolar Sorting Receptor Leads to Non-Specific Missorting of Soluble Vacuolar Proteins in Arabidopsis Seeds. *Traffic* **2008**, *9* (3), 408–416. https://doi.org/10.1111/j.1600-0854.2007.00693.x.
(16) Rojo, E.; Zouhar, J.; Carter, C.; Kovaleva, V.; Raikhel, N. V. A Unique Mechanism for Protein Processing and Degradation in Arabidopsis Thaliana. *Proc. Natl. Acad. Sci. U. S. A.* **2003**, *100* (12), 7389–7394. https://doi.org/10.1073/pnas.1230987100.
(17) Halpin, C.; Knight, M. E.; Foxon, G. A.; Campbell, M. M.; Boudet, A. M.; Boon, J. J.; Chabbert, B.; Tollier, M.-T.; Schuch, W. Manipulation of Lignin Quality by Downregulation of Cinnamyl Alcohol Dehydrogenase. *Plant J.* **1994**, *6* (3), 339–350. https://doi.org/10.1046/j.1365-313X.1994.06030339.x.
(18) Panstruga, R.; Antonin, W.; Lichius, A. Looking Outside the Box: A Comparative Cross-Kingdom View on the Cell Biology of the Three Major Lineages of Eukaryotic Multicellular Life. *Cell. Mol. Life Sci. CMLS* **2023**, *80* (8), 198. https://doi.org/10.1007/s00018-023-04843-3.
(19) Johnston, G. C.; Ehrhardt, C. W.; Lorincz, A.; Carter, B. L. Regulation of Cell Size in the Yeast Saccharomyces Cerevisiae. *J. Bacteriol.* **1979**, *137* (1), 1–5. https://doi.org/10.1128/jb.137.1.1-5.1979.
(20) Pan, H.; Zhou, R.; Louie, G. V.; Mühlemann, J. K.; Bomati, E. K.; Bowman, M. E.; Dudareva, N.; Dixon, R. A.; Noel, J. P.; Wang, X. Structural Studies of Cinnamoyl-CoA Reductase and Cinnamyl-Alcohol Dehydrogenase, Key Enzymes of Monolignol Biosynthesis. *Plant Cell* **2014**, *26* (9), 3709–3727. https://doi.org/10.1105/tpc.114.127399.

# Chapter 4: Discussion & Future Directions

## 4.1 Discussion of BiFC Results

Through *A. tumefaciens*-mediated infiltration of BiFC-tagged *C. roseus* proteins into *N. benthamiana* epidermal cells, followed by confocal fluorescence microscopy, I systematically investigated protein–protein interactions (PPIs) among 11 enzymes in the core MIA biosynthetic pathway leading to important pharmaceuticals such as vinblastine. This analysis revealed a highly interconnected PPI network that, to my knowledge, has not been previously reported. Except for ASO, which did not yield positive BiFC signals with any tested partners, all other 10 enzymes showed positive pairwise interactions, indicating an extensive interaction landscape within the pathway.

Subcellular localization patterns of these interactions were also informative. When testing SGD, a nuclear-localized enzyme, I observed BiFC signals exclusively in the nucleus. When I tested GO, an ER-associated enzyme, most interactions localized to the ER. However, GO and GS exhibited both cytoplasmic and ER fluorescence depending on the orientation of the mVenus tag, which may indicate a spatially dynamic interaction. Notably, when SGD and GO are co-expressed, BiFC signals are detected at the nuclear envelope, consistent with the physical continuity between the nucleus and ER. In contrast, interactions among the remaining soluble enzymes are primarily observed in the cytosol and in the nucleus, likely caused by passive diffusion from the cytosol to the nucleus.

Notably, CAD2 that mediates the interaction between GS and SGD also exhibites interactions with all tested enzymes except ASO. This suggests that CAD2 may play a broader role in mediating PPIs beyond its established scaffolding function in the GS–

SGD interaction. However, an important caveat must be considered: CAD2 homologs are widely conserved across the plant kingdom[1], including in *N. benthamiana*. Earlier work in our lab, currently unpublished, demonstrated that endogenous CAD2 homolog(s) in *N. benthamiana* can interact with SGD in the nucleus and with GS in the cytosol. Furthermore, in this study, GS and SGD showed positive BiFC signals even in the absence of co-expressed *C. roseus* CAD2, in contrast to analogous experiments in yeast, which lacks plant CAD homologs involved in lignin biosynthesis.

These observations suggest that some of the detected PPIs in the plant system may be facilitated by endogenous host proteins, such as *N. benthamiana* CAD homologs, leading to indirect or "apparent" interactions. This limitation should be carefully considered not only in this study but also in other *in vivo* PPI analyses, where native cellular factors may influence observed interactions. Orthogonal approaches are therefore necessary to distinguish direct interactions from those mediated by auxiliary proteins.

Despite these caveats, my results clearly support a high degree of connectivity among MIA biosynthetic enzymes in plant cells. Whether mediated by CAD2, CAD-like proteins, or other auxiliary factors, it is highly likely that these enzymes physically associate in their native context in *C. roseus*. The observed interactions across multiple subcellular compartments further suggest the potential formation of dynamic, possibly transient metabolons that facilitate the efficient transfer of labile intermediates during MIA biosynthesis across different cellular compartments.

Given that CAD and CAD-like proteins such as CrCAD2 are broadly conserved across plant species, an intriguing hypothesis emerging from this work is that CAD-mediated PPIs may represent a widespread organizational principle in plant metabolism,

rather than a feature unique to *C. roseus*. Future studies involving diverse plant systems—both MIA-producing and non-producing—will be essential to fully elucidate the scope and functional significance of CAD-mediated protein interaction networks *in planta*.

### 4.1.1 Overexpression of Cytosolic Proteins and Nuclear Localization

A common theme among my results is that cytosolic proteins are naturally diffusing into the nucleus. Importantly, we see this diffusion with the free RFP, which is approximately 28 kDa and contains no localization signal, in Figure 3.1. It was previously thought that the nuclear pore complex (NPC) on the nuclear membrane would allow passive diffusion of proteins up to 60 kDa. However, more recently the consensus has shifted away from this and more towards a soft cut-off, where diffusion into the nucleus decreases gradually with increased protein size rather than a strict cutoff[2,3]. This is important, as all our fluorescent fusion proteins are greater than 60 kDa, yet still exhibit clear diffusion into the nucleus, presumably through the NPC.

While I cannot reliably quantify the amount of fluorescent protein inside vs. outside the nucleus, I speculate that a confounding factor here may be the overexpression of the fusion proteins. In my agrobacterium-mediated BiFC experiments, all proteins were expressed under the control of a strong, constitutive promoter 35S. Although the promoter is commonly used for heterologous protein expression in *N. benthamiana*, its overexpression of proteins beyond their natural levels may cause the cytoplasm to be crowded, causing diffusion through the nuclear pore and enhancing interactions with SGD beyond what would truly occur in the plant[4]. The nuclear localization of some or all the soluble proteins that lack a nuclear targeting motif in GFP-fusion or BiFC results may

be subjected to this artifact. There is also a possibility that this confounds the observed nuclear interactions between SGD and GS. A weaker promoter may be used in future studies to reduce the level of protein expression.

### 4.1.2 Negative BiFC Observed for ASO

An intriguing observation in this study is the consistently negative BiFC results obtained for ASO. One possible interpretation, supported by previous reports of negative BiFC results between ASO and other enzymes such as DPAS and HL1/2[5], is that ASO may not engage in stable or direct interactions with other proteins in the core MIA biosynthetic pathway. Alternatively, the lack of BiFC signal may arise from technical limitations related to tag placement. In this study, the BiFC tag was fused to the C-terminus of ASO, and it is possible that this topology prevents productive fluorophore complementation. While N-terminal tagging is often used as an alternative, ASO contains an N-terminal signal peptide that is cleaved during protein maturation, which would also remove any fused tag. In future work, a potential strategy would be to insert the BiFC tag between the signal peptide and the mature ASO sequence, although the impact of such modification on protein folding, localization, and function would need to be experimentally validated.

Another possibility is that proteolytic cleavage removes the C-terminal BiFC tag, leading to false-negative results. This could be tested by analyzing total protein extracts from infiltrated *N. benthamiana* leaves via SDS-PAGE followed by western blotting using an anti-mVenus antibody. Detection of smaller-than-expected bands would indicate proteolysis. However, our previous observation that ASO–GFP fusion proteins localize correctly to the tonoplast makes this explanation less likely.

## 4.2 Future Directions

### 4.2.1 Removing the CAD background

To determine whether the PPIs observed in *Nicotiana benthamiana* are direct, it will be essential to repeat BiFC experiments in a heterologous system such as *Saccharomyces cerevisiae*. Yeast lacks endogenous CAD enzymes involved in plant lignin biosynthesis, thereby eliminating potential interference from host CAD homologs. Conducting BiFC assays in yeast would help clarify whether the observed interactions occur directly between the tested proteins or are mediated by endogenous plant factors. In addition, it is important to strengthen evidence for proposed PPIs using orthogonal approaches, including split-luciferase complementation assays and *in vitro* pull-down experiments (discussed in Section 1.6). While such methods can establish whether a direct interaction occurs, understanding the mechanistic basis of these interactions will require further investigation.

### 4.2.2 Molecular Modelling

To address how these interactions occur at the molecular level, structural modeling of the native proteins will be necessary. Such analyses should consider both protein–protein interfaces and the positioning of catalytic sites relative to their substrates. This approach can help identify key residues involved in mediating interactions.

Targeted mutagenesis can then be used to disrupt these interfaces, for example, by introducing charge repulsion at predicted contact points. Comparing the catalytic properties of wild-type and interaction-deficient mutants through enzyme kinetics will reveal whether these interactions influence catalytic efficiency.

In our unpublished work, such an approach demonstrated that CAD2 facilitates substrate channeling by enhancing GS catalytic efficiency through remodeling of its substrate access channel at the GS–CAD2 heterodimer interface. This mechanism likely enables rapid transfer of the highly labile strictosidine aglycone from SGD (which also interacts with CAD2), thereby minimizing substrate degradation. These findings help address a long-standing gap in understanding vinblastine biosynthesis in *Catharanthus roseus*, highlight the value of biosynthetic gene cluster mining, and provide new insight into how MIA pathways are organized *in planta*.

### 4.3 Final Remarks

Beyond mechanistic insights, our investigation of subcellular localization of PPIs—from strictosidine to downstream products such as catharanthine and vindoline—provides a framework for rational engineering of microbial production systems. Manipulating enzyme localization and interactions could significantly improve metabolic flux toward desired products. For example, altering localization signals such as removing the bipartite C-terminal nuclear localization signal (NLS) from SGD, may enhance catalytic efficiency by co-localizing it with cytosolic partners such as GS and CAD2.

While many questions remain, this study establishes a broad foundation for future investigation of PPIs in MIA biosynthesis. The identification of 45 distinct PPIs and their subcellular localizations significantly advance our understanding of plant specialized metabolism and offers valuable guidance for developing efficient heterologous systems for large-scale production of MIA-derived pharmaceuticals.

## Bibliography 4


(1) Guo, D.-M.; Ran, J.-H.; Wang, X.-Q. Evolution of the Cinnamyl/Sinapyl Alcohol Dehydrogenase (CAD/SAD) Gene Family: The Emergence of Real Lignin Is Associated with the Origin of Bona Fide CAD. *J. Mol. Evol.* **2010**, *71* (3), 202–218. https://doi.org/10.1007/s00239-010-9378-3.

(2) Lin, D. H.; Hoelz, A. The Structure of the Nuclear Pore Complex (An Update). *Annu. Rev. Biochem.* **2019**, *88*, 725–783. https://doi.org/10.1146/annurev-biochem-062917-011901.

(3) Timney, B. L.; Raveh, B.; Mironska, R.; Trivedi, J. M.; Kim, S. J.; Russel, D.; Wente, S. R.; Sali, A.; Rout, M. P. Simple Rules for Passive Diffusion through the Nuclear Pore Complex. *J. Cell Biol.* **2016**, *215* (1), 57–76. https://doi.org/10.1083/jcb.201601004.

(4) Zhang, Y.; Chen, M.; Siemiatkowska, B.; Toleco, M. R.; Jing, Y.; Strotmann, V.; Zhang, J.; Stahl, Y.; Fernie, A. R. A Highly Efficient Agrobacterium-Mediated Method for Transient Gene Expression and Functional Studies in Multiple Plant Species. *Plant Commun.* **2020**, *1* (5), 100028. https://doi.org/10.1016/j.xplc.2020.100028.

(5) Carr, S. C.; McDonald, A.; Langley, C.; Grabe, V.; Gase, K.; O'Connor, S. E. Protein–Protein Interactions Modulate a Key Branch Point in Monoterpene Indole Alkaloid Biosynthesis. *ACS Chem. Biol.* **2026**, *21* (1), 8–13. https://doi.org/10.1021/acschembio.5c00485.

# Appendix I Supplementary Information for Chapter 2

**Supplementary Table 1:** Primers used in this study.

| # | primer | sequence (5′-3′) |
|---|---|---|
| 1 | Gateway-F | GGGGACAAGTTTGTACAAAAAAGCAGGCTTC |
| 2 | Gateway-R | GGGGACCACTTTGTACAAGAAAGCTGGGTC |
| 3 | CrSGD-BamHI-F | gtcaaggagaaaaaaccccggatccCATGGGATCTAAAGATGATCAGTC |
| 4 | CrSGD-SalI-R | aaatcaacttctgttccatgtcgacTCGACGTATTTTTGCTTCTT |
| 5 | Gal1-CYCT_fwd | tttaagaaggagatatacatCGTCAAGGAGAAAAAACCC |
| 6 | Gal1-CYCT_rev | gcagcagcggtttctttcatCTTAGCTAGCCGCGGTAC |
| 7 | CrGO-Gib-F | *CGAATTCAACCCTCACTAAAGGGCCTGCAGGATGGAGTTTTCTTTCTCCTCACCA* |
| 8 | CrGO-Gib-R | *AACCTCTGGCGAAGAATTGTTAATCCCGGGTTAATCGTTAACAAGATGAGGAACCA A* |
| 9 | 10H7-attb-F | AAAAAAGCAGGCTCTATGGCTGATCGCGTGAAGA |
| 10 | 10H7-attb-R | CAAGAAAGCTGGGTCGACAGCTACTGTTGC |
| 11 | CatR-attb-F | AAAAAAGCAGGCTCTATGGAAAAGCAAGTTGAGAT |
| 12 | CatR-attb-R | CAAGAAAGCTGGGTCCAAGTCTCCATCCCAAAG |
| 13 | attb-CrSAT-F | AAAAAAGCAGGCTTCATGGCACCCCAGATGCAGATA |
| 14 | attb-CrSAT-R | CAAGAAAGCTGGGTCATTGCTAAAATCAGTGTCCAGA |
| 15 | Attb-CrRO-F | AAAAAAGCAGGCTCTATGATAAAAAAAGTCCCAATAGT |
| 16 | Attb-CrRO-R | CAAGAAAGCTGGGTCAAGTTCGACTTGTAAATGG |
| 17 | attb-DPAS-F3 | GGGGACAAGTTTGTACAAAAAAGCAGGCTTCATGGCCGGAAAATCAGCAGA |
| 18 | attb-DPAS-R3 | GGGGACCACTTTGTACAAGAAAGCTGGGTCTAACTCTGACGGAGGAGTCA |
| 19 | attb-HL1-F | GGGGACAAGTTTGTACAAAAAAGCAGGCTTCATGAATTCCTCAACTGATCCAAC |
| 20 | attb-HL1-R | GGGGACCACTTTGTACAAGAAAGCTGGGTCCTCATGTTTGATGAAAGATGCTA |
| 21 | HL2-attb-F | AAAAAAGCAGGCTTCATGGGTTCCTCAGATGAGA |
| 22 | HL2-attb-R | CAAGAAAGCTGGGTCCTTGATGAAAGAAGCTAAACG |
| 23 | BamH1-CrCAD1/2-F | TTAACGTCAAGGAGAAAAAACCCCGATGGCCGGAAAATCACCAG |
| 24 | CrCAD1/2-linker-R | gctaccgctaccgctaccAGGAGCTTTCAAGGTGTT |

| | | |
|---|---|---|
| 25 | linker-<br>NbCAD100-F | CGAATTCCATAGTACCACCAGAACCTTCTGCTTTGAGGGTCTTAGC |
| 26 | Gal10-<br>NbCAD100-R | CGAATTCCATAGTACCACCAGAACCTTCTGCTTTGAGGGTCTTAGC |

**Supplementary Table 2:** cDNA sequences of proteins used in this study.

| | |
|---|---|
| CrSGD | ATGGGATCTAAAGATGATCAGTCCCTTGTTGTTGCCATTTCTCCAGCTGCTGAACCAAATGGAAA<br>TCATTCTGTCCCCATCCCATTCGCCTACCCCAGTATCCCCATTCAACCTAGAAAGCACAACAAGC<br>CCATCGTTCATCGTCGAGATTTCCCCTCAGATTTCATCTTGGGTGCCGGAGGATCTGCTTATCAG<br>TGTGAGGGTGCATATAATGAAGGCAACCGCGGTCCCAGTATATGGGATACTTTCACAAACCGATA<br>TCCAGCCAAAATAGCTGATGGATCTAATGGCAATCAAGCCATCAATTCTTACAATTTGTACAAGG<br>AAGATATCAAGATTATGAAGCAAACAGGCTTGGAATCATATAGGTTTTCAATTTCATGGTCAAGA<br>GTATTGCCAGGTGGAAATCTATCCGGTGGAGTGAATAAAGATGGTGTCAAGTTCTATCATGACTT<br>TATAGATGAGCTTCTAGCCAATGGCATCAAACCCTTTGCAACTCTCTTCCACTGGGATCTTCCCC<br>AAGCTCTTGAAGACGAGTATGGAGGCTTCTTGAGTGATCGAATTGTGGAAGATTTTACGGAGTAT<br>GCAGAATTTTGCTTTTGGGAATTCGGTGACAAAGTAAAATTTTGGACGACTTTCAATGAACCACA<br>TACTTATGTTGCAAGTGGATATGCCACTGGTGAATTTGCACCAGGAAGAGGTGGTGCAGATGGCA<br>AGGGGAACCCTGGCAAAGAACCCTATATAGCGACACATAATTTACTTCTTTCTCACAAAGCTGCT<br>GTGGAAGTATATAGGAAAAATTTTCAGAAATGTCAAGGAGGTGAAATTGGAATTGTACTTAATTC<br>AATGTGGATGGAGCCTCTCAATGAAACCAAAGAAGATATTGATGCTCGGGAAAGGGGTCTTGATT<br>TCATGCTCGGATGGTTCATAGAGCCATTAACAACGGGTGAATACCCAAAATCCATGAGAGCTCTT<br>GTAGGAAGCCGTCTTCCAGAATTTTCAACAGAAGATTCCGAAAAATTAACAGGATGCTATGATTT<br>TATCGGAATGAATTATTATACAACTACTTATGTTTCTAATGCAGACAAAATTCCCGATACTCCGG<br>GTTACGAAACAGATGCTCGAATTAATAAGAATATTTTTGTCAAAAAAGTTGATGGGAAGGAAGTG<br>CGCATTGGTGAACCGTGCTATGGGGGATGGCAGCATGTTGTTCCATCTGGACTCTACAATCTCTT<br>GGTTTACACTAAGGAGAAATACCATGTTCCAGTGATTTATGTCTCAGAATGTGGTGTGGTTGAGG<br>AAAATAGAACCAACATATTACTTACAGAAGGTAAAACCAACATATTACTTACAGAAGCTCGTCAC<br>GATAAACTCAGGGTTGATTTTCTACAAAGTCATCTCGCTAGCGTGCGAGATGCTATTGATGATGG<br>TGTGAATGTAAAAGGATTCTTTGTTTGGTCATTCTTCGACAACTTCGAATGGAATTTGGGATATA<br>TATGCCGTTATGGAATTATCCATGTTGATTATAAAACTTTTCAAAGATATCCAAAGGATTCTGCC<br>ATATGGTACAAGAATTTCATTAGTGAAGGATTTGTTACGAATACAGCTAAAAAGAGATTCCGAGA<br>AGAAGATAAACTAGTTGAGTTAGTCAAGAAGCAAAAATACTAA |
| CrGS2 | ATGGCTGGAGAAACAACAAAACTAGACCTTTCAGTGAAGGCCATCGGATGGGGTGCTGCAGATGC<br>ATCTGGCGTTCTTCAGCCCATTAGGTTCTATAGAAGAGCCCCTGGTGAACGGGATGTGAAGATTA<br>GAGTTTTGTACTGTGGTGTGTGCAATTTCGATATGGAAATGGTCAGAAACAAGTGGGGTTTCACT<br>AGATACCCTTATGTTTTTGGACATGAGACCGCCGGTGAGGTGGTAGAAGTTGGGAAGAAAGTAGA<br>GAAATTCAAGGTTGGAGATAAGGTGGGCGTGGGATGTATGGTCGGATCTTGTGGCAAATGTTTCC<br>ATTGTCAAAACGAAATGGAGAATTACTGCCCGGAGCCTAATTTGGCTGATGGATCTACTTACCGT<br>GAAGAAGGAGAACGTTCCTATGGAGGTTGTTCAAATGTCATGGTTGTTGATGAAAAATTCGTCCT<br>TAGATGGCCCGAAAATTTGCCTCAAGATAAAGGAGTTCCTCTCCTCTGTGCTGGGGTTGTTGTTT<br>ATAGCCCCATGAAATATATGGGATTTGATAAGCCAGGAAAGCATATTGGGGTTTTTGGGTTGGGT<br>GGTCTTGGTTCCATTGCTGTTAAGTTTATTAAAGCTTTTGGTGGTAAGGCTACTGTTATTAGTAC<br>ATCAAGGCGTAAAGAGAAGGAAGCCATTGAAGAGCATGGAGCTGATGCTTTTGTTGTCAACACTG<br>ACTCTGAACAATTGAAGGCTCTGGAAGGTACTATGGATGGTGTTGTGGACACCACCCCAGGTGGC<br>CGCACTCCTATGCCACTTATGCTCAATTTGGTTAAGTTTGACGGCGCCGTTATACTCGTCGGTGC<br>ACCGGAGACGCTATTTGAGCTCCCGTTGGAGCCTATGGGAAGGAAAAAGATAATCGGAAGCTCCA<br>CTGGAGGTCTCAAAGAGTATCAAGAAGTGCTTGATATTGCAGCCAAACACAACATTGTATGTGAT<br>ACTGAGGTTATTGGGATTGATTATCTCAGCACTGCTATGGAACGCATCAAGAATTTGGATGTCAA<br>GTACCGATTCGCGATCGACATTGGGAATACATTGAAATTTGAGGAATAA |
| CrGO | ATGGAGTTTTCTTTCTCCTCACCAGCTCTCTACATAGTTTATTTCTTGCTTTTCTTTGTGGTAAG<br>GCAATTATTGAAACCCAAAAGTAAGAAAAAATTGCCACCAGGTCCAAGAACACTACCCTTAATTG<br>GAAACCTTCATCAACTCTCGGGACCTTTACCTCATCGTACCCTAAAAAATTTGTCCGATAAACAT<br>GGTCCTTTGATGCACGTGAAAATGGGCGAACGTTCGGCAATTATAGTATCAGATGCAAGAATGGC<br>AAAAATAGTTCTTCATAATAACGGTTTAGCCGTTGCAGATCGGTCAGTAAATACTGTCGCAAGTA<br>TTATGACTTATAATAGTTTGGGTGTTACCTTTGCTCAGTATGGAGATTACTTAACAAAATTACGT |

| | |
|---|---|
| | CAAATCTATACTTTGGAACTTTTAAGTCAGAAAAAAGTTCGATCTTTCTACAGTTGTTTTGAAGA<br>TGAACTCGATACTTTTGTTAAGTCAATTAAGTCTAACGTTGGACAACCTATGGTTTTGTACGAGA<br>AAGCTTCTGCTTATTTGTATGCTACCATTTGTAGAACTATTTTTGGGAGTGTTTGCAAGGAAAAG<br>GAGAAAATGATTAAGATAGTGAAGAAAACGTCGTTACTGTCTGGAACACCACTTAGATTGGAGGA<br>TCTTTTTCCTTCTATGAGCATTTTTTGTAGATTTAGTAAAACTTTGAATCAATTGAGAGGACTTT<br>TGCAAGAAATGGATGATATTTTGGAAGAAATCATAGTTGAAAGGGAAAAGGCTTCTGAAGTCTCA<br>AAAGAGGCAAAGGATGATGAAGATATGCTTAGTGTTCTGTTGAGGCATAAATGGTACAATCCAAG<br>TGGTGCTAAATTCAGAATCACTAATGCAGACATCAAAGCCATTATCTTTGAGTTGATCTTAGCAG<br>CAACCCTAAGTGTAGCAGATGTTACAGAATGGGCTATGGTTGAAATTCTAAGGGATCCCAAAAGT<br>TTGAAAAAAGTGTACGAAGAAGTACGAGGTATTTGTAAAGAAAAGAAAAGAGTGACAGGATACGA<br>CGTTGAAAAAATGGAATTTATGCGTCTTTGTGTGAAGGAATCAACAAGAATACATCCAGCTGCTC<br>CTCTTTTAGTTCCTAGAGAATGCAGAGAAGATTTTGAAGTAGATGGATACACAGTTCCAAAAGGG<br>GCTTGGGTTATAACAAATTGCTGGGCTGTTCAAATGGATCCTACAGTATGGCCCGAACCAGAGAA<br>GTTTGATCCAGAAAGATATATTCGTAACCCAATGGATTTCTATGGAAGTAACTTTGAATTGATAC<br>CATTTGGGACAGGTAGAAGAGGATGTCCTGGTATTTTATATGGAGTGACAAATGCTGAGTTTATG<br>TTGGCTGCTATGTTTTATCATTTTGATTGGGAAATAGCAGATGGTAAAAAACCAGAAGAAATTGA<br>TTTGACTGAGGACTTTGGTGCTGGTTGCATTATGAAGTATCCTTTGAAATTGGTTCCTCATCTTG<br>TTAACGATTAG |
| CrRedox1 | ATGGCTGATCGCGTGAAGACCGTAGGATGGGCAGCTCACGACAGCTCCGGCTTCCTCTCTCCCTT<br>CCAATTCACTCGAAGGGCAACAGGTGAAGAAGATGTGAGGTTGAAGGTGTTGTACTGTGGTGTCT<br>GTCACTCAGACCTTCATAACATCAAGAACGAAATGGGATTCACCTCCTACCCTTGTGTCCCCGGG<br>CATGAGGTTGTGGGGGAAGTGACGGAAGTGGGGAACAAAGTAAAGAAATTCATAATTGGTGATAA<br>AGTTGGGGTTGGATTATTCGTTGACTCATGTGGCGAATGCGAACAATGTGTGAATGATGTAGAAA<br>CCTATTGTCCCAAATTGAAAATGGCTTATTTATCCATTGATGATGATGGAACTGTGATTCAAGGA<br>GGGTACTCAAAGGAAATGGTCATCAAAGAACGCTACGTTTTCCGGTGGCCGGAAAATCTTCCTCT<br>ACCCGCCGGTACACCGCTTCTGGGTGCCGGTAGTACAGTTTATAGTCCAATGAAATACTATGGAC<br>TTGATAAGTCAGGACAACATCTAGGAGTTGTTGGCCTTGGTGGACTTGGTCATTTAGCTGTTAAA<br>TTTGCAAAGGCTTTTGGACTTAAAGTTACTGTCATTAGTACCTCTCCTAGCAAGAAGGATGAAGC<br>CATCAATCACCTTGGTGCTGATGCATTTTTAGTTAGCACTGATCAAGAGCAAACCCAGAAAGCAA<br>TGAGCACAATGGATGGCATAATTGACACAGTATCAGCTCCTCATGCATTGATGCCATTGTTTTCC<br>CTATTGAAACCAAATGGGAAGCTAATTGTTGTTGGTGCACCAAATAAACCAGTTGAATTAGATAT<br>TCTATTTCTTGTCATGGGAAGGAAAATGCTCGGAACATCTGCTGTTGGGGGAGTGAAGGAGACAC<br>AAGAGATGATCGATTTTGCAGCAAAACATGGTATAGTTGCAGATGTAGAAGTTGTGGAAATGGAG<br>AATGTGAACAATGCAATGGAGCGGCTTGCGAAGGGGGATGTTAGATATAGATTTGTTCTTGATAT<br>TGGGAATGCAACAGTAGCTGTCTGA |
| CrRedox2 | ATGGAAAAGCAAGTTGAGATCCCTGAAGTAGAATTGAATTCAGGACATAAAATGCCAATTGTGGG<br>ATACGGAACATGCGTGCCAGAACCCATGCCACCGTTGGAAGAACTAACCGCAATCTTCTTAGATG<br>CAATAAAGGTTGGTTACCGGCACTTCGACACGGCTTCGAGTTACGGCACAGAGGAGGCACTTGGT<br>AAAGCCATAGCTGAGGCTATAAACAGCGGTTTGGTTAAAAGTAGGGAGGAATTCTTCATCAGTTG<br>TAAGCTGTGGATTGAAGATGCAGATCATGACCTTATCTTGCCTGCCCTCAACCAGTCACTTCAGA<br>TTCTTGGGGTTGATTATTTGGATCTATATATGATACACATGCCGGTGAGAGTGAGGAAAGGTGCT<br>CCCATGTTCAATTATTCAAAAGAGGATTTCCTTCCATTTGACATACAAGGTACATGGAAGGCCAT<br>GGAAGAGTGCAGCAAACAAGGATTGGCCAAGTCTATTGGTGTCAGCAACTACTCTGTTGAAAAAC<br>TCACTAAACTCCTAGAAACCTCCACTATTCCCCCCGCCGTTAATCAGGTTGAGATGAATGTAGCT<br>TGGCAACAGAGAAAATTGCTGCCATTTTGCAAAGAGAAAAACATTCATATAACATCATGGTCTCC<br>ACTCCTATCTTATGGTGTCGCTTGGGGAAGTAATGCTGTCATGGAAAATCCTGTTCTCCAACAAA<br>TTGCGGCTTCCAAAGGCAAAACTGTGGCACAGGTGGCACTAAGATGGATATACGAGCAAGGAGCA<br>AGTCTCATTACAAGGACTTCCAACAAGGACAGAATGTTTGAAAATGTTCAAATTTTTGATTGGGA<br>ACTCAGTAAAGAAGAATTGGATCAAATTCATGAAATCCCACAACGTAGGGGTACTTTAGGTGAAG<br>AATTTATGCATCCAGAAGGACCGATCAAATCCCCAGAGGAGCTTTGGGATGGAGACTTGTGA |
| CrSAT | ATGGCACCCCAGATGCAGATATTGTCAGAGGAACTGATTCAACCATCATCTCCGACACCCCAAAC<br>CTTGAAAACCCATAAACTTTCCCATCTTGATCAAGTTTTATTAACATGTCATATCCCTATTATTC<br>TCTTTTATCCAAATCAATTGGACTCAAATCTCGATCGAGCCCAAAGATCTGAGAATCTAAAACGA<br>TCTTTATCAACAGTGTTAACTCAATTTTACCCTTTAGCCGGAAGAATCAATATAAATTCTTCCGT<br>AGATTGTAATGATTCCGGAGTCCCTTTTCTTGAAGCTCGAGTTCATTCCCAACTCTCAGAAGCAA<br>TTAAAAATGTCGCCATAGATGAACTCAATCAATACCTGCCATTCCAACCTTATCCCGGTGGGGAG<br>GAAAGTGGGTTGAAAAAAGATATCCCCTTAGCTGTAAAAATCAGTTGTTTCGAATGTGGCGGAAC<br>AGCAATTGGGGTCTGTATTTCCCACAAGATTGCCGATGCGTTGTCCTTGGCTACCTTCCTCAATT<br>CATGGACCGCAACATGCCAGGAAGAGACTGATATTGTTCAACCTAATTTCGATCTGGGATCCCAT<br>CATTTTCCGCCTATGGAAAGCATCCCAGCACCTGAATTTCTACCGGATGAAAATATTGTGATGAA<br>ACGGTTCGTGTTCGATAAAGAAAAATTAGAAGCTCTAAAAGCCCAATTAGCTTCCTCTGCAACAG<br>AAGTGAAGAATTCAAGTCGGGTACAAATTGTTATTGCTGTTATATGGAAGCAATTCATTGACGTG<br>ACCCGGGCAAAATTCGATACCAAGAACAAATTAGTAGCAGCTCAAGCAGTGAATTTGAGATCAAG |

| | |
|---|---|
| | AATGAATCCACCATTTCCTCAATCTGCTATGGGGAATATAGCCACAATGGCATATGCCGTTGCAG<br>AGGAGGATAAGGATTTTTCAGATCTTGTCGGTCCATTGAAAACCAGTCTTGCAAAAATTGATGAT<br>GAACATGTTAAAGAATTACAAAAAGGAGTAACATATTTGGATTATGAAGCTGAACCACAAGAATT<br>GTTCTCTTTTAGTAGTTGGTGCAGGCTTGGGTTTTATGATTTGGATTTTGGATGGGGAAAGCCTG<br>TTTCTGTTTGTACAACAACTGTGCCTATGAAGAATTTGGTATATTTGATGGATACAAGAAATGAA<br>GATGGAATGGAAGCATGGATCAGCATGGCTGAAGATGAGATGTCTATGCTTTCCTCTGATTTTCT<br>TTCACTTCTGGACACTGATTTTAGCAATTGA |
| CrASO | ATGATAAAAAAAAGTCCCAATAGTTCTTTCAATTTTCTGCTTTCTTCTTCTACTCTCATCATCCCA<br>TGGCTCAATTCCTGAAGCTTTTCTCAATTGTATTTCCAATAAATTTTCATTAGATGTATCCATTT<br>TAAACATTCTTCATGTTCCCAGCAATTCTTCCTATGATTCTGTTCTCAAATCTACTATCCAAAAT<br>CCAAGATTCCTCAAATCACCCAAGCCCTTAGCTATAATCACCCCAGTACTTCACTCCCATGTCCA<br>ATCTGCTGTTATCTGTACCAAACAAGCCGGTTTACAAATTAGAATCCGAAGCGGAGGAGCTGATT<br>ACGAGGGCTTATCCTATCGTTCTGAGGTTCCCTTTATTCTGCTAGATCTCCAGAATCTTCGATCA<br>ATTTCCGTTGATATTGAAGACAACAGCGCTTGGGTCGAATCAGGAGCAACAATTGGTGAATTCTA<br>TCATGAGATAGCTCAGAACAGCCCTGTTCATGCGTTTCCAGCTGGGGTCTCTTCCTCTGTTGGAA<br>TTGGCGGCCATTTGAGTAGCGGCGGTTTTGGTACATTGCTTCGGAAATATGGATTAGCAGCCGAT<br>AATATAATCGATGCAAAAATTGTTGATGCCAGAGGCAGAATTCTTGATAGGGAATCAATGGGAGA<br>AGATCTATTTTGGGCTATTAGAGGAGGAGGAGGAGCTAGTTTTGGTGTTATAGTTTCTTGGAAGG<br>TTAAACTTGTAAAAGTCCCTCCGATGGTAACTGTTTTCATCTTGTCCAAGACTTATGAAGAAGGA<br>GGTTTAGATCTTCTACACAAATGGCAATATATAGAACACAAACTCCCTGAAGATTTATTCCTTGC<br>TGTAAGCATCATGGATGATTCATCTAGTGGAAATAAAACACTTATGGCAGGTTTTATGTCTCTGT<br>TTCTTGGAAAAACAGAGGACCTTCTGAAAGTAATGGCGGAAAATTTCCCACAACTTGGATTGAAA<br>AAGGAAGATTGCTTAGAAATGAATTGGATTGATGCAGCAATGTATTTTTCAGGACACCCAATTGG<br>AGAATCCCGATCTGTGCTTAAAAACCGAGAATCTCATCTTCCAAAGACATGCGTTTCGATCAAAT<br>CAGACTTTATTCAAGAACCACAATCCATGGATGCATTGGAAAAGTTATGGAAGTTTTGTAGGGAA<br>GAAGAAAATAGTCCCATAATACTGATGCTTCCACTGGGGGGAATGATGAGTAAAATATCAGAATC<br>AGAAATCCCATTTCCTTACAGAAAAGATGTGATTTACAGTATGATATACGAAATAGTTTGGAATT<br>GTGAAGACGATGAATCATCGGAAGAATATATCGATGGATTGGGAAGGCTTGAGGAATTAATGACT<br>CCATATGTGAAACAACCAAGAGGTTCTTGGTTCAGCACCAGAAACCTTTATACCGGTAAAAATAA<br>AGGTCCAGGAACAACTTATTCCAAAGCTAAAGAATGGGGATTTCGGTATTTTAATAATAATTTCA<br>AAAAGTTGGCCCTTATCAAAGGACAAGTTGATCCAGAAAACTTCTTCTACTATGAACAAAGCATT<br>CCCCCTCTCCATTTACAAGTCGAACTTTGA |
| CrDPAS | ATGGCCGGAAAATCAGCAGAAGAAGAACATCCCATTAAGGCTTACGGATGGGCTGTTAAAGATAG<br>AACAACTGGGATTCTTTCTCCCTTCAAATTTTCCAGAAGGGCAACAGGTGATGATGATGTCCGAA<br>TTAAGATACTCTACTGTGGAATTTGTCACACTGATCTTGCCTCAATCAAGAACGAATACGAGTTT<br>CTTTCTTATCCTCTTGTGCCCGGGATGGAGATCGTAGGAATAGCAACGGAGGTTGGAAAAGATGT<br>CACAAAAGTGAAAGTTGGCGAAAAAGTAGCATTATCAGCCTATTTAGGATGTTGTGGCAAATGCT<br>ATAGTTGTGTAAATGAACTCGAGAATTATTGTCCGGAAGTAATCATAGGTTATGGCACCCCATAC<br>CATGACGGAACAATTTGCTATGGGGGCCTTTCAAACGAAACTGTCGCAAATCAAAGTTTTGTTCT<br>TCGTTTTCCTGAAAGACTTTCTCCAGCTGGCGGAGCTCCTTTGCTTAGCGCCGGAATTACTTCGT<br>TTAGTGCAATGAGAAATAGCGGCATCGACAAACCTGGATTACACGTGGGAGTCGTCGGTCTCGGC<br>GGATTAGGTCATCTTGCTGTAAAATTTGCTAAGGCTTTTGGTCTTAAAGTAACTGTTATTAGCAC<br>CACTCCCAGCAAGAAGGATGATGCTATAAATGGTCTTGGTGCTGATGGATTCTTACTCAGCCGCG<br>ATGATGAACAAATGAAGGCTGCTATTGGAACCTTTGATGCAATTATTGATACACTGGCGGTTGTT<br>CATCCCATAGCACCATTGCTTGATCTCCTGAGAAGTCAAGGGAAATTTTTGTTACTTGGGGCGCC<br>ATCTCAATCACTTGAGTTGCCACCTATTCCTTTATTATCAGGTGGGAAATCTATCATTGGAAGTG<br>CGGCCGGAAATGTGAAGCAAACTCAAGAAATGCTTGATTTTGCAGCGGAGCATGATATAACTGCA<br>AATGTTGAGATTATTCCAATAGAGTACATAAATACTGCAATGGAACGTTTAGACAAGGGCGATGT<br>TAGATACCGATTTGTAGTTGACATCGAAAATACCTTGACTCCTCCGTCAGAGTTATAA |
| CrHL1 | ATGAATTCCTCAACTGATCCAACTTCAGATGAGACTATTTGGGATCTTTCTCCATATATTAAAAT<br>TTTCAAAGATGGAAGAGTAGAAAGACTCCATAATAGTCCTTATGTTCCCCCATCACTTAATGATC<br>CAGAAACTGGCGTTTCTTGGAAAGATGTCCCGATTTCATCACAAGTTTCCGCTAGGGTATACATT<br>CCAAAAATCAGCGACCATGAAAAACTCCCTATTTTTGTGTATGTGCATGGGGCTGGCTTTTGTCT<br>AGAATCTGCCTTCAGATCATTTTTCCACACTTTTGTCAAACACTTCGTAGCCGAAACCAAAGTTA<br>TTGGGGTTTCGATTGAATATAGACTTGCCCCAGAGCACCTTTTACCCGCAGCTTATGAAGATTGT<br>TGGGAAGCCCTTCAATGGGTTGCTTCTCATGTGGGTCTCGACAATTCCGGCCTAAAGACAGCTAT<br>TGATAAAGATCCATGGATAATAAACTATGGTGATTTCGATAGACTGTATTTGGCGGGTGACAGTC<br>CTGGTGCTAATATTGTTCACAACACACTTATCAGAGCTGGAAAAGAGAAACTGAAGGGCGGAGTG<br>AAAATTTTGGGGGCAATTCTTTACTACCCATATTTCATTATCCCAACCAGCACGAAACTTAGTGA<br>TGATTTTGAGTATAACTACACATGTTACTGGAAATTGGCTTATCCAAATGCTCCTGGCGGGATGA<br>ATAACCCAATGATAAACCCCATAGCTGAAAATGCTCCAGACTTGGCTGGATACGGTTGCTCGAGG<br>TTGTTGGTTACCCTGGTTTCCATGATTTCAACGACTCCAGATGAGACTAAAGACATAAATGCGGT<br>TTATATTGAGGCATTAGAAAAGAGTGGATGGAAAGGGGAATTGGAAGTGGCTGATTTTGACGCAG |

| | |
|---|---|
| | ATTATTTTGAACTCTTCACCTTGGAAACGGAGATGGGCAAGAATATGTTCAGACGTTTAGCATCT<br>TTCATCAAACATGAGTAA |
| CrHL2 | ATGGGTTCCTCAGATGAGACTATTTTTGATCTTCCTCCATACATCAAAGTCTTCAAAGATGGAAG<br>AGTAGAAAGACTCCATTCTTCCCCATATGTTCCCCCATCTCTTAATGATCCAGAAACCGGTGGAG<br>TCTCTTGGAAAGACGTCCCAATTTCTTCAGTAGTTTCAGCTAGAATTTACCTTCCTAAAATCAAC<br>AACCATGATGAAAAACTCCCCATTATAGTCTATTTCCATGGAGCTGGTTTTTGTCTTGAATCGGC<br>CTTCAAATCATTTTTCCACACTTATGTGAAACACTTTGTAGCAGAAGCCAAAGCTATTGCGGTTT<br>CTGTTGAGTTCAGGCTCGCCCCTGAAAACCATTTACCCGCAGCTTATGAAGATTGCTGGGAAGCC<br>CTTCAATGGGTTGCTTCTCATGTGGGTCTCGACATTTCCAGCTTGAAGACATGTATTGATAAAGA<br>TCCATGGATAATCAACTATGCCGATTTCGATAGACTCTATTTGTGGGGTGATAGCACCGGTGCCA<br>ATATTGTTCACAACACACTTATCAGATCTGGTAAAGAGAAATTGAACGGCGGCAAAGTGAAGATT<br>TTGGGGGCAATTCTTTACTACCCATATTTCTTAATCAGGACGAGTTCAAAACAGAGTGATTATAT<br>GGAGAATGAGTATAGATCTTACTGGAAATTGGCTTACCCAGATGCTCCTGGTGGAAATGATAACC<br>CAATGATAAACCCTACAGCTGAGAATGCTCCTGATCTGGCTGGATATGGTTGCTCGAGGTTGCTG<br>ATTTCC*ATGGTTGCCGATGAAGCTAGA*GATATAACTCTTCTTTATATTGATGCATTGGAAAAGAG<br>TGGATGGAAAGGTGAATTAGATGTGGCTGATTTTGATAAACAGTATTTTGAACTGTTTGAAATGG<br>AAACAGAGGTTGCCAAGAACATGCTCAGACGTTTAGCTTCTTTCATCAAGTAA |
| CrCAD2 | ATGGCCGGAAAATCACCAGAAGAGGAGCACCCAGTCAAGACCTATGGATTGGCTGCTCATGATTC<br>ATCTGGGGTTTTATCTCCGTTCAAATTCTCCAGGAGGGCAACTCTTGAGGATGATGTGAGGTTCA<br>AGGTGCTATATTGTGGGATTTGTCATACTGACCTTCATTTCGCTAAGAATGAGTGGGGTATTTCG<br>ACCTATCCTCTTGTACCAGGACATGAAATCGTAGGGGAAGTTACAGAGGTCGGCGGCAAAGTTAC<br>AAAGGTCAAGGTTGGAGATAAAGTTGGTGTTGGCTGCTTGGTTGGTTCATGCCGCACTTGTGATA<br>ATTGTCGTGCAGATCTTGAGAACTATTGTCCCAAAATGGTGCTAACCTATGCAAGTCCAAACGTT<br>GATGGAACGATTACCTATGGAGGCTATTCCAATGAGATGGTATGCAATGAACACTTTATTGTTCG<br>TTTCCCAGAGAACCTACCACTTGATGGTGGGGCACCATTGCTTTGTGCCGGTATTACTGTGTACA<br>GTCCAATGAAATACTATGGCTTTGCCAAACCCGGGAGCCACATAGCTGTTAATGGTCTTGGTGGA<br>CTTGGCCATGTGGCTGTTAAGTTTGCAAAGGCCATGGGAGCAAAAGTGACAGTTATAAGTACATC<br>TGAGGGCAAGAAAGACGATGCCCTCAATCGTTTGGGTGCAGATGCATTTTTGTTGAGCAGTAATC<br>CAGAAGCACTGCAGGCTGCAACAGGCACATTTGATGGCATACTTAATACTATTTCTGCTAAGCAC<br>GCTATTATCCCATTGCTTGGTCTACTAAAGTCTCATGGCAAGCTTGTTCTTCTTGGGGCACCCCC<br>GGAACCACTTGATCTTCACTCTGCTCCTTTGCTTATGGGGAGGAAGATGGTTGCTGGAAGTAGCA<br>TTGGAGGATTGAAGGAGACCCAAGAGATGCTTGATTTTGCCGGAAAGCATAACATTACTGCAGAT<br>ATAGAACTCATTTCCGCGGACAATATCAACACAGCTTTGGAGCGTCTGGCCAAGGGTGATGTTAG<br>ATATCGCTTTGTCCTTGACGTTGCAAAGACCTTGAAAGCTCCTTAA |
| mCherry | ATGGTGAAGCGTGAGGAGGATAACATGGCCATCATCAAGGAGTTCATGCGCTTCAAGGTGCACAT<br>GGAGGGCTCCGTGAACGGCCACGAGTTCGAGATCGAGGGCGAGGGCGAGGGCCGCCCCTACGAGG<br>GCACCCAGACCGCCAAGCTGAAGGTGACCAAGGGCGGCCCCCTGCCCTTCGCCTGGGACATCCTG<br>TCCCCTCAGTTCATGTACGGCTCCAAGGCCTACGTGAAGCACCCCGCCGACATCCCCGACTACTT<br>GAAGCTGTCCTTCCCCGAGGGCTTCACATGGGAGAGAGTCACCACATACGAAGACGGGGGCGTGC<br>TGACCGCTACCCAGGACACCAAGGTGGAGGAGTACAACTACAACAGCCACAACGTCTATATCATG<br>GCCGACAAGCAGAAGAACGGCATCAAGGTGAACTTCAAGATCCGCCACAACATCGAGGACGGCAG<br>CGTGCAGCTCGCCGACCACTACCAGCAGAACACCCCCATCGGCGACGGCCCCGTGCTGCTGCCCG<br>ACAACCACTACCTGAGCACCCAGTCCGCCCTGAGCAAAGACCCCAACGAGAAGCGCGATCACATG<br>GTCCTGCTGGAGTTCGTGACCGCCGCCGGGATCACTCTCGGCATGGACGAGCTGTACAAGTAA |
| GFP | ATGGTGAGCAAGGGCGAGGAGCTGTTCACCGGGGTGGTGCCCATCCTGGTCGAGCTGGACGGCGA<br>CGTAAACGGCCACAAGTTCAGCGTGTCCGGCGAGGGCGAGGGCGATGCCACCAACGGCAAGCTGA<br>CCCTGAAGTTCATCTGCACCACCGGCAAGCTGCCCGTGCCCTGGCCCACCCTCGTGACCACCCTG<br>ACCTACGGCGTGCAGTGCTTCAGCCGCTACCCCGACCACATGAAGCAGCACGACTTCTTCAAGTC<br>CGCCATGCCCGAAGGCTACGTCCAGGAGCGCACCATCTTCTTCAAGGACGACGGCAACTACAAGA<br>CCCGCGCCGAGGTGAAGTTCGAGGGCGACACCCTGGTGAACCGCATCGAGCTGAAGGGCATCGAC<br>TTCAAGGAGGACGGCAACATCCTGGGGCACAAGCTGGAGTACAACTACAACAGCCACAACGTCTA<br>TATCATGGCCGACAAGCAGAAGAACGGCATCAAGGTGAACTTCAAGATCCGCCACAACATCGAGG<br>ACGGCAGCGTGCAGCTCGCCGACCACTACCAGCAGAACACCCCCATCGGCGACGGCCCCGTGCTG<br>CTGCCCGACAACCACTACCTGAGCACCCAGTCCGCCCTGAGCAAAGACCCCAACGAGAAGCGCGA<br>TCACATGGTCCTGCTGGAGTTCGTGACCGCCGCCGGGATCACTCTCGGCATGGACGAGCTGTACA<br>AGTAA |
| mVenus | ATGGTGAGCAAGGGCGAGGAGCTGTTCACCGGGGTGGTGCCCATCCTGGTCGAGCTGGACGGCGA<br>CGTAAACGGCCACAAGTTCAGCGTGTCCGGCGAGGGCGAGGGCGATGCCACCTACGGCAAGCTGA<br>CCCTGAAGCTGATCTGCACCACCGGCAAGCTGCCCGTGCCCTGGCCCACCCTCGTGACCACCCTG<br>GGCTACGGCCTGCAGTGCTTCGCCCGCTACCCCGACCACATGAAGCAGCACGACTTCTTCAAGTC<br>CGCCATGCCCGAAGGCTACGTCCAGGAGCGCACCATCTTCTTCAAGGACGACGGCAACTACAAGA<br>CCCGCGCCGAGGTGAAGTTCGAGGGCGACACCCTGGTGAACCGCATCGAGCTGAAGGGCATCGAC<br>TTCAAGGAGGACGGCAACATCCTGGGGCACAAGCTGGAGTACAACTACAACAGCCACAACGTCTA |

| | |
|---|---|
| | TATCACCGCCGACAAGCAGAAGAACGGCATCAAGGCCAACTTCAAGATCCGCCACAACATCGAGG<br>ACGGCGGCGTGCAGCTCGCCGACCACTACCAGCAGAACACCCCCATCGGCGACGGCCCCGTGCTG<br>CTGCCCGACAACCACTACCTGAGCTACCAGTCCAAGCTGAGCAAAGACCCCAACGAGAAGCGCGA<br>TCACATGGTC |

# Curriculum Vitae

Candidate's Full Name: Hannah Caroline Tran

Universities Attended (with dates and degrees obtained): University of New Brunswick, Bachelor of Science in Biology-Chemistry, 2020-2024

Conference Presentations:

- Phytochemical Society of North America 64th Annual Meeting, York University, June 2025, poster titled: Mapping the Subcellular Compartmentalization of Enzymes in Monoterpene Indole Alkaloid Biosynthesis
- Canadian Society of Plant Biologists 2025 Annual General Meeting, Dalhousie University, August 2025, poster titled: Mapping the Subcellular Compartmentalization of Enzymes in Monoterpene Indole Alkaloid Biosynthesis